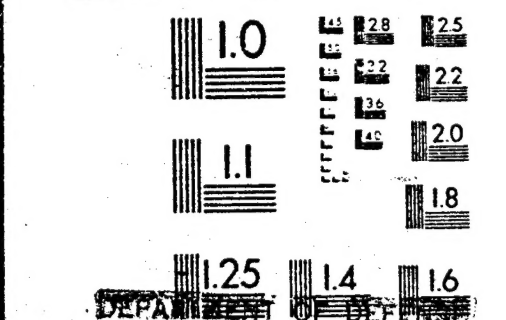

DISCLAIMER NOTICE

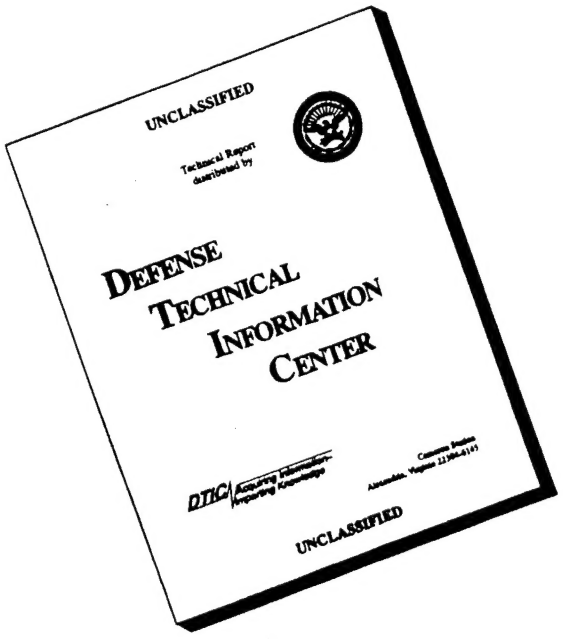

THIS DOCUMENT IS BEST QUALITY AVAILABLE. THE COPY FURNISHED TO DTIC CONTAINED A SIGNIFICANT NUMBER OF PAGES WHICH DO NOT REPRODUCE LEGIBLY.

Date: 7/15/95 Time: 7:24:23PM

Page: 1 Document Name: untitled

2 OF 4

-- ***DTIC DOES NOT HAVE THIS ITEM***

-- 1 - AD NUMBER: D436351

-- 5 - CORPORATE AUTHOR: VIRGINIA POLYTECHNIC INST AND STATE UNIV
-- BLACKSBURG DEPT OF CHEMISTRY

-- 6 - UNCLASSIFIED TITLE: AN INVESTIGATION OF ADHESIVE/ADHEREND AND
-- FIBER/MATRIX INTERACTIONS. PART A- SURFACE CHARACTERIZATION OF
-- TITANIUM DIOXIDE, TITANIUM AND TITANIUM 6% AL-40% V POWDERS:
-- INTERACTION WITH WATER, HYDROGEN CHLORIDE AND POLYMERS.

-- 9 - DESCRIPTIVE NOTE: FINAL REPT.,

--10 - PERSONAL AUTHORS: SIRIWARDANE,R. V. ;WIGHTMAN,J. P. ;

--11 - REPORT DATE: MAY , 1982

--12 - PAGINATION: 204P

--15 - CONTRACT NUMBER: NAG-127

--18 - MONITOR ACRONYM: NASA

--19 - MONITOR SERIES: CR-169009

--20 - REPORT CLASSIFICATION: UNCLASSIFIED

--22 - LIMITATIONS (ALPHA): APPROVED FOR PUBLIC RELEASE; DISTRIBUTION
-- UNLIMITED. AVAILABILITY: NATIONAL TECHNICAL INFORMATION SERVICE,
-- SPRINGFIELD, VA. 22161. N82-25367.

--33 - LIMITATION CODES: 1 24

-- END Y FOR NEXT ACCESSION END

y

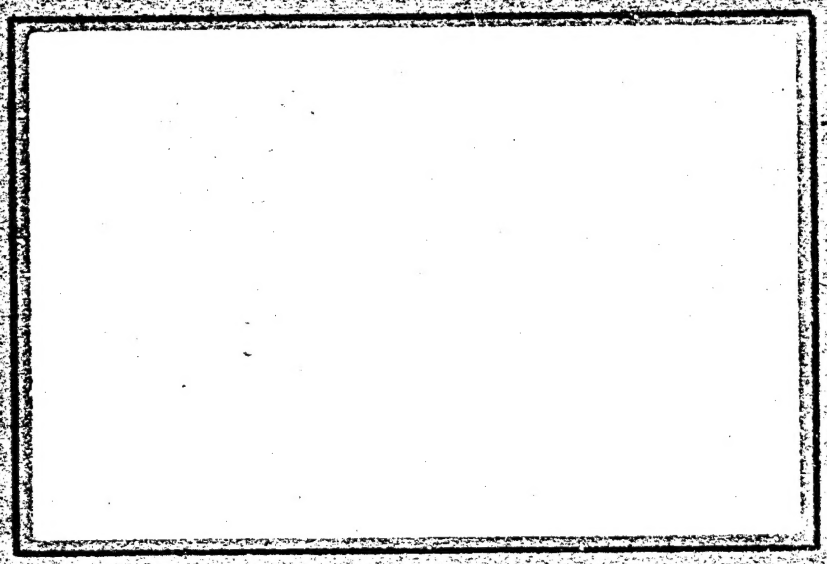

Virginia Polytechnic Institute and State University

Blacksburg, Virginia 24061

FINAL TECHNICAL REPORT

AN INVESTIGATION OF ADHESIVE/ADHEREND AND FIBER/MATRIX INTERACTIONS

PART A - SURFACE CHARACTERIZATION OF TITANIUM DIOXIDE, TITANIUM AND TITANIUM 6% Al - 4% V POWDERS: INTERACTION WITH WATER, HYDROGEN CHLORIDE AND POLYMERS

by

Ranjani V. Siriwardane and J. P. Wightman

Prepared for

National Aeronautics and Space Administration

May, 1982

Grant NAG1-127

NASA-Langley Research Center
Hampton, Virginia 23665
Materials Division
Donald J. Progar

Department of Chemistry
Virginia Polytechnic Institute and State University
Blacksburg, Virginia 24061

FOREWARD

This final technical report (Part A) summarizes our work on the characterization of the surface oxide on titanium. A summary of our work on the analysis of fractured Ti 6-4 lap shear specimen and on the analysis of composite samples is given in Part B.

ACKNOWLEDGEMENTS

We acknowledge the work of Mr. Andy Mollick and other members of the University Glass Shop for their great help in providing the necessary custom made glassware for the adsorption studies and for the calorimetry work. We thank Dr. Lucian Zelazny for the use of the surface area analyzer and the x-ray diffractometer and Mr. Bob Honeycutt for obtaining the SEM photomicrographs.

The technical assistance of Paul Hergenrother, Don Progar and Terry St. Clair at the NASA-Langley Research Center is recognized.

TABLE OF CONTENTS

LIST OF FIGURES

LIST OF TABLES

I. INTRODUCTION

Adhesives are being used increasingly to bond metal structural components. For example, an extensive effort is underway to adhesively bond Ti (6% Al -4% V) sections in advanced aircraft (1). Several chemical pretreatments have been developed to clean the alloy surface to obtain better adhesive bonding (2). The strength and durability of these adhesive bonds depend in part on the properties of the oxide layer present on the alloy surface. A number of experimental techniques including electron spectroscopy for chemical analysis (3,4), scanning (transmission) electron microscopy (4,5), reflectance visible-infrared spectroscopy (6), secondary ion mass spectrometry (7), Auger electron spectroscopy (2,8), and ion scattering spectroscopy (7) have been used to characterize this oxide layer. The surface oxide layer is generally accepted to be titanium dioxide. It has been reported that the layer on the Ti 6-4 surface may, indeed, be the rutile (8) phase of TiO_2. However, because of its low surface area it is difficult to characterize the oxide layer directly on the metal surface, and to study the interaction of the oxide layer with polymer adhesives.

To overcome this difficulty, titanium metal, titanium 6-4 metal in the form of powders, and pure crystalline titania powders were used to study the interaction with polymeric adhesives. These results were used to examine the relationship between the oxide layer present on the alloy surfaces and pure crystalline titanium oxide surfaces.

In addition to applications in adhesion, the knowledge of the

surface properties of titania powders is useful in pigment technology. Titanium dioxide is widely used as a pigment and is considered superior to many other pigmentary products. Some of the reasons for the superiority of the TiO_2 pigments are their very high refractive index, relatively low density and fairly narrow particle size range which gives maximum scattering of visible light (9). Total production of TiO_2 in the United States in 1980 was estimated to be about 700 thousand tons. Out of this, 50% was used as surface coatings and fillers, 15% for plastic and rubber fillers and 5% for ceramics (10).

In all of these applications, the properties of TiO_2 pigments are directly related to the interactions between the surface of the pigments and the various media into which they are dispersed. The surface chemistry of the pigments plays a leading role in determining the nature of these interactions. Thus, an increase in knowledge of the surface properties of TiO_2 is essential in pigment technology.

Titanium dioxide is also a well known photocatalyst. For instance, in the presence of oxygen and ultra-violet light, many compounds undergo oxidation on TiO_2 surfaces (11). These catalytic properties of TiO_2 surfaces are determined by the degree of hydration, the extent to which hydroxyl groups cover the surface, and the ease with which these groups can be removed (12). Furthermore, some interesting catalytic properties may also be obtained by exchange of oxygen atoms or hydroxyl groups by chlorine atoms (13). Therefore, the study of the interaction of TiO_2 surfaces with both water and hydrogen chloride would be of great interest.

The objectives of this work were to characterize titanium and titanium (6% Al -4% V) metal powders and five titania powders in both the

rutile and anatase crystalline forms and to study the interaction of these surfaces with polymers, water and hydrogen chloride. The characterization of these oxide surfaces was done by X-ray diffraction, electron spectroscopy for chemical analysis (ESCA), scanning electron microscopy (SEM), microelectrophoresis, and vacuum infrared transmission spectroscopy. Interaction with polymers was studied using immersional calorimetry and ESCA. Interaction with water and hydrogen chloride was studied by gas phase adsorption, immersional calorimetry, ESCA and vacuum infrared transmission spectroscopy.

II. LITERATURE SURVEY

Part 1: Titanium Dioxide Surface

This section contains a summary of previous work related to titanium dioxide. Excellent review papers (14,9) have been written in this area.

1. Structure

There are three naturally occurring crystallographic forms of titanium dioxide, namely, anatase, brookite and rutile. However, only rutile and anatase are produced on a large scale (9). The name 'rutile' is derived from Latin, meaning 'red' due to its association in bauxite and laterite deposits. The rutile crystal is tetragonal (ditetragonal-dipyramidal) P $4_2/mnm$, a=4.58, c=2.95, z=2, and it has a structure similar to AX_2 compounds as shown in Figure 1a. It consists of $[TiO_6]$ octahedra linked by two common edges to form chains parallel to the c-axis (15).

Anatase also has a tetragonal structure (I $4_1/amd$) as shown in Figure 1b. In anatase, the shared edges at the top and bottom of the octahedra are at right angles to each other, while in rutile two opposite parallel edges are shared. Although rutile has been accepted to be the most stable form, recent thermochemical data indicate that anatase is 2-3 kcal/mole more stable than rutile (16).

2. Nature of the Hydroxyl Groups and Interaction with Water

The hydroxyl groups on anatase and rutile titania powders have been studied by Yates (17) using infrared spectroscopy. For anatase after evacuation at 150°C, bands at 3675 and 3350-3100 cm^{-1} were observed.

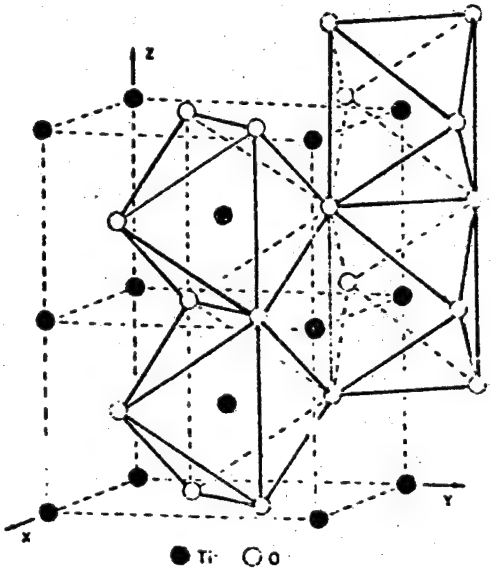

(a)

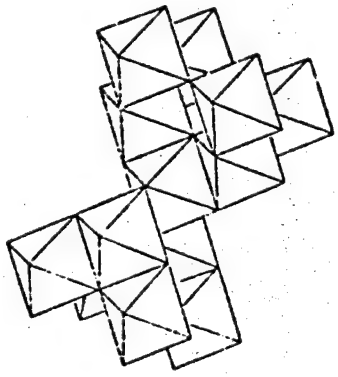

(b)

Figure 1. Structures of (a) Rutile and (b) Anatase Crystalline Forms of Titanium Dioxide

These were caused by hydroxyl stretching vibrations present in water and in hydroxyl groups. An additional band observed at 1605 cm^{-1} was due to bending vibrations of residual adsorbed monomeric water. After evacuation at 350° only two hydroxyl bands at 3715 and 3675 cm^{-1} associated with two crystal planes were observed. After evacuation of rutile at 150°C a spectrum was observed with bands at 3680, 1610, 1420 and 3450-3150 cm^{-1}. The bands at 3680 cm^{-1} which were assigned to 'NH' containing species remained after evacuation at 350°C. The band at 1610 cm^{-1} suggested that adsorbed water was dimeric on rutile.

Interaction of water vapor with rutile has been investigated by Dawson (18). Discontinuity in the adsorption isotherm was found for samples containing small particle sizes, and was explained in terms of localized and condensed states of the adsorbed layer. Isotherms on larger particles had two linear sections between relative pressures about 0.05 and 0.23 torr. Close packed monolayer formation was thought to occur at the beginning of the second linear section. The different behavior between the small and large particles was explained in terms of the predominant crystal planes, (100) for small particles and (110) for large particles. Furthermore, irreversible condensation of hydroxyl groups at 250-450°C was observed for large particles.

Day and Parfitt (19) studied the adsorption of water vapor on rutile calcined at 450°C. Increasing adsorption was found with increasing outgassing temperatures up to 200°C and constant adsorption was reached at temperatures higher than 200°C. Molecular water remained on the surface after outgassing at temperatures lower than 200°C. Quantitative analysis of water vapor adsorption isotherms showed that the surface contained

equal proportion of hydroxylated and non-hydroxylated regions.

Boutin et al. (12) studied the nature of the hydroxyl groups by slow neutron inelastic scattering. It was found that liquid water with lower mobility than bulk water was present on the surface. Incomplete removal of molecular water was found for the solid with high surface area at 200°C. Different kinds of hydroxyl groups were present on the surface and water was weakly bound to them.

Herrington and Lui (20) studied the interaction of water vapor with coated pigments. The adsorptive properties of uncoated pigments were relatively insensitive to outgassing temperature compared to coated materials. Heats of immersion ($\Delta_w H$) showed a similar distinction between the pigments. The number of hydroxyl groups was calculated using the isotherms and the values varied from 1.45 to 13.94. The uncoated rutile pigment gave a $\Delta_w H$ value equal to the surface enthalpy of water after preadsorption of only a monolayer, whereas all coated pigments needed considerably more preadsorbed water to reach this condition.

Primet et al. (21) further investigated the nature of TiO_2 surfaces by infrared spectroscopy. For anatase, infrared bands were observed at 3715 cm^{-1} due to isolated hydroxyl groups and at 3665 cm^{-1} due to hydrogen bonded hydroxyl groups in adjacent unit cells. For rutile, bands were observed at 3685 cm^{-1} due to isolated hydroxyl groups and at 3655 cm^{-1}, 3410 cm^{-1} due to hydrogen bonded hydroxyl groups. The hydroxyl groups in anatase were found to be more polarized than that of rutile. After evacuation of amorphous TiO_2, the initial hydroxyl groups were not restored by exposure to water. Dehydroxylation of crystallized TiO_2 was found to be partly reversible. All hydroxyl groups could be

exchanged with D_2O vapor.

Jones and Hockey (22) described a model for a rutile surface. Major exposed crystal planes for rutile were found to be 60% of (110), 20% of (101) and 20% of (100). The infrared band at 3410 cm^{-1} was assigned to OH- ions which were bidentate while the 3650 cm^{-1} band was due to monodentate OH- ions in the (110) plane. The bands at 3610 cm^{-1} was due to molecular water held on the (101) plane and the band at 3550 cm^{-1} was due to molecular water adsorbed on the (100) plane. Removal of water from the (100) plane was found to be easier than removal from the (101) plane.

Jones and Hockey (23) studied the hydroxylation and hydration of rutile prepared by $TiCl_4$ and combustion of Ti(isopro)$_4$. Two types of hydroxyl groups and molecular water were present on the rutile surface after out-gassing at ambient temperatures. The hydroxyl groups were found to be ionic by adsorption of SO_2Cl_2, SO_2 and HCl. Evidence for two types of coordinately bonded water was found by HCl adsorption. The sample prepared from $TiCl_4$ contained chlorine and was more readily dehydroxylated than the chlorine free sample.

Munuera et al. (24) used a combination of thermogravimetric analysis, adsorption isotherms, temperature programmed desorption (TPD) and infrared spectroscopy to study the anatase surface. Three forms of water were desorbed from the surface. The sum of all three forms of water was 6.5-7.9 H_2O/nm^2 and residual hydroxyl groups amounted to 0.3-0.5 OH/nm^2. From TPD traces, it followed that 2 H_2O/nm^2 were more tenaciously held to the surface. The heat of desorption of this mode was 50 kJ/mol. The infrared spectra of anatase showed bands at 3720, 3680, 3300 and 1615 cm^{-1}. At 350°C, only bands at 3730, 3680, 3620 and 3480 cm^{-1} were

observed. Based on the experimental data, a surface model was developed assuming that the (111) plane is the most likely exposed plane.

Munuera and Stone (25) continued the study of interaction of water vapor with the surface of rutile using adsorption isotherms, TPD and infrared spectroscopy. It was found that dissociative chemisorption of water occurred on Ti-O pairs while strong and weak forms of molecular water were adsorbed on isolated titanium and oxygen ions. Non-dissociatively adsorbed water was removed totally at 325°C.

The adsorption of water vapor on pure and phosphate-covered anatase samples has been examined using infrared spectroscopy and TPD techniques by Munuera (26). Only a small amount of water remained on the surface after outgassing at 350°C. Infrared analysis showed the presence of a small amount of molecular water and strongly adsorbed hydroxyl groups. The phosphate-covered surface had fewer adsorbed water molecules than the uncovered surface. It was suggested that basic anions such as $H_2PO_4^-$ with a short oxygen-oxygen distance fulfill the steric requirements and preferentially adsorb as bidentated ligands displacing water, to complete the octahedral coordination of the cations in the (111) plane.

Deuterium exchange with surface hydroxyl groups on rutile was studied using D_2 and D_2O by Jackson and Parfitt (27). It was found that D_2 completely exchanged at 300°C but did not exchange with saturated vapor at room temperature. The infrared studies after deuteration verified that the surface species were hydrogenic. Labile bicarbonate species were formed by reaction with CO_2 and two types of hydroxyl groups were identified.

Jones and Hockey (28) studied water vapor adsorption on rutile by infrared spectroscopy. Hydrogen bonded molecular water corresponding to an infrared band at 1630 cm^{-1} was found on the surface. The heat of adsorption was estimated to be 70-80 kJ/mol at 300K. Two types of hydroxyl groups gave infrared bands at 3650 and 3410 cm^{-1}. The dehydroxylation proceeded in accord with reactions [1] and [2].

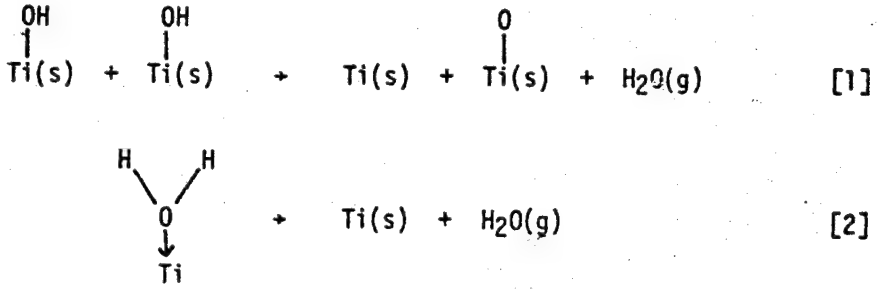

$$\begin{matrix} OH & & OH & & & & O \\ | & & | & & & & | \\ Ti(s) & + & Ti(s) & \rightarrow & Ti(s) & + & Ti(s) \end{matrix} + H_2O(g) \qquad [1]$$

$$\begin{matrix} H & & H \\ \diagdown & & \diagup \\ & O & \\ & \downarrow & \\ & Ti & \end{matrix} \rightarrow Ti(s) + H_2O(g) \qquad [2]$$

Quantitative measurements of water adsorption suggested that rutile consisted of (110), (100) and (101) planes in the ratio of 3:1:1.

Iwaki et al. (29) studied the interaction of water vapor with calcined and uncalcined rutile samples. It was found that the uncalcined sample had a higher water content than the calcined sample. The sample which was calcined twice showed a small maximum in $\Delta_w H$ around 400°C, which was explained as the stabilization of well defined oxo structure by heating in vacuum. The sample which was calcined once did not show a maximum in $\Delta_w H$ while the uncalcined sample showed a maximum in $\Delta_w H$ at 300°C. This peculiar behavior was explained in terms of an ill-defined oxo structure of the uncalcined sample.

The interaction of water vapor with the rutile surface was further studied by Day et al. (30). Adsorption isotherms had turning points

(knees) at relative pressures of 0.03 and 0.22. With increasing coverage the isosteric heats varied linearly from 12.75 to 10.75 Kcal/mol between the two knees. Considerable dehydration also occurred between 200-400°C, and on subsequent exposure to water vapor at ambient temperatures, the surface was fully rehydroxylated. The differential entropies of adsorption gave further evidence for the formation of a close packed monomolecular water layer at the second knee.

Gas adsorption and tritium exchange studies on TiO_2 have been carried out by Yates et al. (31). Significant porosity was found by gas adsorption data. After a short outgassing time at room temperature, the number of surface protons was found to be 12.5 protons/100 $\AA^2$. From this data it was suggested that the exposed crystal planes were the (110) and the (101) planes. Further outgassing at room temperature gave evidence for the removal of chemisorbed water.

Dawber and Guest (32) studied the heats of immersion of partially dried anatase and rutile pigments in mixtures of water with methanol, ethanol and n-propanol. Thermogravimetric analysis showed that rutile possessed more adsorbed water than anatase due to the porous nature of the coating. By immersion in water, it was estimated that anatase gained one monolayer of water while rutile gained six molecular layers of water.

Nagao et al. (33) studied the interaction of water with rutile. It was found that the surface hydroxyl groups decreased monotonously with increasing outgassing temperature. Content of surface hydroxyl groups varied from 4 H_2O molecules/100 $\AA^2$ to zero over the outgassing temperature range 50°C-600°C, while heats of immersion varied from 300 to

600 mJ/m^2. Differential heats of chemisorption of water on TiO_2 decreased with increasing amount of chemisorbed water indicating a heterogeneous surface.

3. Interaction with HCl

Only a few studies have been carried out in this area. Some infrared investigations have been made, but the adsorption of hydrogen chloride has not been reported.

Primet et al. (13) studied the reaction of gaseous HCl with anatase. After evacuation at 200°C, bands were present at 3715, 3660 and 3410 cm^{-1}. After reaction with HCl(g), a sharp band was present at 3540 cm^{-1} along with a broad band centered around 3330 cm^{-1}. The band at 3540 cm^{-1} was due to the hydroxyl groups adjacent to chlorine which were formed by reaction of Ti $\overset{O}{}$ Ti groups with HCl. The broad band at 3330 cm^{-1} and the band at 1595 cm^{-1} were due to molecular water formed by the reaction of superficial hydroxyl groups with HCl.

Parfitt et al. (34) studied the reaction of HCl with rutile using infrared spectroscopy. A dry rutile surface gave infrared bands at 3700 cm^{-1} with a shoulder at 3660 cm^{-1}. Initial doses of HCl to the dry surface formed more hydroxyl groups increasing the intensity of the band at 3660 cm^{-1}. Based on the data, two possible reactions were suggested.

$$Ti^{4+}\ O^{2-}\ Ti^{4+} + HCl \underset{}{\overset{45^\circ C}{\rightleftharpoons}} Ti^{4+}\ OH - Ti^{4+}\ Cl^- \qquad [3]$$

$$Ti^{4+}\ OH + HCl \underset{400^\circ C}{\overset{45^\circ C}{\rightleftharpoons}} Ti^{4+}\ O\begin{matrix}H\\H\end{matrix}\ Cl^- \rightleftharpoons Ti^{4+}\ Cl^- + H_2O \qquad [4]$$

Water treated rutile surface gave an additional reaction

$$HCl + H_2O(\text{adsorbed}) \quad H_3O^+ Cl^- \qquad [5]$$

HCl pretreated rutile surface showed Bronsted acidity. The functional group that was responsible for the Bronsted acidity was identified as $Ti^{4+}\ O\begin{matrix}H\\H\end{matrix}\ Cl^-$ which could be removed at elevated temperature.

4. Studies Related to the Electrical Double Layer

Electrophoresis studies of rutile has been carried out by Parfitt et al. (35). It was found that the surface chloride and chloride in the bulk had the effect of lowering the isoelectric point. This showed that chloride present on the surface was ionic in nature. Bulk chloride had a tendency to diffuse to the surface on heating and was removed as hydrogen chloride gas or as Cl^- by subsequent washing. After the reaction with hydrogen chloride, the isoelectric point increased indicating that the chloride produced on the surface after reaction with hydrogen chloride was different from the chlorine originally present on the sample.

Tschapak et al. (36) studied the point of zero charge (p.z.c.) and the isoelectric point (i.e.p.) of TiO_2 in LiCl, KCl and $CaCl_2$ solutions. KCl and LiCl were indifferent electrolytes for TiO_2. However, the p.z.c. of TiO_2 in $CaCl_2$ decreased about 1-1.5 pH units indicating specific adsorption of the electrolyte.

The i.e.p. of different titanias have been reported by Parks (37). The i.e.p. of natural rutile varied from 3.5-5.5. Synthetic rutile gave an i.e.p. of 6.7 while synthetic anatase had an i.e.p. of 6.0. Structural impurities present in the solids changed the i.e.p. significantly.

Changes in the i.e.p. were also observed on TiO_2 by heat treatment. This was interpreted as loss of oxygen leading to a nonstoichiometric oxide.

Healy et al. (38) found a quantitative relationship between heats of immersion and the p.z.c. of inorganic oxides including TiO_2. The basis of the correlation was also examined in terms of electrostatic field strengths of the oxide surfaces. It was found that the larger the value of the field strength, the more extensive the interaction between water molecules and the oxide surface.

A detailed thermodynamic analysis of the electrical double layer at the rutile-solution interface has been carried out by Berube and DeBruyn (39). The p.z.c. of TiO_2 at room temperature was 6.0 independent of its crystalline modification, but was lowered to 4.0 by heat treatment.

Berube and DeBruyn (40) developed a model for the electrochemical double layer at the rutile/solution interface. Differential capacity curves on rutile were obtained by graphical differentiation of adsorption isotherms. The experimental curves paralleled those calculated from simple diffuse layer theory. Specific adsorption of inorganic ions decreased in the order $Li^+ > Na^+ > Cs^+$ and $Cl^- \cong ClO_4^- \cong NO_3^- \cong I^-$. The presence of a waterlike atmosphere in the double layer was also established.

Levine and Smith (41) investigated the conditions under which an oxide surface in aqueous solution would obey the Nernst equation with respect to H^+/OH^- as potential determining ions. A modified form of the Nernst equation was derived. This was combined with a model of the inner part of the double layer involving adsorption of both anions and cations of the supporting univalent electrolyte.

Kumagi and Fukushima (42) studied the adsorption of nonionic

ethoxylated surfactants onto TiO_2 in water using microelectrophoresis. It was found that the carbonyl group was responsible for surfactant adsorption on rutile TiO_2. Adsorption occurred onto the TiO_2 having positive charge in water.

5. Acid-Base Properties

Parfitt et al. (43) studied the reaction of rutile with NH_3 to investigate Bronsted and/or Lewis acid sites on the surface. Two types of Lewis acid sites were identified. Bronsted acid sites were not present and addition of water did not change the Lewis acid sites to Bronsted sites. However, the addition of HCl produced Bronsted acid sites. Significant changes in acidity were not observed on the reduced surface.

For anatase and rutile, the adsorption of three acidic compounds (CH_3COOH, C_6H_5OH, CO_2) and three basic compounds (NH_3, C_5H_5N, $(CH_3)_3N$) has been studied by Primet et al. (44). Hydroxyl groups on rutile did not show an acidic character to any of the basic compounds while hydroxyl groups on anatase showed protonic character towards $(CH_3)_3N$. Two kinds of Lewis acid sites were observed with NH_3 and pyridine.

Parfitt et al. (45) studied the adsorption of pyridine on rutile surface using infrared spectroscopy. Two stereochemically distinct Lewis sites were identified. Only one of them was sufficiently acidic to react with pyridine which is a weak Lewis base. Rutile did not show Bronsted acidity even after pretreatment with water vapor.

Acidic and basic properties of hydroxylated anatase and rutile surfaces have been studied by Boehm (46). Hydroxyl groups on the surface were found to be amphoteric in character. Half of the hydroxyl groups

were acidic in character and the other half were mainly basic and could be exchanged with other anions. The acidic character was strong on TiO_2 which had a p.z.c. of 6.5.

6. Interaction with Other Substances

Interactions of CO and CO_2 with TiO_2 have been studied by Yates (17). It was found that the CO was weakly chemisorbed while CO_2 was much more strongly chemisorbed as CO_2 species.

Day and Parfitt (19) studied the interaction of N_2 with rutile calcined at 450°C. The presence of micropores (7Å) was found by t-plots. For surfaces containing preadsorbed water, surface areas obtained from the t-plot showed excellent agreement with minimum BET values. Erroneous BET results were obtained for the dry surface.

Reaction of CCl_4 with anatase has been studied by Primet et al. (13) using infrared spectroscopy. Two different reactions took place at room temperature and at high temperature. The reaction at room temperature was with the surface while the one at high temperature was with lattice oxygens.

Competitive adsorption of isopropanol, acetone and water on rutile was studied by Munuera (11,47). Isopropanol and acetone vapors gave type I isotherms. Isopropanol displaced acetone in a 1:1 ratio. Gaseous acetone and water did not displace chemisorbed isopropanol.

Parfitt et al. (48) studied the interaction of trimethylchlorosilane, dimethyldichlorosilane and methyltrichlorosilane with rutile. After reactions with trimethylchlorosilane and dimethylchlorosilane, the surface became resistant to uptake of molecular water. However, reaction with methyltrichlorosilane was less complete and the surface did not

become resistant to water after the reaction.

Sorption of N_2, water, ethanol and n-pentane has been studied by Day et al. (49), on rutile modified by presorption of water, ethanol, hexan-1-ol and hexan-1:6 diol. Hydrophobic character was found in those surfaces modified by organic pretreatment. Hexan 1:6 diol was oriented parallel to the surface while hexanol had this configuration only at high relative pressures.

Furlong et al. (50) determined the differential energies of adsorption ($\Delta_a U$) of argon and nitrogen on pure rutile and silica-coated rutile by microcalorimetry. It was found that the surface was heterogeneous. N_2-cation interaction contributed an appreciable amount to $\Delta_a U$ for pure rutile but after coating with silica (0.9-2.6 wt%), the surface properties became more like silica than rutile.

Eltekov et al. (51) studied the adsorption of C_5-C_8 n-alkanes, benzene, diethylether and C_1-C_4 n-alcohols on polyethylene glycol layers deposited on rutile. This modification of rutile gave a rather homogeneous surface.

Adsorption of N_2, O_2, CO on TiO_2 which was used as a catalyst support material has been studied by Dollimore and Pearce (52). Tubular pores with various cross sectional areas were identified. Both N_2 and CO adsorption-desorption isotherms were similar in type but O_2 isotherms showed enhanced adsorption.

Adsorption from binary liquid mixtures of p-xylene and n-heptane on rutile has been studied by Day et al. (53). A dual nature of the surface was observed. One-half of the surface which was hydrophobic showed preferential adsorption of xylene. Molecular water on the surface markedly

affected adsorption.

Water vapor adsorption isotherms have been determined on TiO_2, previously conditioned in n-dodecylamine solutions by Pope and Sulton (54). The oxide surface became partially hydrophobic by conditioning. The dodecylamine was oriented horizontally at low concentrations but forced to vertical orientation at high concentrations.

James et al. (55) analyzed the models for the adsorption of hydrolysable metal ions at the oxide/water interface. Five different mechanisms were proposed. It was noted that the studies on adsorption of relatively simple metal aquohydroxo complexes could not distinguish between each mechanism.

Specific surface areas of TiO_2 by physical adsorption of Ar, Kr, and Xe were determined by Basilova (56). The DKR and BET methods and electron microscopy were used to determine the surface areas. Possible reasons were discussed for the differences in the values of the specific surface areas determined by the different methods.

7. Photo-activity of TiO_2 and Catalysis

Boonstra and Mutsaers (57) studied the photoadsorption of oxygen onto the TiO_2 surface. A strong linear correlation was found between the photo-adsorption of oxygen and the number of hydroxyl groups. A decrease in photo-activity was found after HCl adsorption due to the formation of TiCl bonds.

The isomerization of cis-2-butene on modified anatase surface has been studied by Leal and Andrew (58). Isomerization was not observed when cis-2-butene was adsorbed on the surface at room temperature. However,

chemisorption with the formation of a carbonium ion complex was observed at 100°C.

Iyengar et al. (59) studied the migration of oxygen vacancies formed at the TiO_2 surface during hydrogen reduction into the interior by ESR spectroscopy. The presence of Ti^{3+} ions was found on reduced samples. After exposure to low O_2 pressures, O_2^- signals were observed on vacuum reduced samples and these were absent in hydrogen reduced samples. This was attributed to the migration of anion vacancies to the interior.

The role of ammonia in promoting radical species in precipitated TiO_2 has been studied by Iyengar et al. (60) using ESR. The species resulting from photochemical or thermal oxidation of traces of ammonia were found to be firmly held to the surface.

Bickley and Stone (61) studied the oxygen adsorption on rutile under the influence of illumination in the near ultra-violet. The presence of water enhanced the photo adsorption process. Rutile which had been subjected to prolonged outgassing and subsequent reoxidation was found to be inactive.

Munuera et al. (62) studied the photo activity of TiO_2 samples in the presence of O_2. Fast adsorption of O_2 was found in the early stages of illumination and a slow photo desorption afterwards. Thermal removal of water reduced photo adsorption.

The surface reduction of anatase and rutile under vacuum, in the presence of CO and H_2, u.v. radiation has been studied by Gravelle et al. (63). Formation of two types of paramagnetic centers as Ti^{3+} ions were observed by ESR spectroscopy. Adsorption of oxygen formed O_2^- species. These results paralleled the photocatalytic partial oxidation of

isobutane on TiO_2 at room temperature.

Fukuzawa et al. (64) studied the interaction of O_2 with TiO_2 during photoillumination by ESR. Two paramagnetic signals were detected and were attributed to solid state defects and to adsorbed oxygen species.

Electron donor properties of TiO_2 have been studied by Che et al. (65) using ESR. Tetracyanoethylene and trinitrobenzene adsorption revealed that electron donor centers were associated with OH^- groups. At high temperatures weakly coordinated O^{2-} ions were formed and these were responsible for the reducing properties of the solid.

ESCA investigation of V_2O_5 + TiO_2 catalysts for vapor phase oxidation of alkyl pyridines has been carried out by Anderson (66). Sintered powder mixtures yielded higher surface vanadium concentration than the bulk composition. The catalyst used in the oxidation of alkyl pyridines was only reduced in the thin surface layer. Surface compositional changes in V, Ti and O were observed after the catalytic reaction.

8. Miscellaneous

Chung et al. (67) used low energy electron diffraction (LEED), Auger electron spectroscopy (AES), electron energy loss spectroscopy (EELS) and ultra-violet photoemission spectroscopy (UPS) to study the single crystal faces of rutile. The (110) and (100) planes were found to be the stable planes.

The formation of large spheres of TiO_2 prepared by fusion of five kinds of fine TiO_2 powder particles has been investigated by Morimoto and Kittaka (68). Each TiO_2 particle formed, contained both anatase and rutile structures; the former constituted mainly the outer phase.

Pope and Sutton (69) studied the flotation response of TiO_2 conditioned in n-dodecylamine solutions. A strong correlation was found for the flotation response and the adsorption of cationic conditioning agent.

Surface properties of rutile single crystals using d.c. electrical conductivity were studied by Iwaki (70). The electrical conductivity on the (110) plane increased after thermal treatment in vacuo over the temperature range 25-550°C. A decrease in conductivity was found by the addition of O_2 and an increase was found by addition of H_2.

Part 2: Interaction of TiO_2, Ti and Ti-6-4 With Polymers

1. Nature of The Titanium Metal Surface

Titanium has a hexagonal close packed crystal structure (71). This transforms to a body centered cubic crystal structure called beta at 883°C. Aluminum stabilizes the alpha crystal structure by raising the alpha-beta transformation temperature. Vanadium stabilizes the beta crystal structure. Alpha-beta alloys contain a mixture of alpha and beta phases at room temperature.

Low energy electron diffraction and Auger electron spectroscopy have been used to study the reaction of a clea Ti (0001) surface with oxygen gas at low pressures and room temperature by Shih and Jona (72). It was found that the final structure of the oxide was probably TiO, not TiO_2.

Senzaki et al. (73) studied the structure of Ti surface at elevated temperatures. Hexagonal field emission patterns were observed at temperatures near 800°C. At temperatures above 882°C, the body centered cubic beta phase was observed instead of the hexagonal close packed alpha phase.

Oxidation of Ti and Ti 6-4 metal has been studied by Motte et al. (8). At low temperatures, pure titanium oxidized more rapidly than the alloy. The difference was attributed to the existence of an alumina layer on the alloy. The rutile (TiO_2) form of the oxide was found on both Ti and Ti 6-4 surfaces contradictory to the work of Shih (72). Pure titanium had two layers of rutile while the alloy contained three layers at 750-900°C. It was also found that the behavior of the growing oxide in oxygen and water vapor was different. In the temperature range 650-900°C, oxidation with oxygen took place by means of successive

cracking of the scale leading to a multilayered oxide structure. In the presence of water vapor, a recrystallization process led to the two layered oxide structure.

Dumas and John (74) studied the oxidation of titanium alloy after deposition of sodium chloride which is known as hot corrosion. This hot corrosion reaction increased the oxidation rate by factor of 100 compared to the simple oxidation. Simple oxidation at 600°C in water saturated air produced an external oxide layer less than 1μ in thickness while hot corrosion produced an oxide layer with a total thickness of about 50μm. The rutile form of TiO_2 was the only compound definitely detected by x-ray analysis.

The oxidation of pure Ti has been studied by Benninghoven et al. (7) using SIMS, AES and XPS. The maxima of the molecular ion emissions due to TiO_n^+ and TiO_n^- were shifted from lower to higher n values with increasing oxygen exposure. The oxygen signals obtained with the three methods showed an identical dependence on oxygen exposure.

The instability of anodically formed TiO_2 films was studied by Quarto et al. (75) using optical and electron microscopy. It was found that the films formed in phosphoric acid had weak spots which permitted the solution to penetrate. The formation of the anatase phase was proposed to be the source of the film instability.

2. Polyimide and Polyphenylquinoxaline

Polyimide synthesis has been discussed by Progar et al. (76). Aromatic polyimides had shown the best thermal stability but had not shown satisfactory adhesion in bonded joints. Some modifications had

been made to polyimide to improve adhesive strength. The synthesis was achieved by adding equimolar quantities of a suitable aromatic dianhydride to a stirred solution of an appropriate aromatic diamine. A similar procedure was used to prepare LARC-13 polyimide (77) used in this study.

Physical and mechanical properties of addition and condensation type polyimides have been investigated by Steger (78). The condensation polyimides showed better strength retention with prolonged aging at 600°F. However, the addition polyimides LARC-13 and LARC-160 exhibited better moisture resistance and less volatile evolution in the polymerization process. It was suggested that addition polyimides were more favorable candidates for high temperature adhesive applications.

The synthesis of polyphenylquinoxaline (PPQ) has been reported by Hergenrother (79,80). This polymer was prepared by reaction of phenyl substituted bis(1,2)-dicarbonyl compounds with aromatic bis(o-diamines). PPQ exhibited good processability relative to other high temperature polymers. The cross linking reaction reduced the thermoplasticity of these polymers at elevated temperatures. The polyphenylquinoxaline had an intrinsic viscosity of 1.19 dℓ/g and a glass transition temperature of 290°C.

3. Pretreated Ti 6-4 Surfaces

Allen and Alsalim (81) studied the nature of the oxide on the surface of Ti and Ti 6-4 after a number of chemical pretreatments. After a phosphate-fluoride pretreatment, the oxide layer present on the surface was found to be rutile. The degree of crystallinity was different for

each treatment. It was also found that a surface coated with a stable oxide in a coherent and rough form was necessary for efficient adhesive bonding.

The surfaces of Ti alloys after various pretreatments have been studied by Hamilton and Lyerly (3). It was suggested that the bonding differences observed with variously treated Ti alloys were caused by variations in the crystalline structure of titanium dioxide. The phosphate-fluoride pretreatment resulted in more durable bonds than the alkaline pretreatment. Alkaline etch favored the formation of rutile TiO_2 while phosphate-fluoride pretreatment produced primarily anatase TiO_2 contradictory to the work of Allen and Alsalim (81). Aging of phosphate-fluoride pretreated surfaces caused anatase TiO_2 to convert to rutile TiO_2. Thin oxide layers were present on phosphate-fluoride etched surfaces. High humidity and stress caused the transition of anatase to rutile TiO_2 on phosphate-fluoride treated Ti 6-4 surfaces. Both alkaline and phosphate-fluoride pretreated surfaces were very hydrophilic.

Wegman (82) studied the nature of Ti 6-4 surface after pretreat-ments. It was found that an increase in humidity caused phosphate-fluoride pretreated Ti 6-4 surface to decrease the durability of the stress bonded joint. The only effect of temperature on the durability of the phosphate-fluoride etched joint was to weaken it initially. The phosphate-fluoride processed Ti 6-4 joints were more durable than the Ti 6-4 treated with alkaline process.

Liverly (83) studied the crystalline forms of thermally aged titanium oxide films after pretreatments. Phosphate-fluoride etched surfaces contained an oxide layer in the anatase TiO_2 form at ambient

temperature and has converted to rutile TiO_2 at 600°F. This agrees with the work by Hamilton and Lyerly (3) but contradictory to the work of Allen and Alsalim (81). After an alkaline (Turco 5578) pretreatment, Ti 6-4 surface contained rutile TiO_2 and remained unchanged at 600°F. The durability of the bonds was highly dependent on the ability of the adhesives to resist moisture penetration. The premise that anatase TiO_2 was more durable than rutile TiO_2 was not confirmed. Indications were that either structure would perform if that particular structure remains unchanged during the life of the adhesive bond.

The effects of commercial treatments on Ti 6-4 has been studied by Baun (2). It was found that the acidic pretreatments selectively etched the alpha-phase. The alloy was found to be covered with a TiO_2 coating. Hydrogen and hydroxyl ions were also detected on these surfaces. The vanadium rich beta phase was mainly exposed after the Turco pretreatment. Aluminum was totally depleted from the surface after the phosphate-fluoride pretreatment. It was suggested that the anatase structure on Ti 6-4 after phosphate-fluoride pretreatment may be stabilized by the presence of Ca^{++} and Na^{+} ions.

Hergenrother and Progar (84) studied the bond durability of polyimide adhesives on Ti 6-4 specimens. The best overall combination of processability and bond strength was found to occur with intermediate molecular weight polymers (η_{int} = 0.5 to 0.8 dℓ/g, T_G = 316-318°C). Adhesive failure was observed on Ti 6-4 specimens pretreated by the phosphate-fluoride process. These specimens severely degraded at the interface after exposure to water. Maximum use temperature of this polymer was found to be 316°C unless a higher temperature and longer time could be used to induce cross linking.

Chen et al. (85) investigated Ti 6-4 surfaces after several pretreatments. Well defined alpha and beta phases were found on the phosphate-fluoride etched surfaces. The growth of alpha phase at the expense of the beta phase was found during thermal oxidation. No clear distinction between the alpha and beta phases was found on Ti 6-4 after the Turco pretreatment.

Chen et al. (86) also investigated the contamination of Ti 6-4 surface after phosphate-fluoride and Turco pretreatments. Traces of P, F, K and Cl were found after phosphate-fluoride pretreatment. Minimum residual contamination was found on Turco pretreated samples.

Beck et al. (5) studied the failure modes of PPQ and LARC-13 bonded Ti 6-4 lap shear samples. LARC-13 polyimide showed mixed mode (interfacial/cohesive) failure. Apparent interfacial failure was noted on phosphate-fluoride treated Ti 6-4 bonded with PPQ. Failure occured at the primer/oxide interface than in the oxide layer.

Ti 6-4 samples after various pretreatments have been studied by Ditchek et al. (87). Phosphate-fluoride etched Ti 6-4 surfaces displayed little macro or micro roughness while Turco etched surface showed large micro roughness. The beta phase was etched slowly during phosphate-fluoride pretreatment, and Na and F ions were retained on the surface. Fe containing substances were found on the Turco etched surface. The oxide layer present on Ti 6-4 was found to be much more stable in humid environments than aluminum oxides. It was stated that the crystalline phase did not affect bond durability but, rather chemical and morphological effects were important factors.

The results of wedge tests on Ti 6-4 panels after eight different

pretreatments were correlated with the studies of the failure surfaces and moisture sensitivity by Ditchek et al. (88). It was found that the prime factor in the durability of a bond was the roughness of the Ti 6-4 surface.

4. Miscellaneous

Huntsberger (89) discussed the important factors in adhesion. It was suggested that insufficient molecular contact at the adhesive/substrate interface was the major cause for poor adhesive performance. Importance of wetting of the adherend by the adhesives was also recognized. Wetting and bond formation was found to be synonymous for the majority of cases. Rates of wetting were dependent on surface energies and the rheological properties of the adhesives. The molecular configurations and conformations of the polymeric adhesives influenced the adhesive performance in number of ways.

De Lollis (90) described the important theories involved in adhesion. It was suggested that in order to bond to a surface, an adhesive must first wet and spread on the surface. The forces responsible for the wetting and spreading phenomena were ascribed to chemical bonds, mechanical entanglement, physical and chemical adsorption and electrostatic forces of attraction. Various theories including mechanical coupling and diffusion were also presented. The problem of preferential adsorption of water was also discussed.

Various mechanisms of adhesion, namely mechanical or interlocking, weak boundary layer, chemical and electrostatic were discussed by Mittal (91). Evidence and mechanisms for charge transfer across the metal

interfaces were reviewed. It was concluded that the electrostatic component of adhesion may have some contribution to adhesion. Evidence for the formation of chemical bonds was discussed.

Kinloch (92) reviewed the mechanisms of environmental failure. The presence of moisture was found to have a deleterious effect on structural adhesives. The first stage was the accumulation of a critical concentration of water in the interfacial region. This was dependent on the rate of water diffusion through the adhesive. This process of water diffusion was accelerated by temperature and stress. The second stage involved a loss in the integrity of the interfacial regions. This includes rupture of secondary bonds, subtle changes in the oxide structure and cohesive failure in a primer layer. The third stage was the ultimate failure of the adhesive joint.

III. EXPERIMENTAL

The materials, characterization techniques, experimental procedures and data reduction methods used in this study are described in this section

Part I. Titania powders

A. Materials

1. Adsorbates

Nitrogen, water and hydrogen chloride were used as the adsorbates. Reagent grade (purity 99%) anhydrous hydrogen chloride and nitrogen (purity 99%) were obtained from the Matheson Company. Water vapor was produced by using distilled-deionized water which had been degassed by repeated freeze-thaw cycles on the vacuum system. Helium obtained from the Airco Company was used for calibration of the dead volume in the adsorption system.

2. Adsorbents

Five titania powders, anatase-A1, rutile-R1 obtained from the Glidden Corporation, anatase-A2 obtained from the Cabot Corporation, rutile-R2 obtained from the Dupont Company, and rutile-R3 obtained from Dr. G. D. Parfitt (Carnegie Mellon University) were used as the adsorbents. A1 was prepared by the sulphate process starting with illmenite while A2, R1, R2 and R3 were prepared by the chloride process starting with $TiCl_4$.

3. Miscellaneous

Analytical grade potassium nitrate (Fisher), nitric acid (Allied

Chemical), potassium hydroxide (Fisher), hydrochloric acid (Fisher), and sodium hydroxide (Fisher) were used in the microelectrophoresis study.

Indicator solutions of p-nitro phenol (Fisher)/toluene, alizarin (Fisher)/toluene, o-nitro phenol (Eastman)/iso octane, benzeneazodiphenyl amine (Eastman)/iso octane, and methyl yellow (Aldrich)/iso octane were used for the acidity measurements.

Hellige standard hydrochloric acid solution (R1193c) was diluted to 1ℓ with deionized water to prepare 0.1N HCl stock solution for the calorimetric studies.

B. Characterization Techniques

1. Surface Area Measurements

Surface areas, based on the BET theory described by Gregg and Sing (93), were measured using the Micromeritics 2100D Orr Surface Area and Pore Volume Analyzer. Prior to the surface area measurements, 0.5 g of each titania sample was outgassed at 100°C, 200°C, 300°C and 400°C for one hour at $<2 \times 10^{-4}$ torr. Calibration of the volume of the pyrex sample bulbs was done with helium, and nitrogen was used as the adsorbate for the measurement. The cross-sectional area of an adsorbed nitrogen molecule was taken as 16.2 $\mathring{A}^2$. A Basic computer program (94) was used to calculate the surface areas.

2. X-Ray Diffraction

A Diano-XRD 8000 diffractometer using Cu K_α radiation and a graphite monochromater were used to determine the X-ray patterns for the titania powders.

3. Scanning Electron Microscopy (SEM) and Energy Dispersive X-Ray Analysis (EDAX)

An Advanced Metals Research Corporation 900 scanning electron microscope operating at 20 KV was used for the SEM analysis. All samples were mounted on conducting copper tape and were coated with a thin film of Au/Pd to prevent charging of the sample surface.

4. Surface Acidity Measurements

Indicator solutions were prepared by dissolving 1 mg of the indicator in 10 cc of the solvent. Color changes of the adsorbed indicators on the solid surface were observed by adding 2 ml of the indicator solution to 1 mg of the solid powder. Indicator measurements were taken on titania powders at room temperature and after outgassing at 400°C. Grey color was observed on R3 after outgassing at 400°C due to the formation of non-stoichiometric oxide. Oxygen at about 300 torr was introduced to this grey colored R3 at 400°C for 30 minutes. Then the powder was allowed to cool back to room temperature. The white color reappeared after this oxygen treatment. The acidity measurements were also taken on R3 after this oxygen treatment.

5. Electron Spectroscopy for Chemical Analysis (ESCA)

The elements within 50Å of the titania surfaces were characterized by using a Dupont 650 electron spectrometer. The sample was bombarded with X-rays from a magnesium target in the analyzer chamber maintained at approximately 5×10^{-7} torr. The energy of the incident Mg K_α X-ray was 1253.6 eV.

Both wide and narrow scan spectra were taken for the elements on

titania before and after HCl adsorption. A value of 284.6 eV (95) for the C1S photopeak resulting from surface contamination was used as the standard value for correcting the binding energy of each element. The photopeak intensities were corrected using published (96) photoionization cross-sections (σ). Atomic fractions (A.F.) were obtained from the following equation

$$A.F. = \frac{A_i/\sigma}{\Sigma A_i/\sigma} \qquad [6]$$

where A_i is the area of each significant peak in the ESCA spectrum.

6. Microelectrophoresis

The electrophoretic mobility (u) and isoelectric point (i.e.p.) of the titania powders were determined using a Rank Mark II microelectrophoresis apparatus. Powders were dispersed ultrasonically in 0.02 M potassium nitrate solutions. By appropriate addition of either nitric acid or potassium hydrcxide, the pH of the solutions was varied. For comparison purposes, the pH was also adjusted by using HCl and NaOH. Then the solutions were transferred to the microelectrophoresis cell which was constructed from silica. The cell was mounted in a perspex thermostatted tank (25°C) attached to the stage of a microscope. The particles were observed by dark field illumination and about five particles were timed at each stationary level in both directions. These measurements were taken with fresh titania powders and powders evacuated at 400°C. The electrophoretic mobility measurements were also taken after oxygen treatment on R3 outgassed at 400°C.

7. Calorimetry

Heats of immersion were determined in a Calvet MS-70

microcalorimeter. A schematic diagram of the calorimeter and sample cell is given in Figure 2. Four sample chambers were matched as two pairs (cells 1 and 2, cells 3 and 4), with one cell being used as a reference while the heat of immersion was measured in the other.

Sample bulbs containing 0.5 g of titania were outgassed at 100°, 200°, 300° and 400°C for 2 hours and sealed under vacuum. Al powder was also outgassed at 100°C and different amounts of water were adsorbed and sealed under vacuum. The sealed sample bulbs were attached to a breaker rod and were placed in a cell containing 2 ml of either deionized water or 1N HCl(aq). This assembly was then placed in the calorimeter and allowed to reach the steady state for about 12 hours. The reaction was initiated after establishment of the initial steady state by pressing the rod to break the fragile tip of the sample bulb.

Heats of immersion ($\Delta_w H$) were calculated using the equation,

$$\Delta_w H = \frac{(SxC - B)}{Wxa_s} \qquad [7]$$

where S is the calorimeter sensitivity, C is the measured number of counts, B is the heat evolved from empty bulb breaking, W is the sample weight, and a_s is the specific surface area. The sensitivity settings of the calorimeter were PS 100 and PS 250.

Heats of immersion were also measured for Al powder after adsorbing known amounts of water vapor. The integral heats of adsorption (ΔH_D) were calculated using equation [8] (97).

$$\Delta H_D = \left(\frac{1}{n}\right) [\Delta H_{E(SL)} - \Delta H_{E(SFL)}] + \Delta H_L \qquad [8]$$

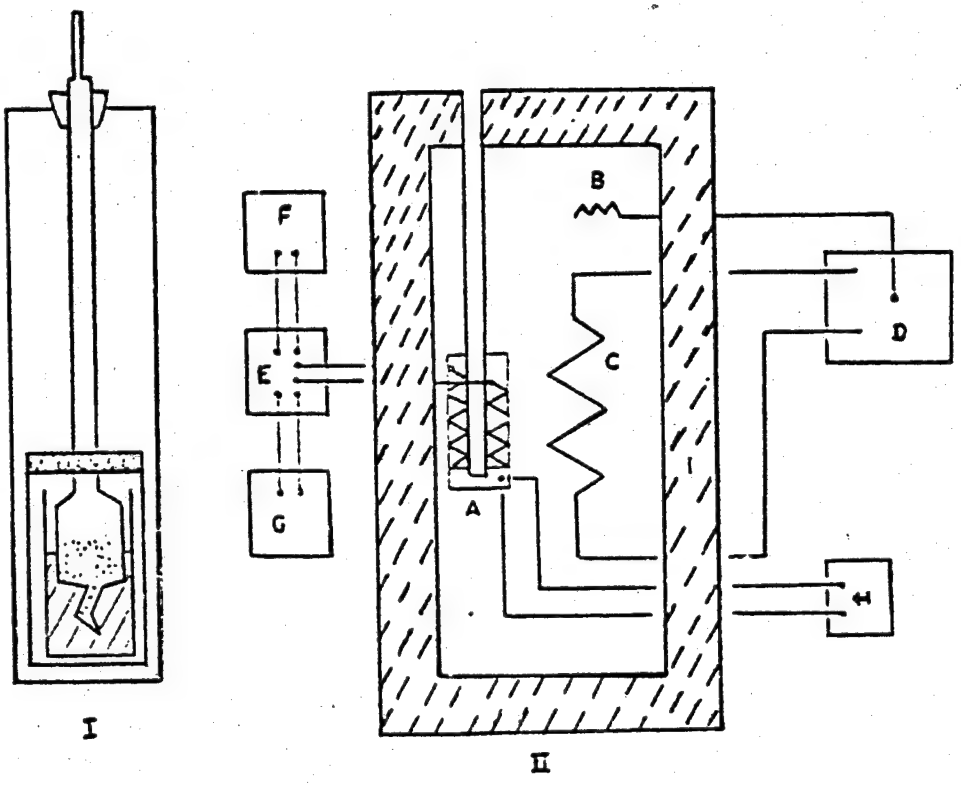

Figure 2. Schematic Diagram of Calorimeter Sample Cell (I) and Chamber (II)

A: Microcalorimetric element (detector)
B: Temperature regulator probe
C: Temperature regulator heater
D: Temperature regulator
E: Amplifier
F: Recorder
G: Integrator counter
H: Platinum resistance thermometer
I: Insulation

where, n = Number of moles of water adsorbed

$\Delta H_{E(SL)}$ = Heat of emmersion of fresh solid in water

$\Delta H_{E(SFL)}$ = Heat of emmersion of solid covered with a film of water

ΔH_L = Heat of liquifaction of water

8. Infrared Spectroscopy

Infrared spectra of titania powders were taken on a Perkin-Elmer 283 spectrophotometer. The TiO_2 pellets were prepared after heating the sample at 100°C in an oven for 15 minutes to remove moisture. About 70 mg of the sample was transferred to the pellet press which was heated to 100°C for 15 minutes. A pressure of 15000 psi was applied for 5 minutes while the press was warm. Then the pressure was released, and the press was allowed to cool before the pellet was taken out. The pellet was placed in a Teflon holder which was then transferred to the glass cell (98) as shown in Figure 3. NaCl windows were placed tightly between the cell and stainless steel holders using rubber 'O' rings. The whole assembly was connected to the vacuum line at 10^{-5} torr, and was heated to appropriate temperatures using heating tape.

The infrared spectra were taken on samples outgassed at room temperature, 100°C, and 200°C for 2 hours. The spectra were also taken after exposing the sample which was outgassed at 200°C to water vapor and gaseous HCl. The reference beam was attenuated during the measurements.

9. Adsorption Measurements

a. Description of the System

Adsorption measurements of hydrogen chloride and water on titania

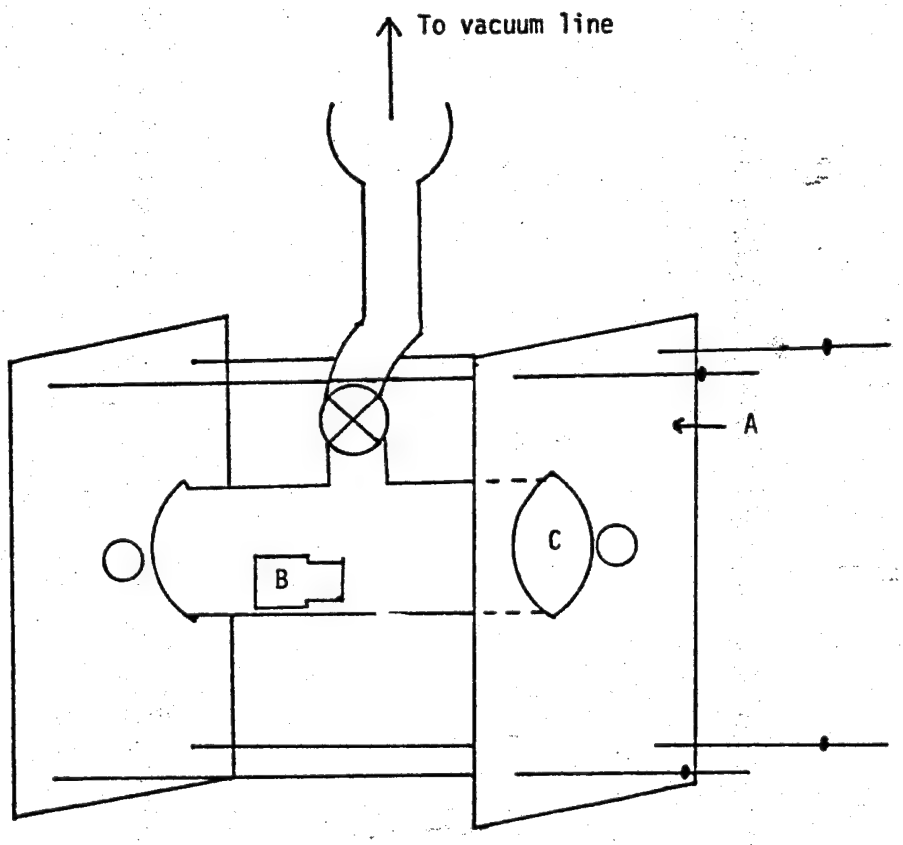

A. Stainless Steel Metal Holders
B. Teflon Holder Containing the Pellet
C. Sodium Chloride Windows

Figure 3. Schematic Diagram of the Vacuum Infrared Cell

samples were conducted in a constant volume apparatus with glass stopcocks lubricated with Apiezon N as shown in Figure 4. The system was maintained at a pressure of 1×10^{-5} torr using a mercury diffusion pump (DP) and a mechanical pump (MPI). The pressure was measured by means of a McLeod gauge (MG). The pumps were accessed to the apparatus via stopcock S1. Helium, hydrogen chloride and liquid water were stored in reservoirs HB, CB and WB and were accessed via stopcocks S7, S5 and S6 respectively. Apiezon W was used to seal the sample bulb SB to the system, and introduction of adsorbate ontc the sample was controlled by stopcock S4. Stopcock S3 connected the system vacuum line to the main vacuum line ML.

The pressures were measured by a MKS Baratron gauge (BG) which is a differential capacitance manometer. The output was displayed on a Baratron meter 144 (BM) with a precision of 0.5 torr and recorded on a Hewlett Packard Mosely 680 strip chart recorder (R). The portion between stopcocks S2 and S8 served as the reference line. A gas buret (GB) consisting of calibrated bulbs containing mercury with known weights was used to regulate the volume of the apparatus. A uniform temperature was maintained by constructing a thermostated air encasement. Heat was supplied by a 100 watt tungsten light bulb. Water was circulated in the air bath and served as the cooling unit. The system was thermostated at 30°C. The sample bulb was surrounded by a constant temperature water bath for the 40°C and 50°C measurements.

b. Introduction and Removal of Gases

The gases were introduced to the main system via valve S14. The

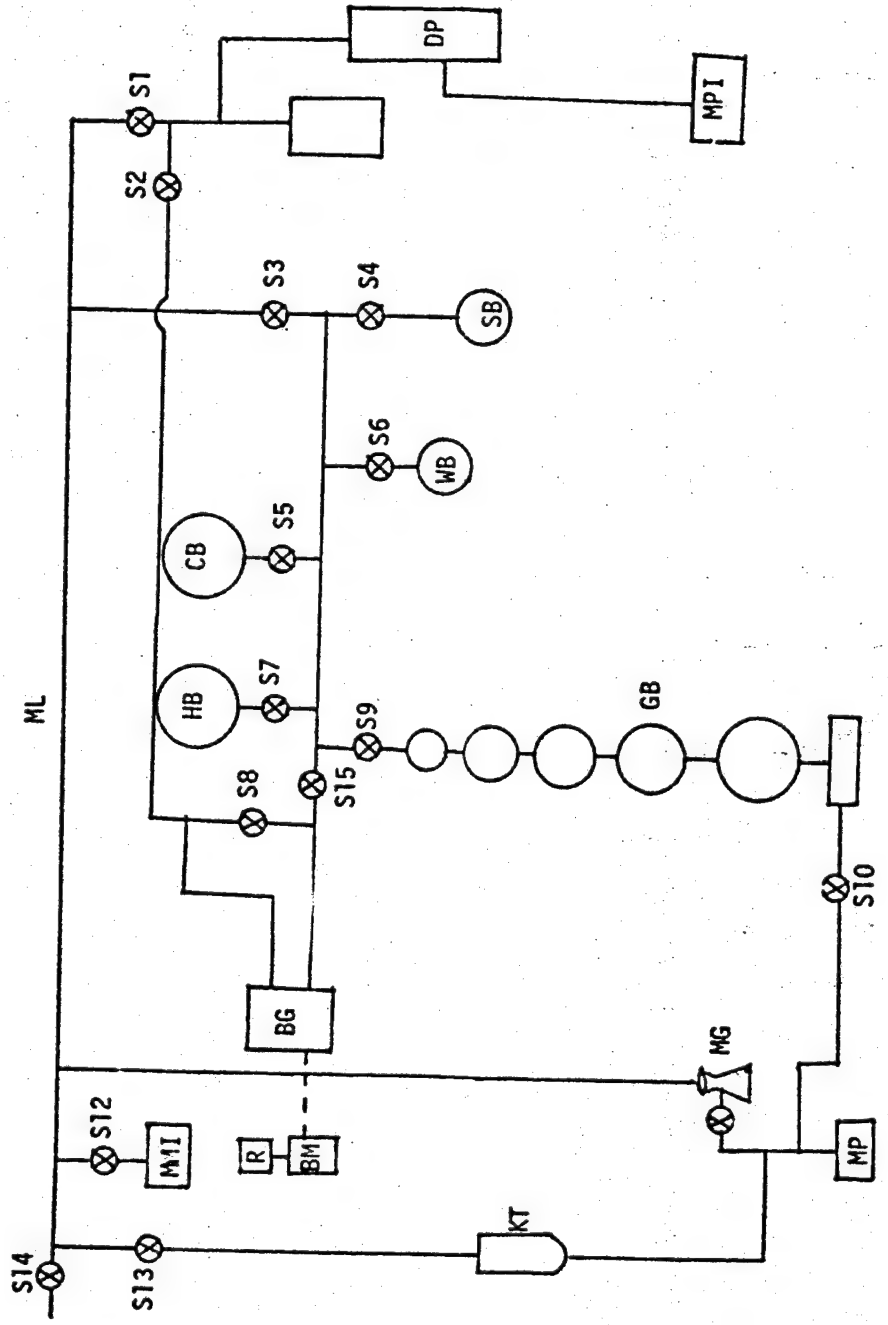

Figure 4. Schematic Diagram of the Adsorption Apparatus

pressure of the gas during the introduction was measured using a manometer MMI, and typically about 760 torr was introduced at one time. All the valves were closed during the introduction except S3 and appropriate valves for the storage bulbs. Then the gases were stored in the storage bulbs. Excess HCl was removed through the KOH trap (KT) through S13 and S3 slowly.

c. Calibration of the Dead Volume (V_S)

The system was first evacuated using the diffusion pump. The stopcocks S2 and S15 were then closed, and the cross member S8 was opened to zero the Baratron meter. Then stopcocks S8, S3, S4 were closed while S2, S15 were opened. Helium was introduced to the system, and the pressure was measured. Then, the meniscus of the mercury inside the doser (GB) was moved down with valve S10 and corresponding pressures were measured. The dead volume of the system was calculated using the ideal gas law and the measured pressures and the known volumes of the bulbs.

d. Adsorption Measurement

Two grams of adsorbent were placed in a sample bulb (SB) and were outgassed at 100°C, 200°C, 300°C and 400°C for 2 hours prior to the adsorption measurement. The adsorption measurements were also taken on oxygen treated R3 outgassed at 400°C. The volume of the sample bulb was determined with helium. The pressure reading was taken after the introduction of helium to the system with valves S3 and S4 closed. Then valve S4 was opened and pressure was measured again. These readings were used to calculate the dead volume of the sample bulb. Then helium was removed from the system. Similarly, water vapor was introduced and the

pressure reading was taken. After opening S4, the system was allowed to equilibriate to reach steady state and the equilibrium pressure was measured. A similar procedure was used for the HCl adsorption measurements.

e. Readsorption Isotherm

The readsorption isotherm was taken to study the reversibility of the adsorption process. After completion of the adsorption isotherm, the sample bulb was reevacuated at the appropriate temperature for 2 hours. Then the readsorption isotherms were taken as described before.

f. Data Reduction

(i) Adsorption Isotherms: Experimental data obtained in the adsorption system was reduced to the amount of gas adsorbed by employing equations based on the ideal gas law.

The number of moles of water or HCl adsorbed (N_i^s) was calculated using the following equations:

$$N_i = \frac{P_i \times V_s}{RT \times W \times a_s} \qquad [8]$$

$$N_f = \frac{P_f \times (V_s + V_{sb})}{RT \times W \times a_s} \qquad [9]$$

$$N_i^s = N_i - N_f + \frac{P_{i-1} \times V_{sb}}{RT \times W \times a_s} + N_{i-1}^s \qquad [10]$$

where P_i is the pressure in the dead volume (V_s) prior to each exposure of adsorbate to the sample, P_f is the equilibrium pressure in the system

after exposure to the adsorbate, V_{sb} is the volume of the sample bulb, W is the weight of the sample, and a_s is the specific surface area. N_i and N_f are the number of gas phase moles in the system before and after exposure to adsorbate, respectively. N^s_{i-1} is the number of gas moles adsorbed before the exposure to the current dose. R is the gas constant and T is the temperature.

g. Monolayer Volume and Adsorbate Area

The Brunauer, Emmett and Teller (BET) method was used to calculate the monolayer volume of water adsorbed on titania. The BET equation was used in the following form:

$$\frac{X}{N(1-X)} = \frac{1}{N_M \cdot C} + \frac{(C-1)X}{N_M \cdot C} \qquad [11]$$

where

$X = P/P_o$

P = Equilibrium pressure of water vapor

P_o = Vapor pressure of water at adsorption temperature

N = Number of moles of water/grams of adsorbent

C = Constant

N_M = Monolayer capacity in moles of water/gram of adsorbent

Here the value of N_M can be expressed as

$$N_M = \frac{1}{m+y}$$

where y and m are the intercept and slope of a plot of $X/N(1-X)$ vs. P/P_o.

The area of the adsorbed water (A) in $\mathring{A}^2$/molecule on TiO_2 was calculated by the following equation:

$$A = \frac{\Sigma}{N_M \cdot N_O} \qquad [12]$$

where, Σ = BET N_2 surface area

N_O = Avogadro number

The monolayer capacity (N_M) of adsorbed hydrogen chloride was calculated employing the following form of the Langmuir equation, using the adsorption data.

$$\frac{P}{N} = \frac{1}{b \cdot N_M} + \frac{P}{N_M} \qquad [13]$$

where

P = Equilibrium pressure of HCl

N = Number of moles of HCl/gram of adsorbent

b = Constant

The monolayer capacity (N_m) is equal to the reciprocal of the slope of the line obtained by plotting P/N vs. P. The adsorbate area of HCl was calculated using equation [12].

h. Calculation of Isosteric Heats of Adsorption

The adsorption isotherms at three temperatures were used to calculate the isosteric heats of adsorption at various surface coverages. The isosteric heat is a differential quantity calculated using isotherm data and a Clapeyron type equation in the following form

$$-q_{st} = R \left[\frac{\delta \ln P}{\delta 1/T}\right]_n \qquad [14]$$

P = Equilibrium pressure

T = Adsorption temperature

N = Moles of adsorbate/unit area of adsorbent

A plot of ln P vs 1/T at constant coverage gives a slope equal to $-q_{st}/R$. Accurate determination of the values of ln P at constant coverage was facilitated by computer fitting of isotherm data using the computer program (99) given in Appendix 1.

Part 2: Interaction with Polymers

A. Materials

The polymers polyphenylquinoxaline and LARC-13 were obtained from personnel at the NASA-Langley Research Center. These polymers were dissolved in 1:1 xylene (Fisher):m-cresol (Matheson, Coleman and Bell) and dimethyl formamide (Mallinckrodt), respectively. The materials used for the pretreatment of the metal powders were hydrofluoric acid (J. T. Baker), methylethyl ketone (Baker), nitric acid (Allied Chemical Corp.), trisodium phosphate (Mallinckrodt Corp.), Turco powder (Purex Corp.), Sprex-AN (NASA-Langley Research Center), and Pasa-Jell (NASA-Langley Research Center). Two metal powders, titanium and titanium 6-4 were obtained from Cerac Corp.

B. Characterization Techniques

Surface areas, scanning electron microscopy (SEM), energy dispersive X-Ray analysis (EDAX), water adsorption isotherms, heats of immersion in water, and electron spectroscopy for chemical analysis (ESCA) were determined by methods described in Part 1.

ESCA measurements were taken on the fresh metal samples and samples outgassed in the vacuum (10^{-7} torr) at 400°C using the variable temperature ESCA probe. SEM pictures were taken for the metal samples at room temperature, after evacuation at 400°C, after heating in air at 400°C and Ti 6-4 after pretreatment with the Turco and phosphate-fluoride processes (6).

C. Interaction With Polymers

Five TiO_2 powders, Ti metal, Ti 6-4 metal powder and Ti 6-4 powder after Turco and phosphate-fluoride pretreatments were used in this study.

A solution of 5% polyphenylquinoxaline was prepared by diluting 5 g of 18% polymer solution in 15 g of 1:1 xylene:m-cresol solution. The 21.5% LARC-13 polymer solution was prepared by dissolving 1g of polymer in 3g of dimethylformamide. Heats of immersion of powders were first measured in the solvent and then in the appropriate polymer solutions. The powders were outgassed at room temperature at 10^{-5} torr for 24 hours. Heats of immersion was also measured after outgassing the metals at 100°, 200°, 300°, 400°C for 2 hours, and at room temperature for 5 minutes at 10^{-5} torr.

IV. RESULTS AND DISCUSSION

Part 1: Titania Powders

A. CHARACTERIZATION OF ADSORBENTS

1. X-ray Diffraction

The crystalline phases determined by X-ray diffraction for the five titania powders A1, A2, R1, R2 and R3 are shown in Table I. The values of d-spacings that were calculated using the X-ray diffraction patterns, for anatase and rutile were 0.352 nm and 0.325 nm, respectively. These values agree well with the reported values (100).

2. Surface Areas

Surface areas of titania powders measured as a function of outgassing temperatures are shown in Figure 5. No significant changes in the surface areas were observed over the outgassing temperature range 100° to 400°C. Similar to the observation in the present study, Herrington and Lui (20) observed minimal changes in surface area in uncoated and coated titania powders with increasing outgassing temperatures. The average surface areas calculated within this outgassing temperature range are listed in Table I.

3. SEM/EDAX Studies on Titania

The scanning electron photomicrographs of A1 powder at two different magnifications are shown in Figure 6. Similar pictures were observed for the other four powders. As shown in Figure 6, the titania powder consists of small primary particles clustered together to give larger secondary particles. EDAX analysis of all powders showed the presence of

TABLE 1

X-RAY DIFFRACTION AND SURFACE AREA RESULTS
FOR TITANIA POWDERS

Sample	Crystalline Phase	Surface Area (m^2/g)
A 1	Anatase (100%)	9 ± 1
A 2	Anatase (87%); Rutile (13%)	48 ± 4
R 1	Rutile (100%)	7 ± 1
R 2	Rutile (100%)	6 ± 2
R 3	Rutile (100%)	22 ± 2

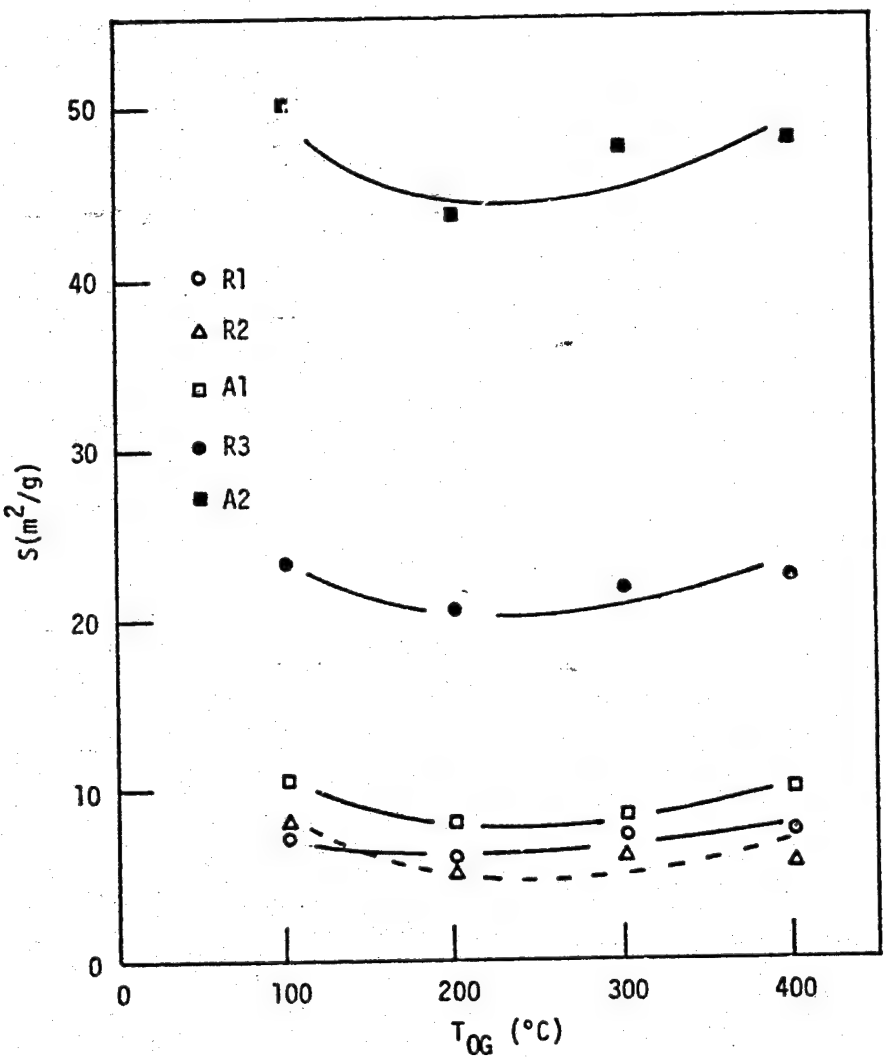

Figure 5. Surface Areas of TiO_2 as a Function of Outgassing Temperature

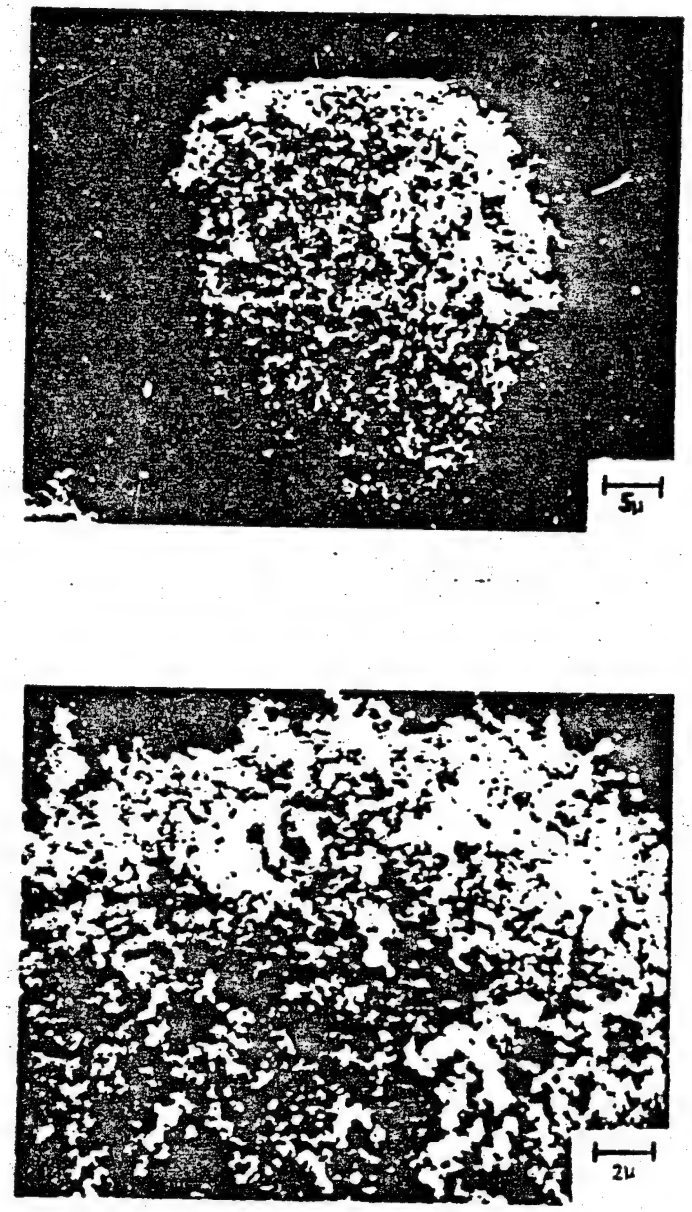

Figure 6. Scanning Electron Photomicrographs of Al

only Ti indicating minimal contamination. However, an alumina coating was known to be present on R1 and R2 powders but no aluminum signal was seen in the EDAX spectra. This observation again demonstrates that EDAX cannot be used in surface analysis.

4. Surface Analysis by ESCA

A qualitative analysis of the surface composition of the titania powders was carried out using ESCA. The results of the ESCA analysis, namely the binding energies (B.E.) and atomic fractions (A.F.) are listed in Table II. The peak corresponding to oxygen of A1 was observed at 530.2 eV. This was assigned to oxygen in the TiO_2 lattice based on previous ESCA studies (66). Trace amounts of phosphorus, potassium and chlorine were observed on A1 powder. A2 and R3 powders were quite pure and only titanium and oxygen and ubiquitous carbon photopeaks were observed. An aluminum photopeak was present on both R1 and R2 samples. The oxygen photopeak for both R1 and R2 powders was a doublet. The photopeak at the lower binding energy was assigned to oxygen in TiO_2 while the peak at the higher binding energy was assigned to oxygen in aluminum oxide. The average binding energy of 531.2 eV agrees well with the binding energy value reported for oxygen on pure Al_2O_3 (101). A trace amount of chlorine was observed on R1 powder.

5. Microelectrophoresis

The TiO_2 powders were dispersed in 0.02 M KNO_3 solution which was known to be an indifferent electrolyte (27). Isoelectric points for the five powders were obtained from the mobility vs pH plots shown in Figures 7-11. The values of the isoelectric points at room temperature

TABLE II

ESCA ANALYSIS OF TITANIA POWDERS

	Anatase-A1		Anatase-A2		Rutile-R1		Rutile-R2		Rutile-R3	
Photopeak	B.E.(eV)	A.F.	B.E.(eV)	A.F.	B.E.(eV)	A.F.	B.E.(eV)	A.F.	B.E.(eV)	A.F.
C 1s	(284.6)	0.24	(284.6)	0.42	(284.6)	0.33	(284.6)	0.36	(284.6)	0.32
O 1s	529.8	0.570	529.2	0.42	529.2		529.2		529.0	0.48
					531.4	0.48	531.0	0.43		
Ti $2p_3$	458.2	0.123	158.0	0.16	457.6	0.11	457.0	0.09	457.2	0.19
Al 2s	-	-	-	-	118.4	0.07	118.8	0.11	-	-
K $2p_3$	292.3	0.021	-	-	-	-	-	-	-	-
Cl 2p	197.6	0.006	-	-	197.4	0.004	-	-	-	-
P $2p_3$	132.8	0.032	-	-	-	-	-	-	-	-

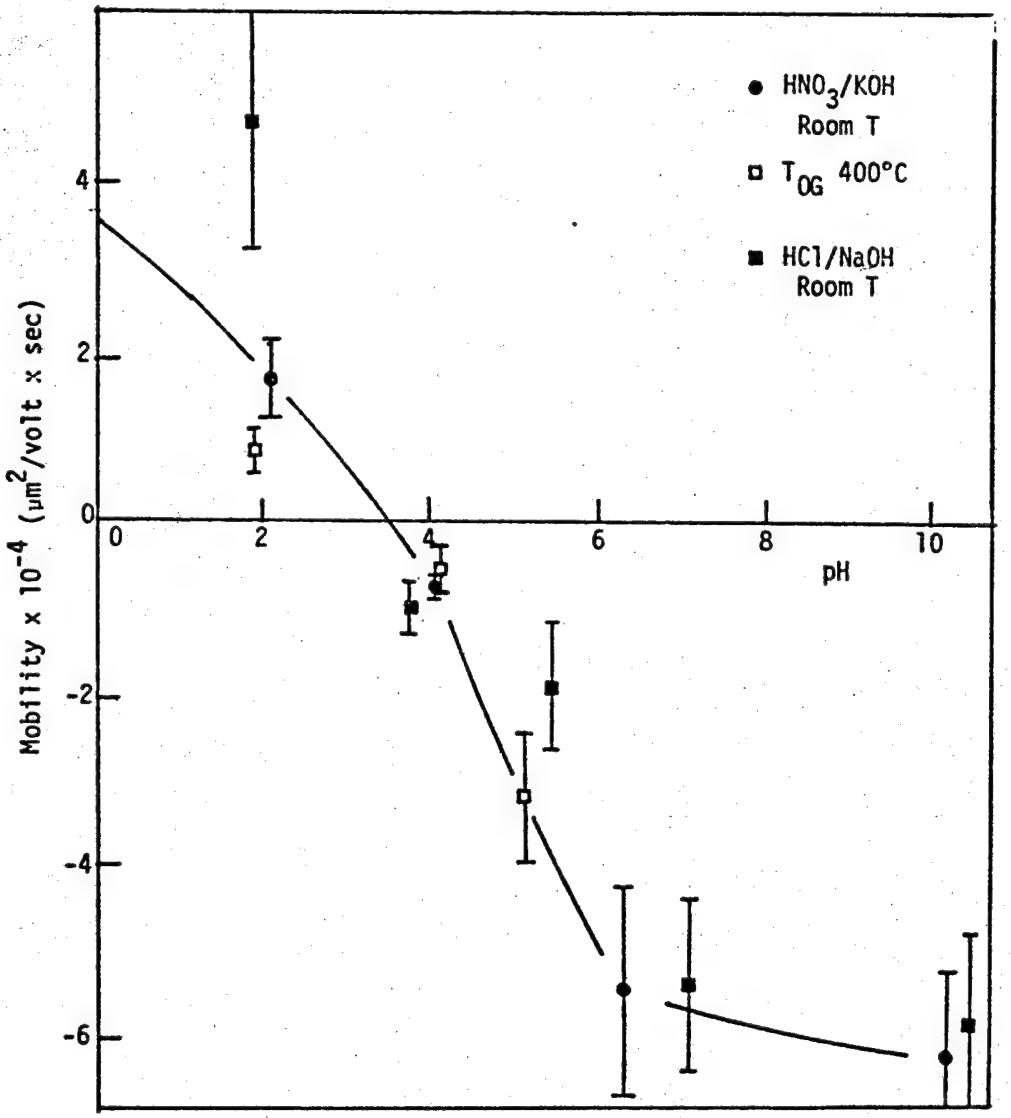

Figure 7. Electrophoretic Mobility of Al as a Function of pH

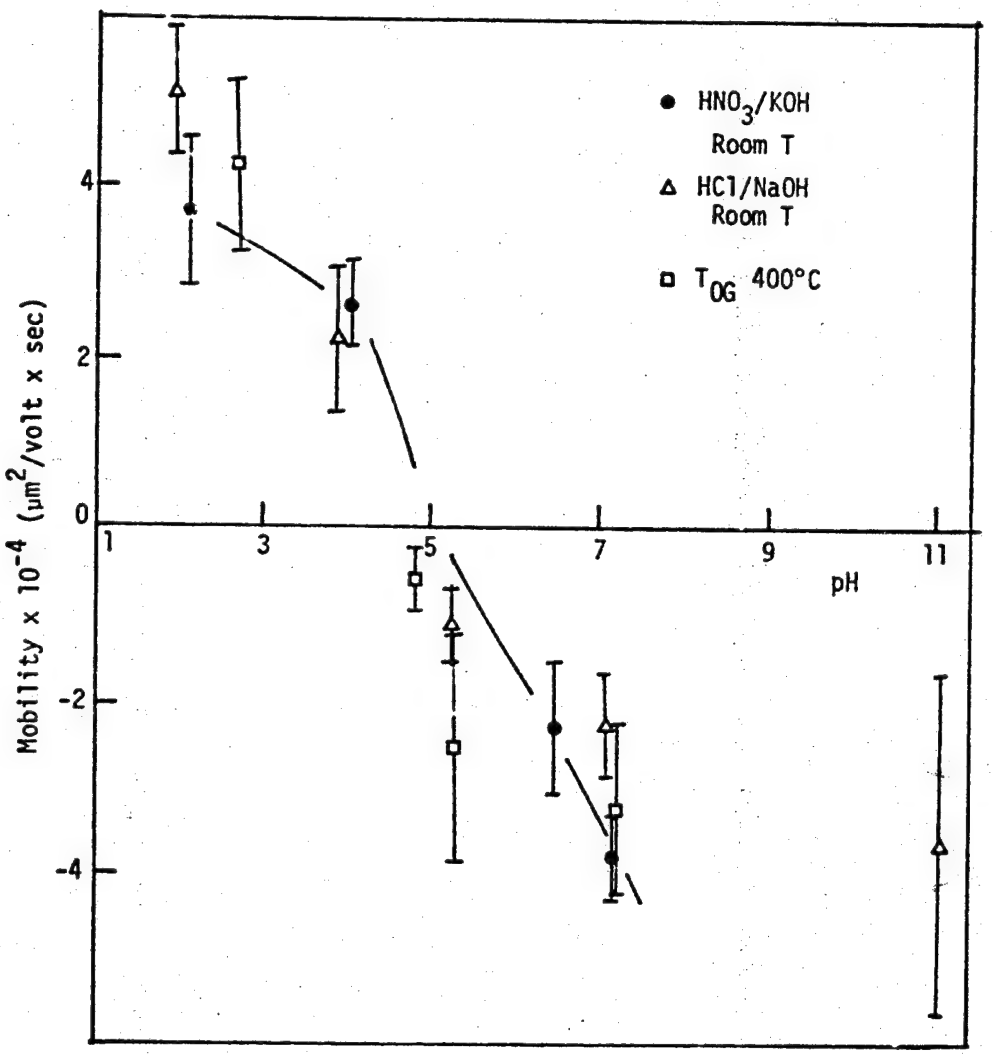

Figure 8. Electrophoretic Mobility of R1 as a Function of pH

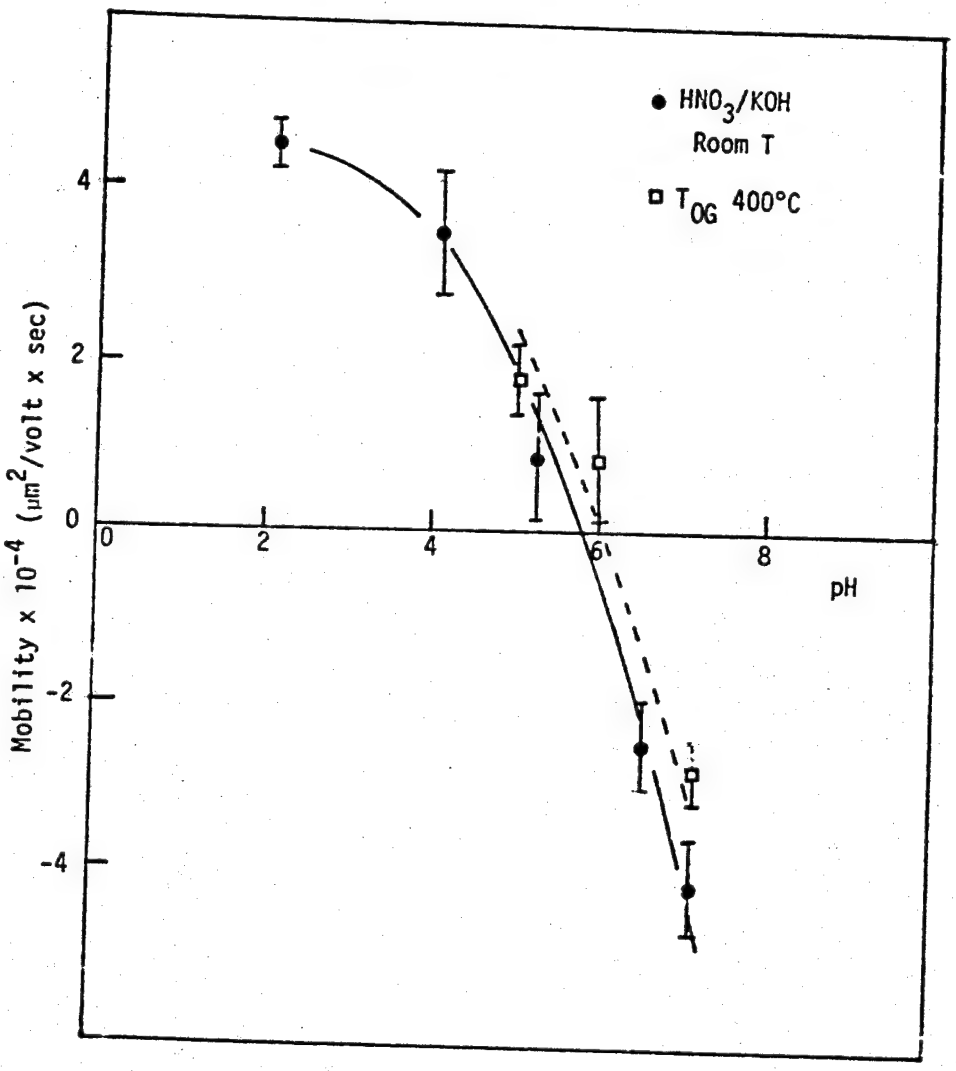

Figure 9. Electrophoretic Mobility of A2 as a Function of pH

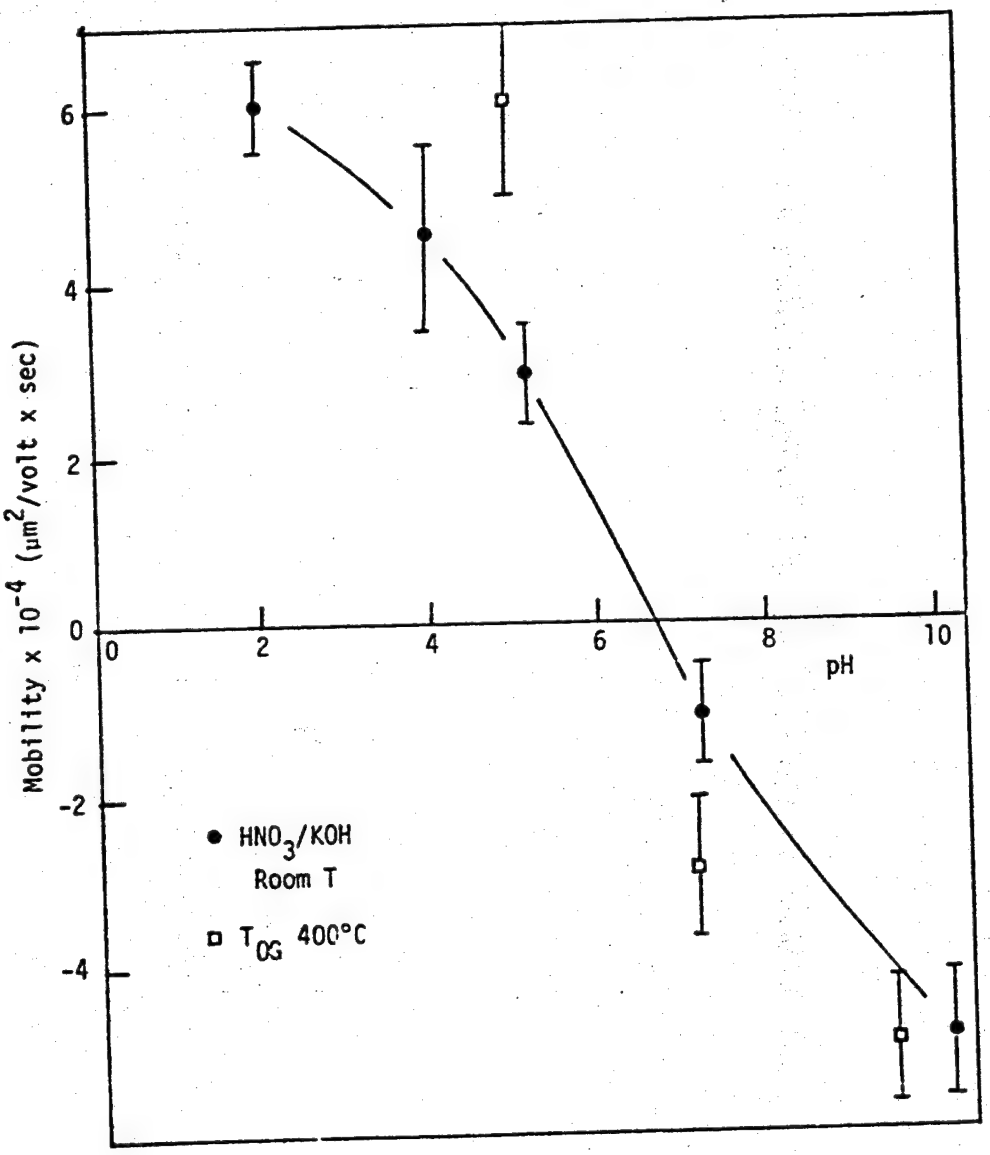

Figure 10. Electrophoretic Mobility of R2 as a Function of pH

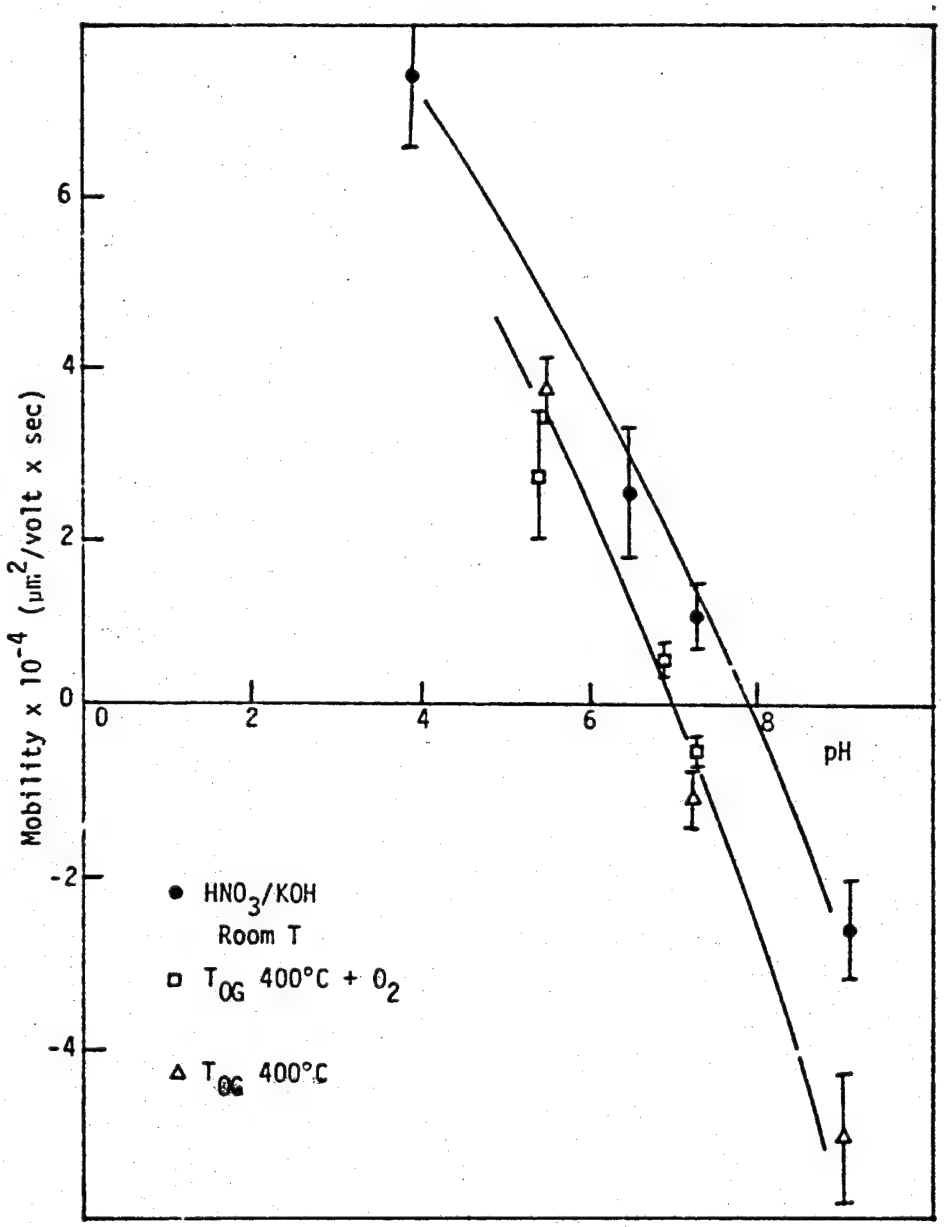

Figure 11. Electrophoretic Mobility of R3 as a Function of pH

and after outgassing at 400°C are listed in Table III. As shown in Figures 7 and 8 for A1 and R1 powders, the isoelectric points were not changed when pH was adjusted by adding $HCl_{(aq)}$ and $NaOH_{(aq)}$ instead of $HNO_{3(aq)}$ and $KOH_{(aq)}$. The isoelectric point of A1 powder was significantly lower than the isoelectric points for the other four powders. Thus, A1 has the highest negatively charged surface among the five powders. Furthermore, R3 has the highest isoelectric point indicating that R3 has the highest positively charged surface of the powders studied. After evacuating at 400°C, no significant change in isoelectric point was observed for A1, A2, R1 and R2 powders. However, a decrease of 1.1 units in the isoelectric point was observed with R3 powder as shown in Figure 11. This may be due to the irreversible condensation of hydroxyl groups which could be responsible for the positive charge observed after outgassing at room temperature. The isoelectric point after outgassing at 400°C for R3 was not affected by oxygen treatment.

6. Surface Acidity

The results of the surface acidity measurements using the indicator method are shown in Table IV. p-Nitro phenol changed from colorless to yellow on A1, A2, R1 and R2 powders. This shows that these four powders are basic and the basicity is greater than 7.6 which is the pk_a value of p-nitro phenol. The acidity was not changed after outgassing these powders at 400°C.

Benzeneazodiphenyl amine changed from yellow to light violet on the surface of R3. Therefore, R3 is quite acidic and has a pK_a value of $\approx$1.5. After outgassing the R3 powder at 400°C, benzeneazodiphenylamine did not

TABLE III

ISOELECTRIC POINTS DETERMINED BY MICROELECTROPHORESIS IN 0.02 M $KNO_{3(aq)}$

Sample	Isoelectric Point at Room T	Isoelectric Point at 400° OGT
A 1	3.6	3.6
A 2	5.8	5.9
R 1	5.1	4.9
R 2	6.7	6.7
R 3	7.9	6.8

TABLE IV

SURFACE ACIDITY MEASUREMENTS OF TITANIA POWDERS
AFTER OUTGASSING AT ROOM TEMPERATURE AND 400°C

Indicator	pK_a	A1 Room T/400	A2 Room T/400	R1 Room T/400	R2 Room T/400	Room T	R3 400	400 + O_2
Benzeneazodiphenyl--amine/Iso Octane	1.5	Y → Y	Y → Y	Y → Y	Y → Y	Y→L.V.	Y→Y	Y → Y
Methyl Yellow/ Iso Octane	2.8	Y → Y	Y → Y	Y → Y	Y → Y	Y → R	Y→P	Y → Y
o-Nitro Phenol/ Iso Octane	7.0	Y → Y	Y → Y	Y → Y	Y → Y	Y → C	Y→C	Y → Y
p Nitro Phenol/ Toluene	7.6	C → Y	C → Y	C → Y	C → Y	C → C	C→C	C → Y

C = Colorless, Y = Yellow, R = Red, P = Pink, L.V. = light violet

change color while methyl yellow changed from yellow to pink. Thus, the surface acidity of R3 powder was decreased as a result of evacuation at 400°C. When the R3 sample was treated with oxygen after outgassing at 400°C, the surface acidity was decreased to a pK_a value >7.6. Since R3 showed a different behavior compared to other samples at 400°C it is important to consider the possible processes that might occur at 400°C. Two processes, namely condensation of hydroxyl groups and formation of coordinately unsaturated Ti^{+3} cations may take place at 400°C in vacuum. The condensation of acidic hydroxyl groups would contribute to a decrease in acidity while formation of Ti^{3+} ions would contribute to an increase in acidity. Since reduction in acidity was observed for R3 at 400°C, the predominant process may be the condensation of hydroxyl groups. By oxygen treatment, the Ti^{3+} cations are removed from the surface. Thus, the complete reduction in acidity after oxygen treatment may be due to the removal of Ti^{3+} cationic Lewis acid sites. However, Parfitt et al. (43) did not observe any significant changes in acidity on reduced rutile samples compared to fresh sample contradictory to the observation made in the present study.

7. Infrared Spectroscopy

The infrared spectra of A2 powder are shown in Figures 12 and 13. In these spectra, broad infrared bands in the 3800-3000 cm^{-1} region and in the 1800-1500 cm^{-1} region were observed before outgassing at room temperature. This was due to the large amount of physisorbed water present on the sample. After outgassing at room temperature, two sharp bands at 3625 cm^{-1} and 1615 cm^{-1}, and a broad band in region 3540-3000 cm^{-1} were

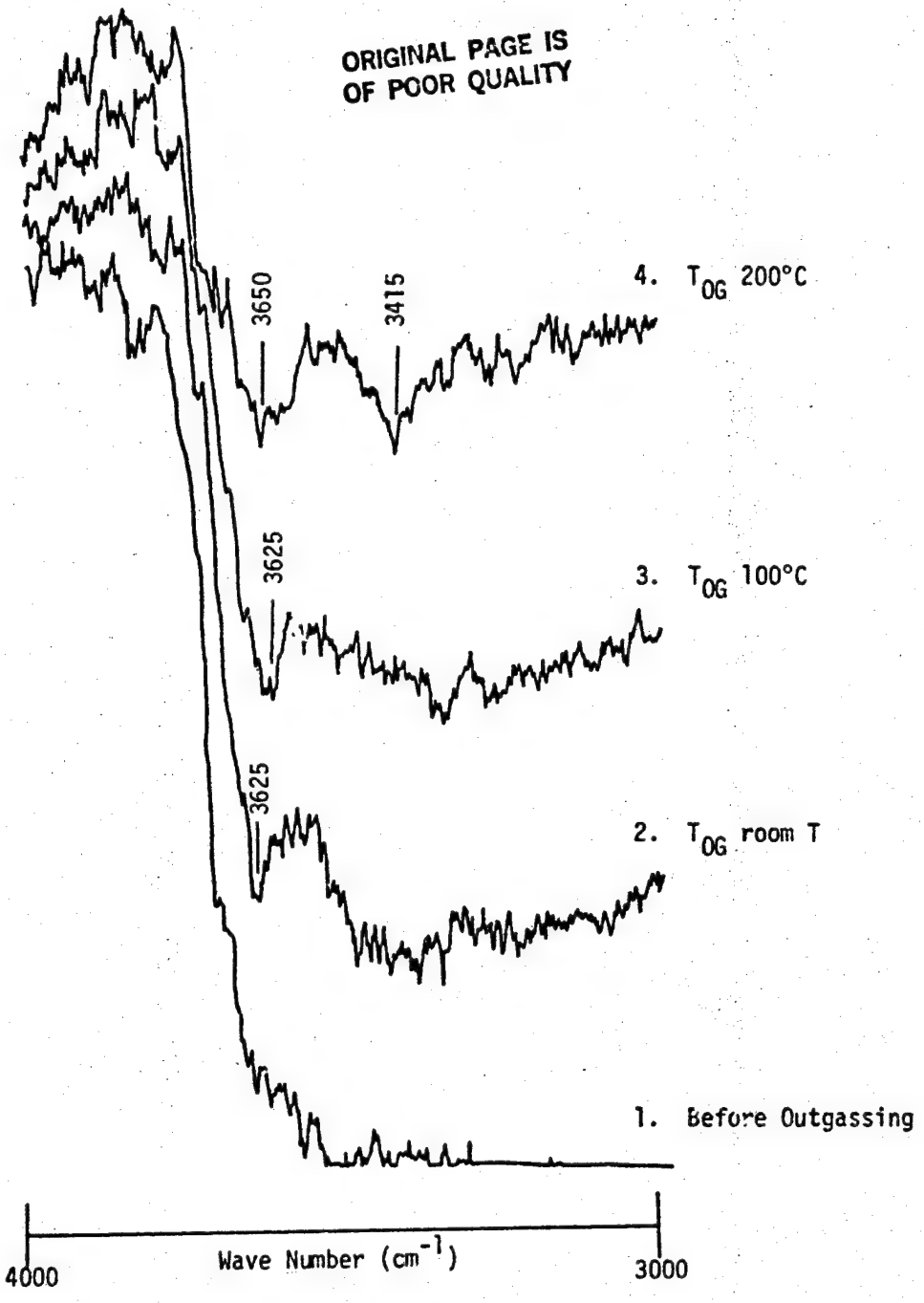

Figure 12. Infrared Spectra (3000-4000 cm^{-1}) of A2 as a Function of Outgassing Temperature

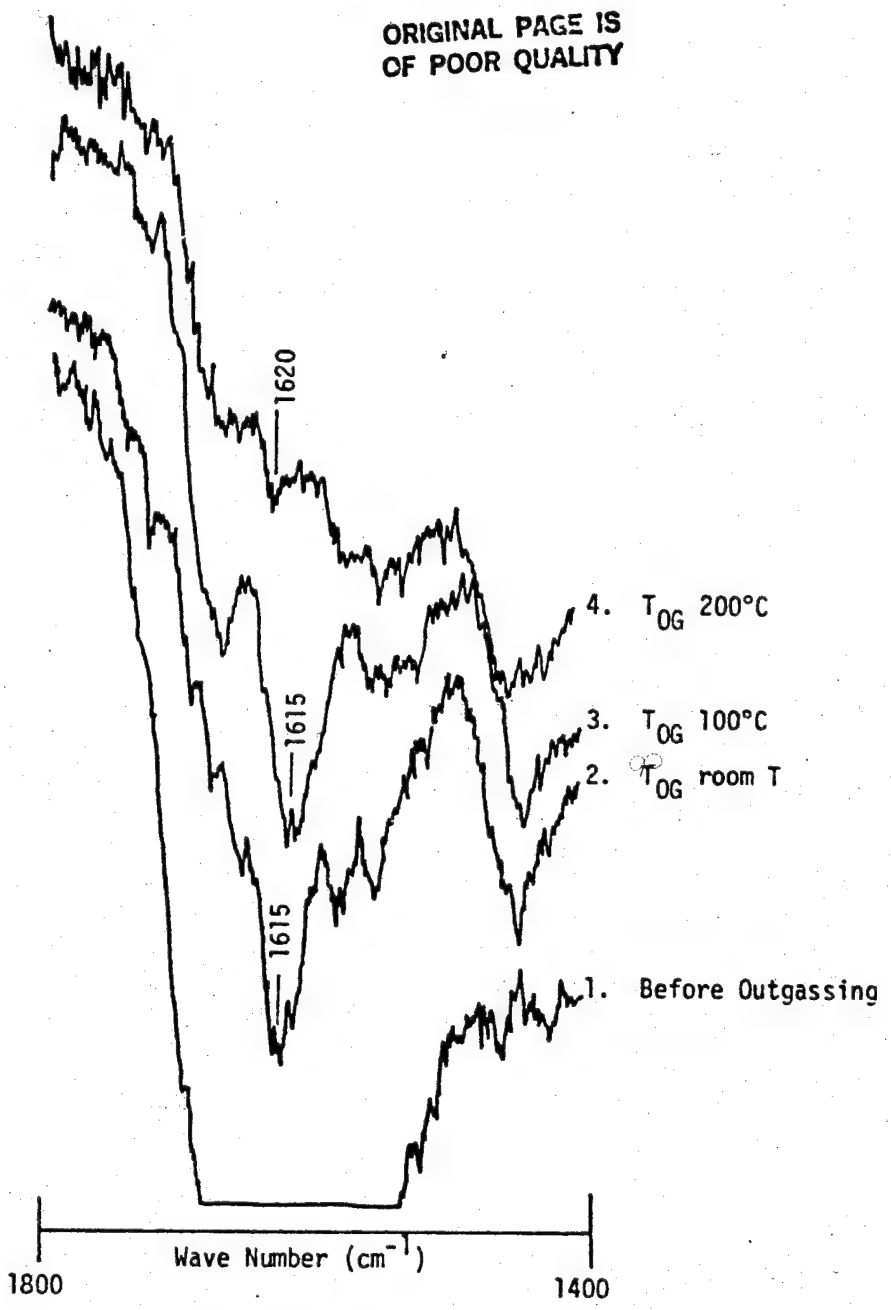

Figure 13. Infrared Spectra (1800-1400) of A2 as a Function of Outgassing Temperature

observed. After evacuation at 100°C, the intensities of all these bands decreased while the positions were not changed. At 200°C, two sharp bands at 3650 cm^{-1} and 3415 cm^{-1} appeared while the intensity of the band at 1620 cm^{-1} decreased. A small band centered at 3720 cm^{-1} was also observed on the sample outgassed at 200°C. The sharpness of these bands at 3650 cm^{-1}, 3415 cm^{-1} and 3720 cm^{-1} indicate that these belong to hydroxyl groups in a well defined structure. It has been observed by Yates (17) that monomeric water has its bending vibration at 1600 cm^{-1}, dimeric water at 1620 cm^{-1}, and polymeric water at 1633 cm^{-1}. The value of 1620 cm^{-1} observed in this study is comparable with the value for bending vibrations of dimeric water. Thus, a small amount of dimeric water was still present on the surface even after evacuation at 200°C.

As shown in Figure 14, the small infrared band at 3720 cm^{-1} on A2 sample outgassed at 200°C is due to a small quantity of isolated hydroxyl groups present on the surface. The infrared band at 3650 cm^{-1} is due to hydrogen bonded hydroxyl groups. The small infrared band at 3415 cm^{-1} may be due either to bridged hydroxyl groups or to water strongly bonded to Ti cations.

Attempts were made to obtain the infrared spectra of A1, R1, R2 and R3 powders. However, transmission was very low due to the large particle sizes of these powders.

B. INTERACTION WITH WATER VAPOR

1. Heats of Immersion in Water

The heats of immersion ($\Delta_w H$) of titania powders as a function of outgassing temperature are shown in Figure 15. Powder A1 showed less

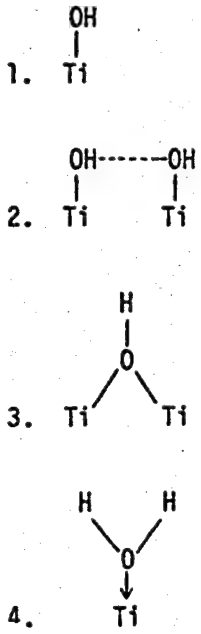

Figure 14. Different Types of Hydroxyl Groups Present on Titania Surfaces

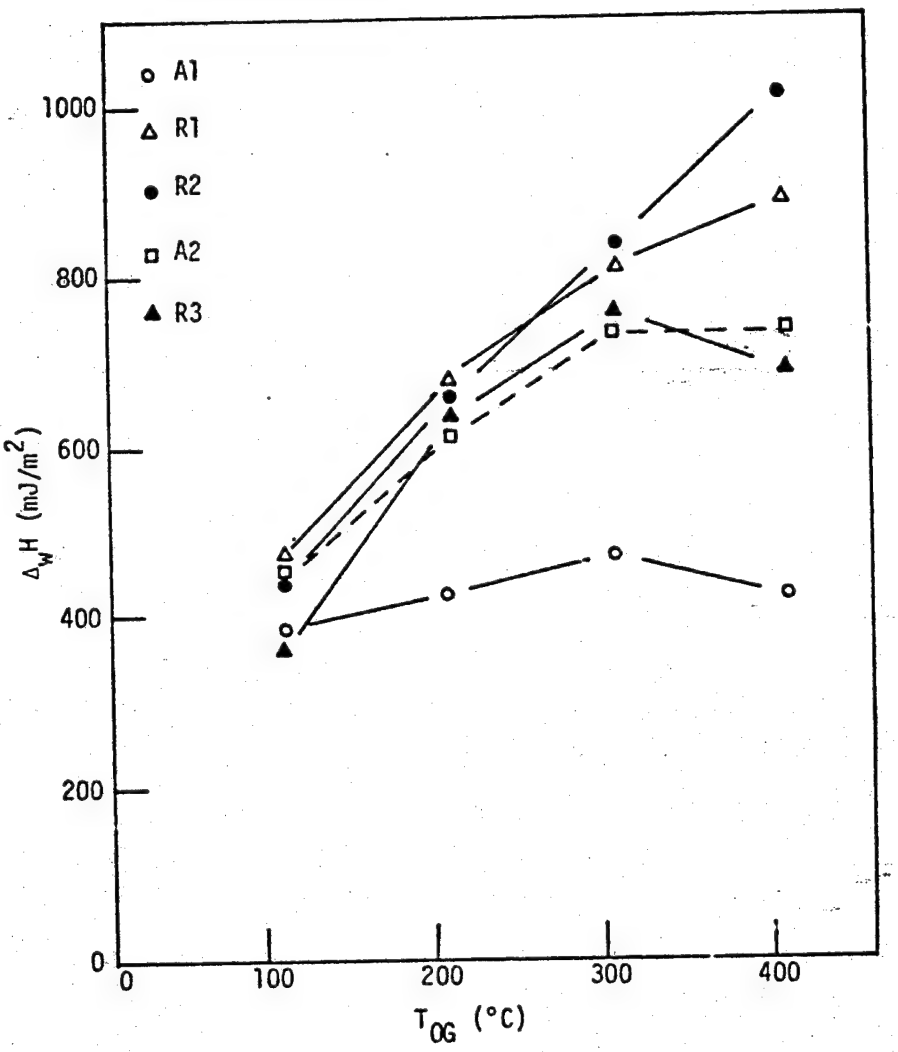

Figure 15. Heats of Immersion of TiO_2 in Water as a Function of Outgassing Temperature

dependence of heat of immersion on outgassing temperature than the other four powders. R3 showed an increase in heat of immersion with increasing outgassing temperature up to 300°C and a decrease at 400°C. Iwaki et al. (29) observed a maximim in heat of immersion around 400°C for rutile samples. Their observation is consistent with the observations made in the present study. A2 which is a mixture of rutile and anatase showed an increase in heat of immersion with increasing outgassing temperatures similar to R3, but it remained constant after 300°C. The rutile samples R1 and R2 which are alumina coated showed marked increase in heat of immersion with increasing outgassing temperature. This increase was more significant for R2 than that for R1. Similar to this observation Herrington and Lui (20) observed an asymptotic increase in heat of immersion with increasing outgassing temperature for alumina coated titania samples.

2. Adsorption of Water Vapor

The adsorption isotherms at 30°C for water vapor on A1 as a function of outgassing temperature are shown in Figure 16. It is clearly seen that the adsorption did not depend on the outgassing temperature. This agrees well with the calorimetric data, in which heat of immersion showed only a minimal dependence on outgassing temperature for A1 powder.

As shown in Figure 17, for A2 powder, there is an increase in adsorption with increasing outgassing temperature up to 300°C, and it remains constant beyond that temperature. Similar behavior was seen with the heat of immersion data.

A different behavior was observed with R3 powder as shown in Figure 18. The adsorption capacity increased up to 300°C outgassing temperature

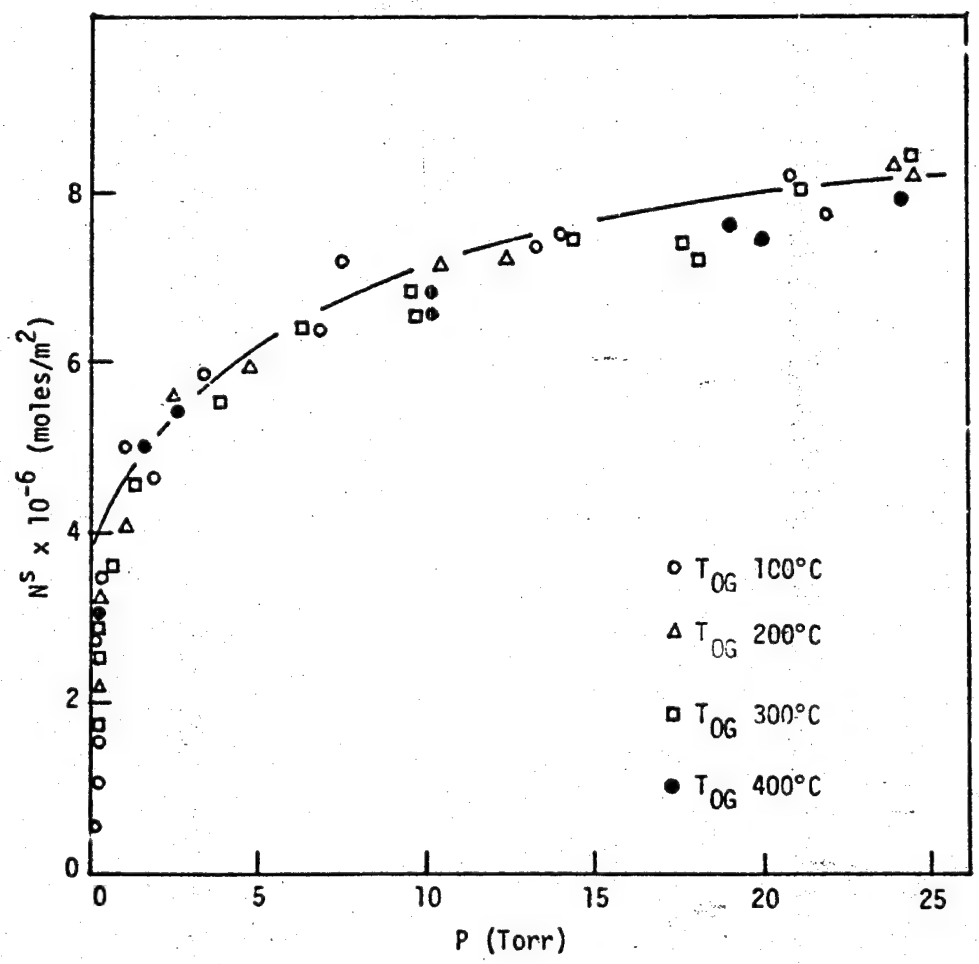

Figure 16. Adsorption Isotherms at 30°C for Water on Al as a Function of Outgassing Temperature

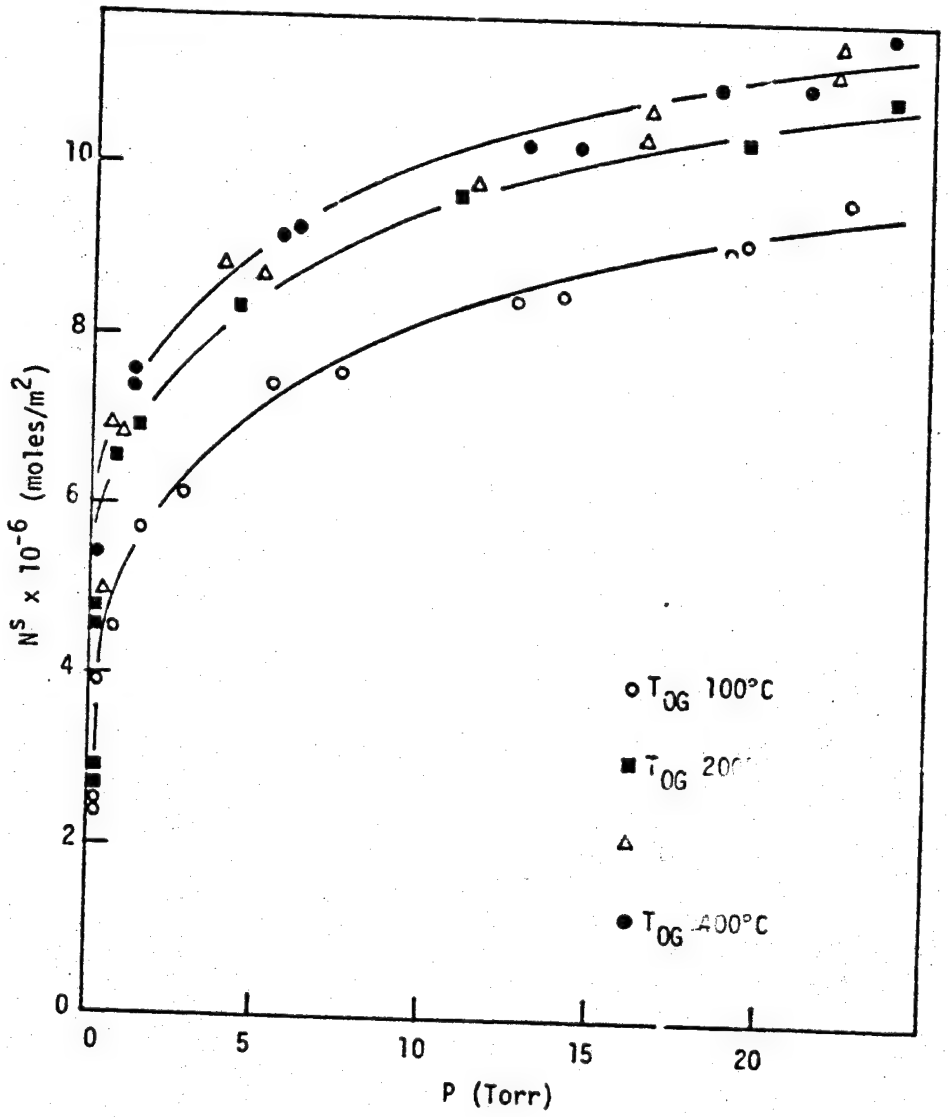

Figure 17 Adsorption Isotherms at 30°C for Water on A2 as a Function of Outgassing Temperature

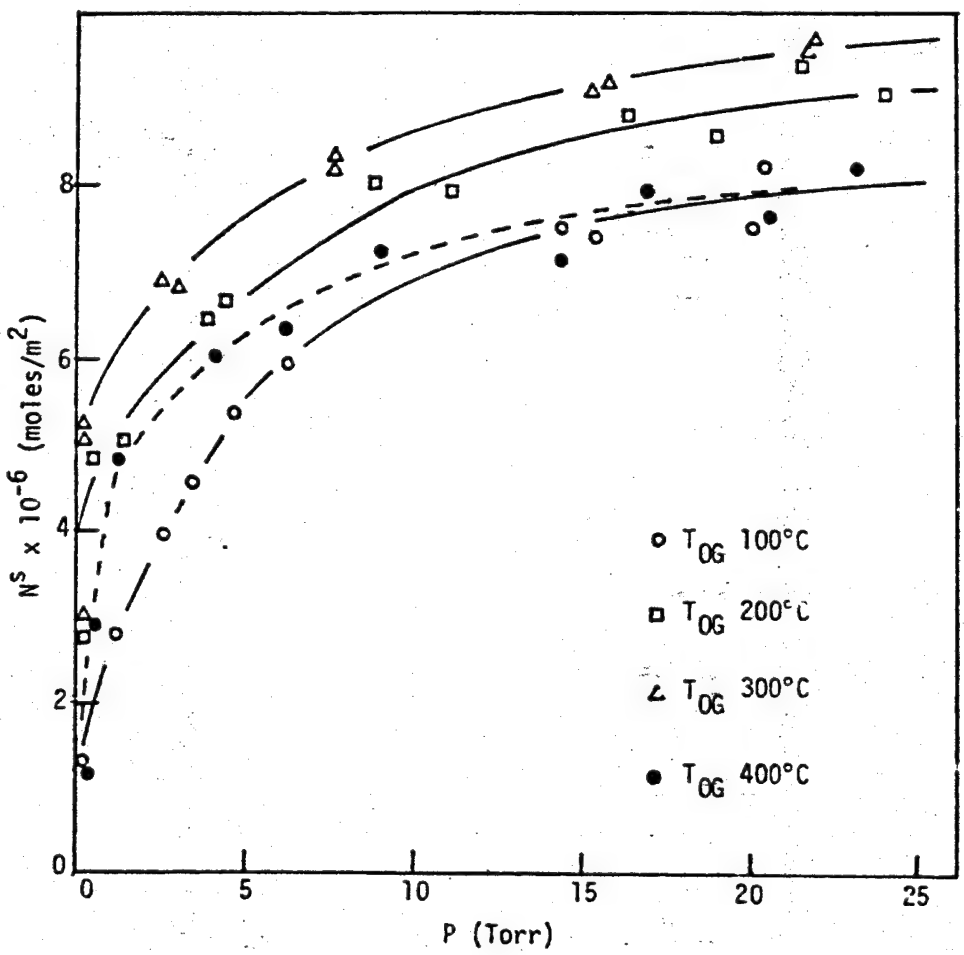

Figure 18. Adsorption Isotherms at 30°C for Water on R3 as a Function of Outgassing Temperature

but there was a marked decrease in adsorption capacity after outgassing at 400°C. Day et al. (19) observed a constant water vapor adsorption after 200°C on rutile contradictory to the observations in the present work. This decrease in adsorption capacity at 400°C for R3 powder paralleled the decrease in heat of immersion, acidity and isoelectric point. The isotherm at 400°C was close to the isotherm at 100°C at high pressure values. A grey color was observed when the R3 sample was outgassed at 400°C indicating the formation of a non-stoichiometric oxide attributed to reduced Ti^{3+} sites. After oxygen treatment the white color characteristic of stoichiometric TiO_2 reappeared. However, the water adsorption isotherm for the oxygen treated sample was similar to that of the untreated sample. The re-adsorption isotherms were similar to the original adsorption isotherms indicating that water adsorption was completely reversible. Thus, the adsorption of water at 30°C is a physisorption process on titania powders outgassed over the temperature range 100-400°C.

It is clear from both the calorimetric and isotherm data that powders A1, A2 and R3 have different surface characteristics. It is interesting to note that the calorimetric data are consistent with the adsorption data. It is also possible to relate the adsorption behavior to the surface composition. The presence of phosphorus was found on A1 powder by ESCA analysis. It has been found by Munuera (26) using temperature programmed desorption studies that $H_2PO_4^-$ containing anatase surface had a low number of adsorbed water molecules. Strongly basic anions such as $H_2PO_4^-$ which have a short oxygen-oxygen distance are

preferentially adsorbed on the surface displacing water molecules as shown in reaction [16].

$$H_2PO_4^-(sol) + H_2O(ads) \rightleftharpoons H_2O(sol) + H_2PO_4^-(ads) \qquad [16]$$

Thus, the presence of phosphorus may be the reason for the low water adsorption capacity. Previous workers (32) showed that the surface of anatase dried at 140°C possessed only one monolayer of water whereas rutile possessed six monolayers of water after the same pretreatment. This is also in agreement with the lower water adsorptive capacity of anatase observed in the present study.

The presence of different kinds of hydroxyl groups was observed with infrared spectroscopy for A2 sample. With increasing outgassing temperatures, the mean kinetic energy of adsorbed hydroxyl groups is increased, and the groups are successively desorbed. Weakly bound hydroxyl groups are removed first while the strongly bound ones are removed at higher temperatures. By exposure to water molecules, these hydroxyl groups are reformed. This explains the reason for the increase in water adsorption capacity for both A2 and R3 powders with increasing outgassing temperatures. The condensation of hydroxyl groups may be occurring at the final stages of dehydroxylation by the following mechanism:

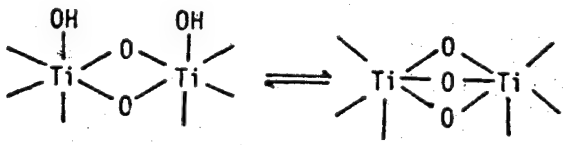

[17]

This reaction was found to be reversible or irreversible depending on the predominantly exposed crystal plane. For instance, in previous work well

calcined rutile samples with the (110) plane as the predominant plane showed irreversibility in the above reaction (18). Thus, instead of formation of two hydroxyl groups only one molecule of water would be coordinatively bound to the surface by exposure to water molecules as shown in reaction [18].

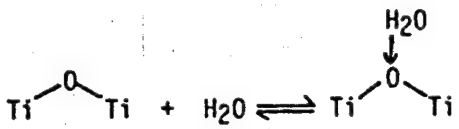

[18]

This would decrease the water vapor adsorption capacity significantly. This irreversible condensation of hydroxyl groups for R3 outgassed at 400°C explains the decrease in heat of immersion and adsorption capacity. These hydroxyl groups are acidic and positively charged at room temperature. Since these hydroxyl groups are removed at 400°C, there was a decrease in acidity and isoelectric point.

The water vapor adsorption isotherms for R1 and R2 powders which are alumina coated are shown in Figures 19 and 20. As shown in these two figures adsorption capacity was strongly dependent on the outgassing temperature. This was more pronounced for the R2 powder. These results are again consistent with the calorimetric data obtained in the present study. This increase in water content is due to the larger number of hydroxyl groups present on the aluminum coating (9) as shown in the following proposed structure [19].

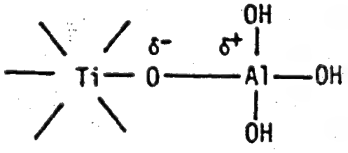

[19]

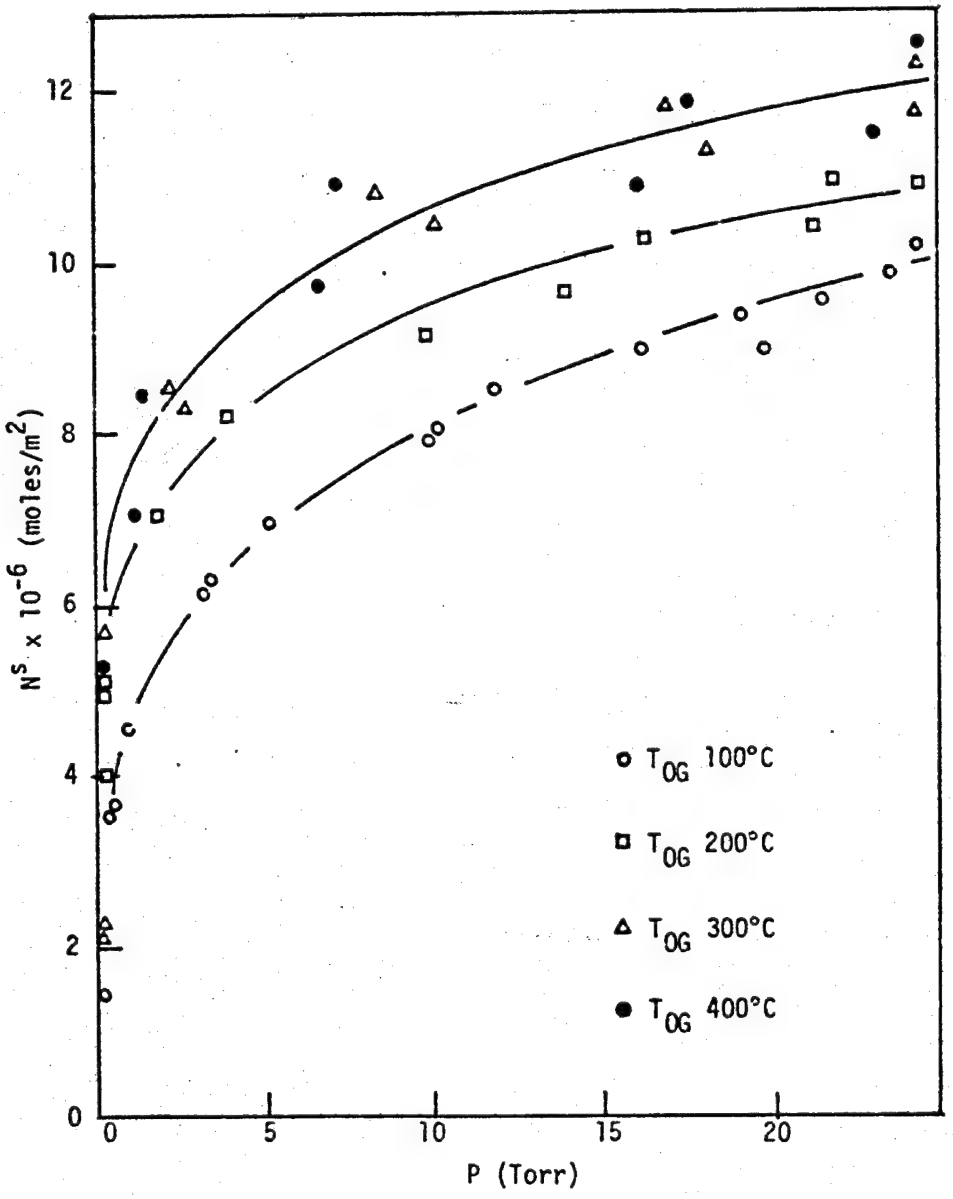

Figure 19. Adsorption Isotherms at 30°C for Water on R1 as a Function of Outgassing Temperature

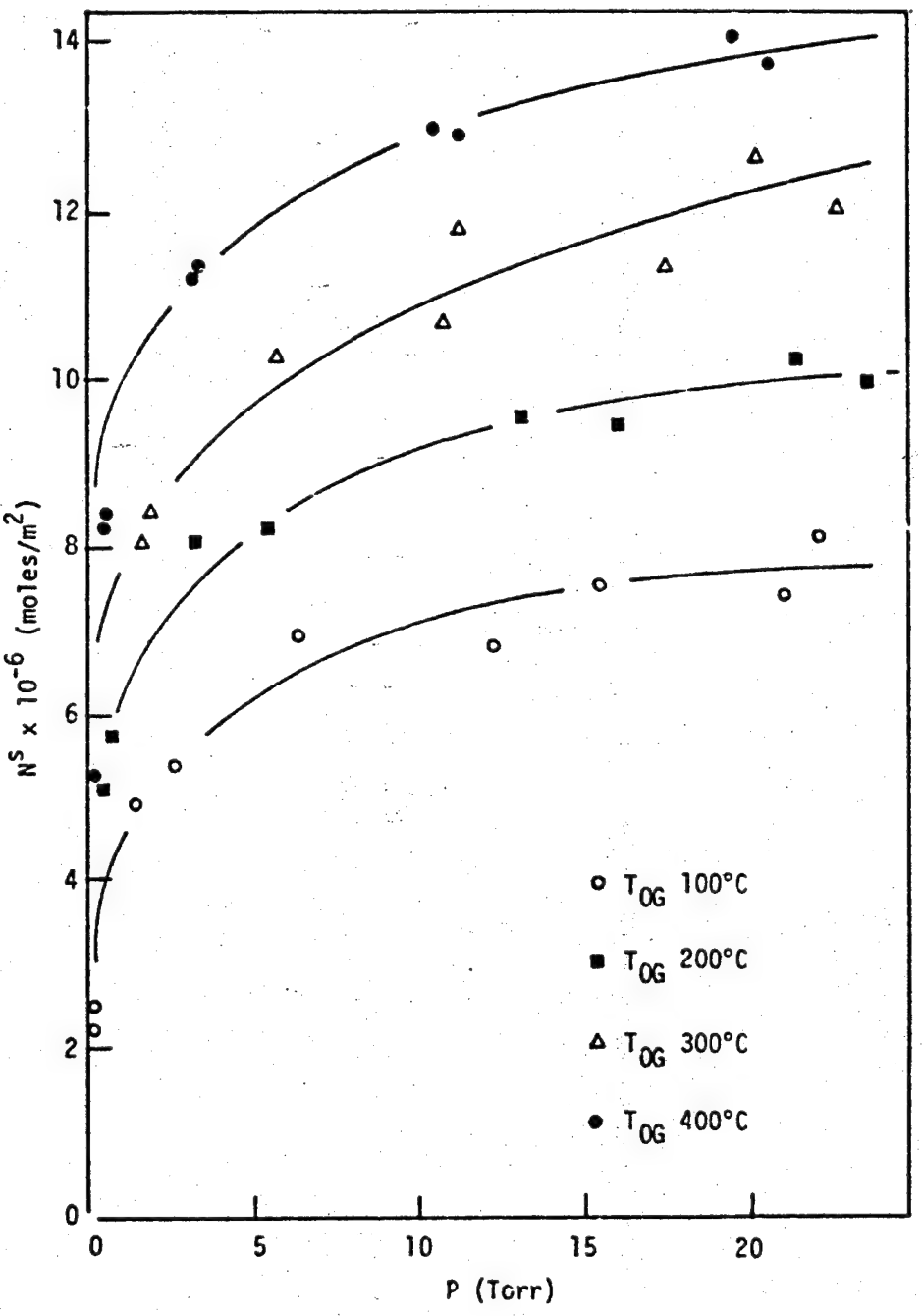

Figure 20. Adsorption Isotherms at 30°C for Water on R2 as a Function of Outgassing Temperature

The calculated monolayer coverages V_m and cross sectional areas (σ) of adsorbed water molecules based on nitrogen surface areas on the five titania powders are given in Table V. The water surface areas (S_{H_2O}) were calculated from the water adsorption data assuming the cross sectional area of water molecule to be 10.8 A^2/molecule. The water surface areas and ratios of water area to nitrogen area (S_{N_2}) are also given in Table V.

3. Infrared Analysis after Water Adsorption

Infrared spectra of the A2 surface after water adsorption is shown in Figures 21 and 22. An outgassing temperature of 200°C was chosen for the study because the peaks corresponding to hydroxyl groups were clearly seen at 200°C. After exposure to water vapor, a broad band in the region 3800 to 3000 cm^{-1} and a band at 1610 cm^{-1} appeared. After reevacuation at 200°C, the original peaks present on the sample outgassed at 200°C, reappeared on the surface. This gave further evidence for the reversibility of the water adsorption process.

4. Variation in Temperature

The adsorption isotherms measured at 30°, 40° and 50°C for A1 powder evacuated at 100° and 400°C are shown in Figures 23 and 24. A strong temperature dependence was observed for adsorption at both outgassing temperatures. The adsorption capacity decreased when the temperature was increased from 30°C to 50°C. At higher isotherm temperatures the kinetic energy of the adsorbed molecules increases and the equilibrium shifts to the gaseous phase. Since three variables are

TABLE V

MONOLAYER COVERAGES OF WATER AND CROSS SECTIONAL AREAS OF ADSORBED WATER, WATER SURFACE AREAS, AND RATIO OF WATER TO NITROGEN SURFACE AREAS OF TITANIA POWDERS

	T_{OG} 100°C					T_{OG} 200°C				
	A1	A2	R1	R2	R3	A1	A2	R1	R2	R3
$V_M \times 10^{-8}$ (Mol/m^2)	519	597	537	410	597	483	660	627	531	594
S_{H_2O} (m^2/g)	3.2	18.5	2.4	1.7	8.5	2.9	20.4	2.8	2.2	8.5
S_{H_2O}/S_{N_2}	0.34	0.39	0.35	0.27	0.39	0.31	0.43	0.41	0.35	0.39
σ ($\AA^2$/mol)	31.9	27.8	30.9	40.4	27.8	34.4	25.2	26.5	31.3	27.9

	T_{OG} 300°C					T_{OG} 400°C				
	A1	A2	R1	R2	R3	A1	A2	R1	R2	R3
$V_M \times 10^{-8}$ (Mol/m^2)	485	824	732	714	637	460	760	816	811	520
S_{H_2O} (m^2/g)	2.9	25.2	3.3	2.9	9.0	2.7	23.3	3.6	3.4	7.4
S_{H_2O}/S_{N_2}	0.32	0.53	0.48	0.46	0.41	0.30	0.49	0.53	0.53	0.34
σ ($\AA^2$/mol)	34.2	20.2	22.7	23.3	26.1	36.1	21.9	20.4	20.5	31.9

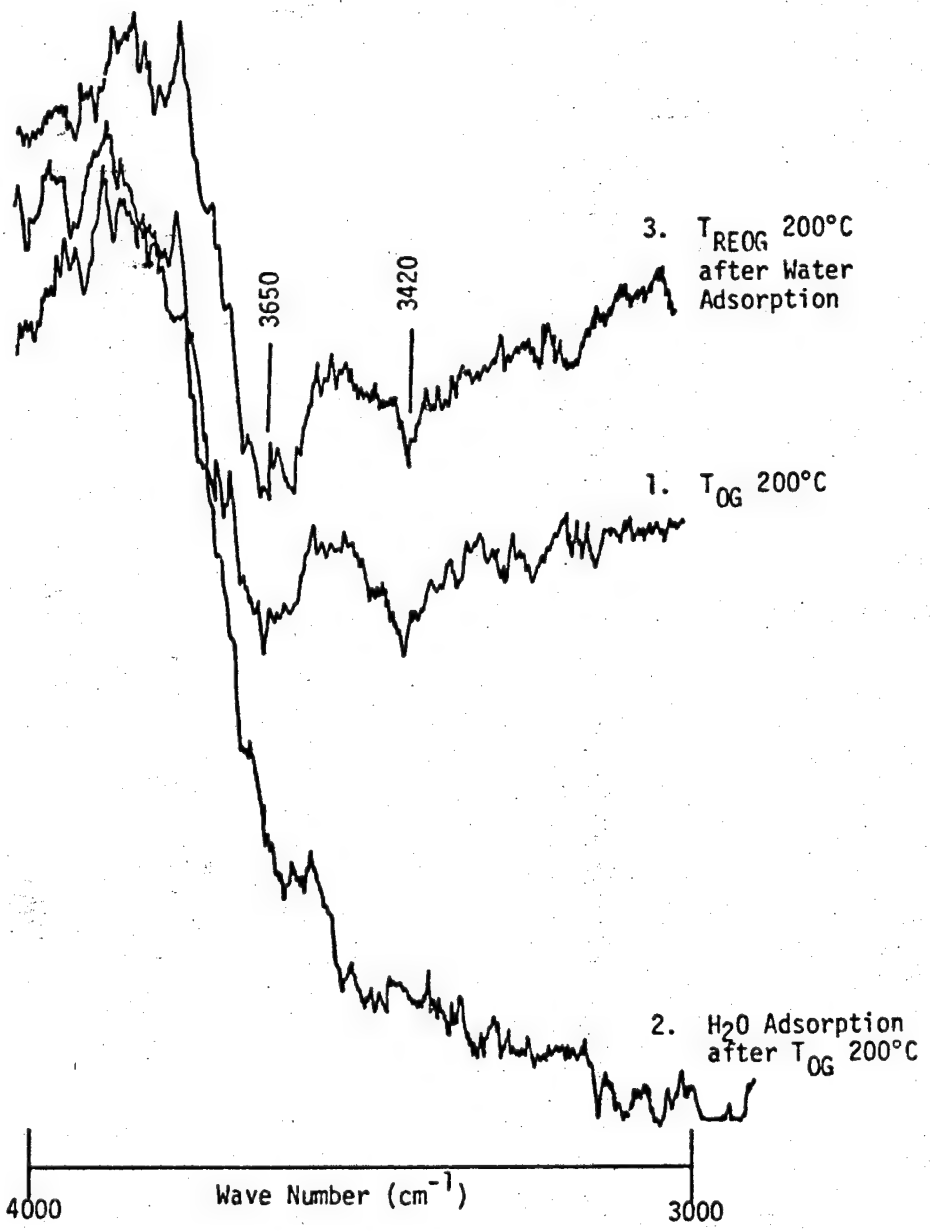

Figure 21. Infrared Spectra (3000-4000 cm^{-1}) of A2 after Water Vapor Adsorption

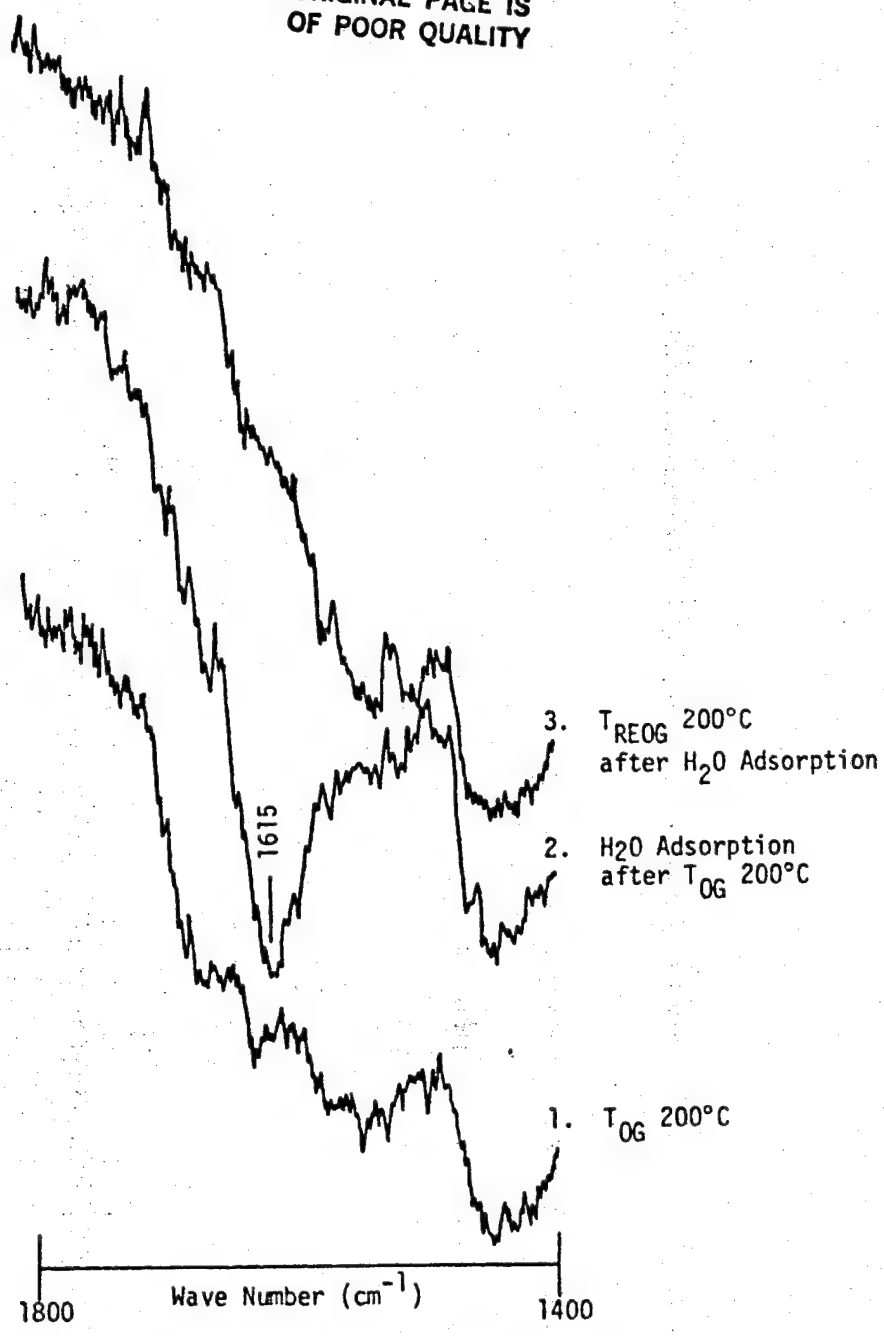

Figure 22. Infrared Spectra (1400-1800 cm^{-1}) of A2 after Water Vapor Adsorption

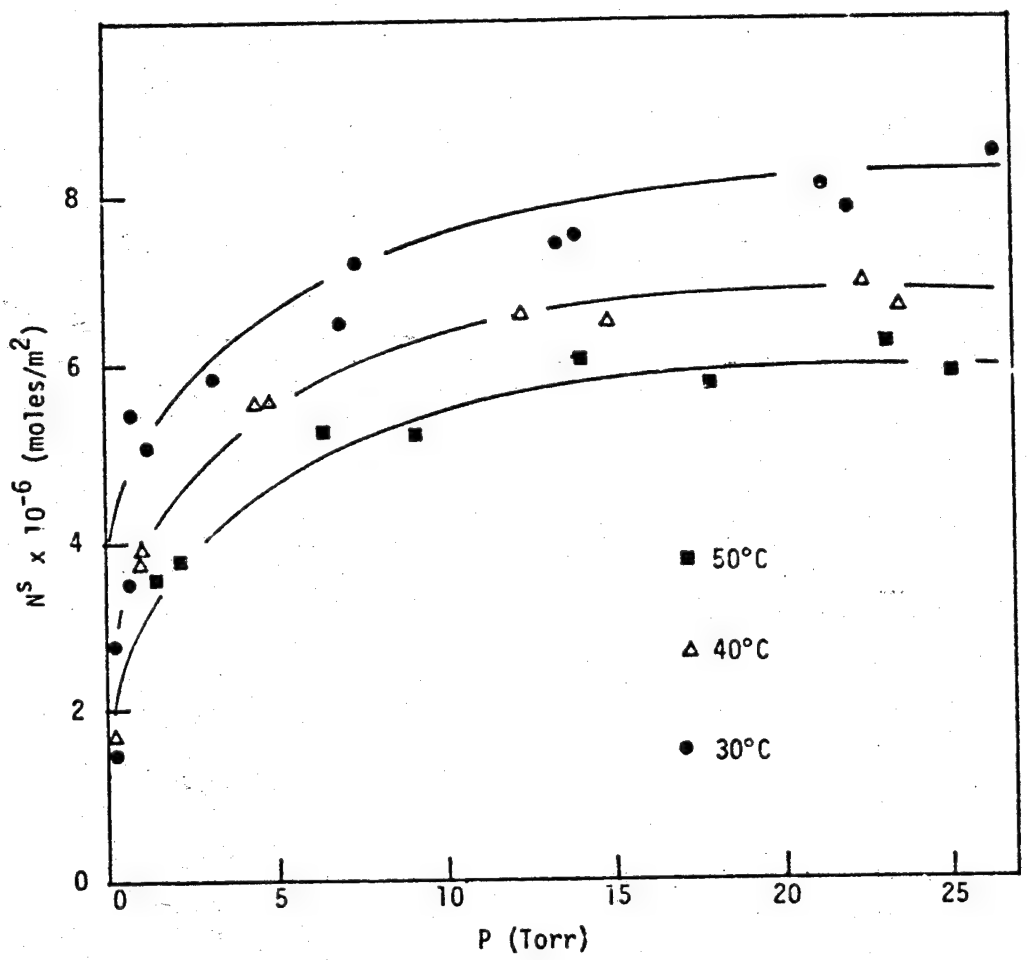

Figure 23. Temperature Dependence on Water Adsorption Isotherms of Al Outgassed at 100°C

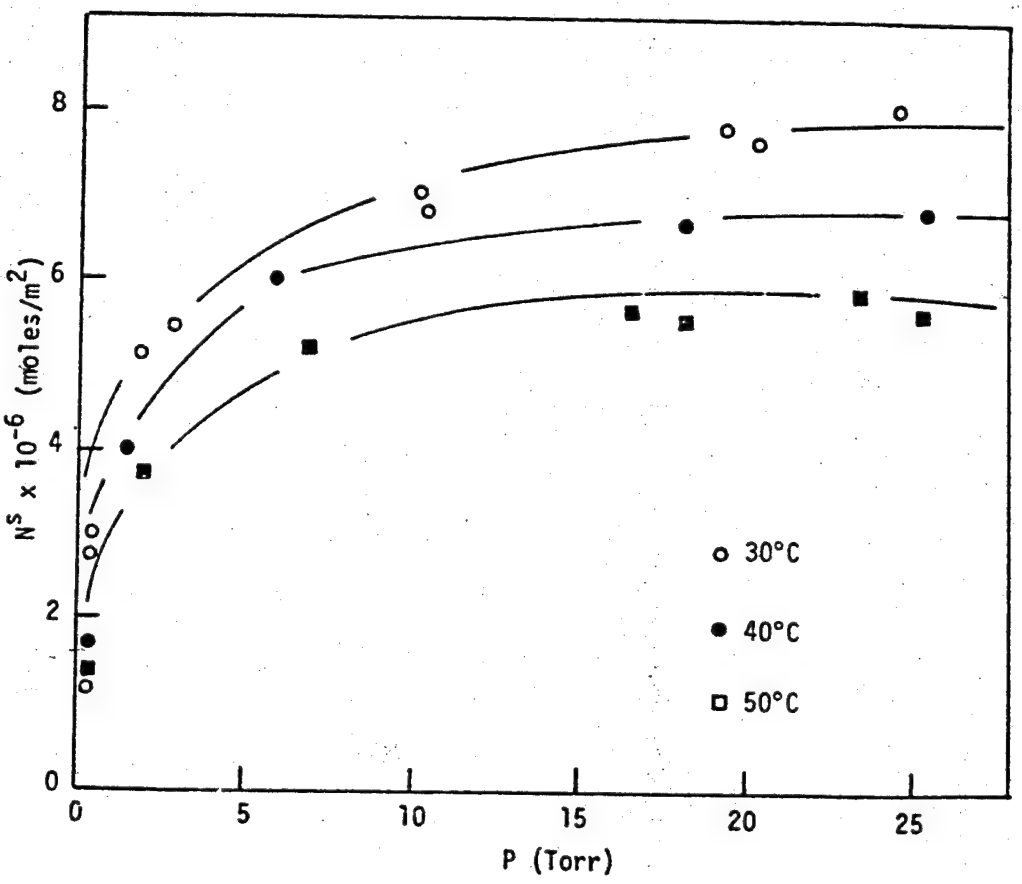

Figure 24. Temperature Dependence on Water Adsorption Isotherms of Al Outgassed at 400°C

available, a three dimensional picture can be drawn using P, n, and T axes as shown in Figure 25. The plane of the adsorption is clearly seen. The lines corresponding to constant pressure values and constant n values are also drawn on the plane.

The adsorption isotherms at 30°, 40° and 50°C for A2 and R1 powders outgassed at 100°, 200° and 400°C are shown in Figures 26-29. The adsorption isotherms at 30°, 40° and 50°C for R3 outgassed at 100°, 200° and 300°C are shown in Figures 30 and 31, respectively. All the adsorption isotherms were strongly dependent on temperature.

The isosteric heats of adsorption were calculated using equation [14] and the isotherms at 30°, 40° and 50°C. The isotherm data were curve fitted using a computer program, and plots obtained from the computer analysis are given in Appendix II. The isosteric heats of adsorption for A1 outgassed at 100° and 400°C, and for A2 outgassed at 100°C and R3 outgassed at 100°C are shown as a function of surface coverage in Figure 32. There is a decrease in the isosteric heat of adsorption with increasing coverage in all four cases. This indicates the heterogeneous nature of the titania samples. A1 sample outgassed at 100°C showed a very low isosteric heat of adsorption of 42 kJ/mole after adsorption of 50 x 10^{-8} moles/m^2 which is close to the heat of liquifaction of water of 44.1 kJ/mole. After outgassing at 400°C, this value increased to 60 kJ $mole^{-1}$. The isosteric heat of adsorption of A1 outgassed at 400°C approached the value corresponding to the heat of liquifaction of water before the completion of a monolayer. A high isosteric heat of adsorption, close to 80 kJ $mole^{-1}$, was found for both

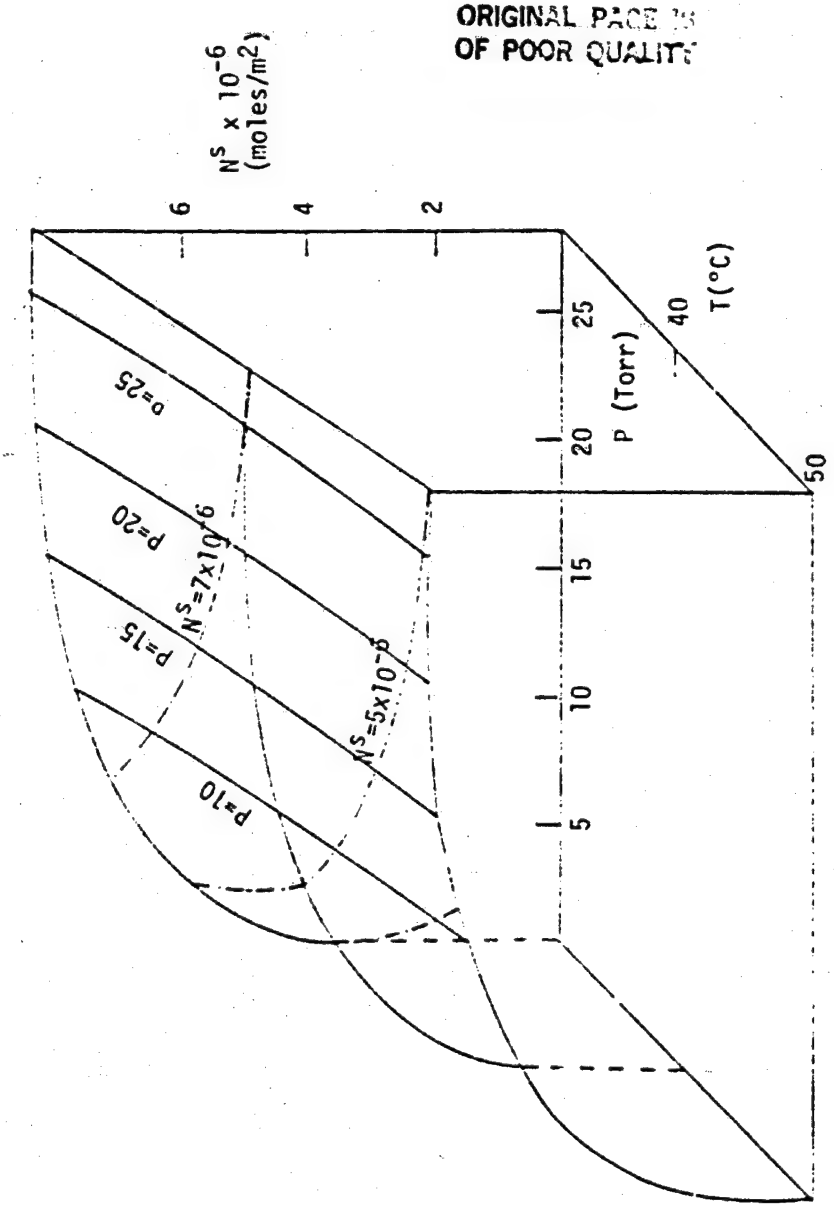

Figure 25. Three Dimensional Plot for Adsorption of Water on Al Outgassed at 100°C

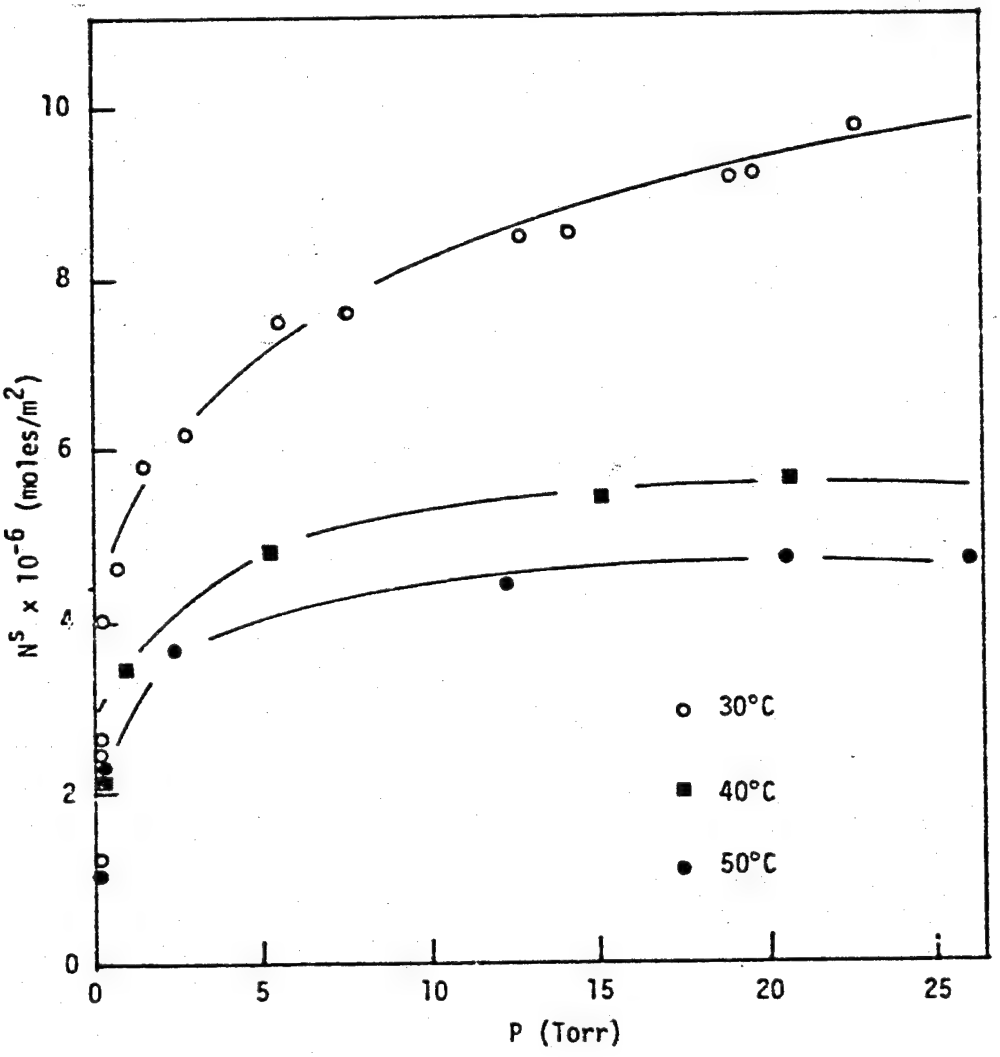

Figure 26. Temperature Dependence on Water Adsorption Isotherms of A2 Outgassed at 100°C

C-2

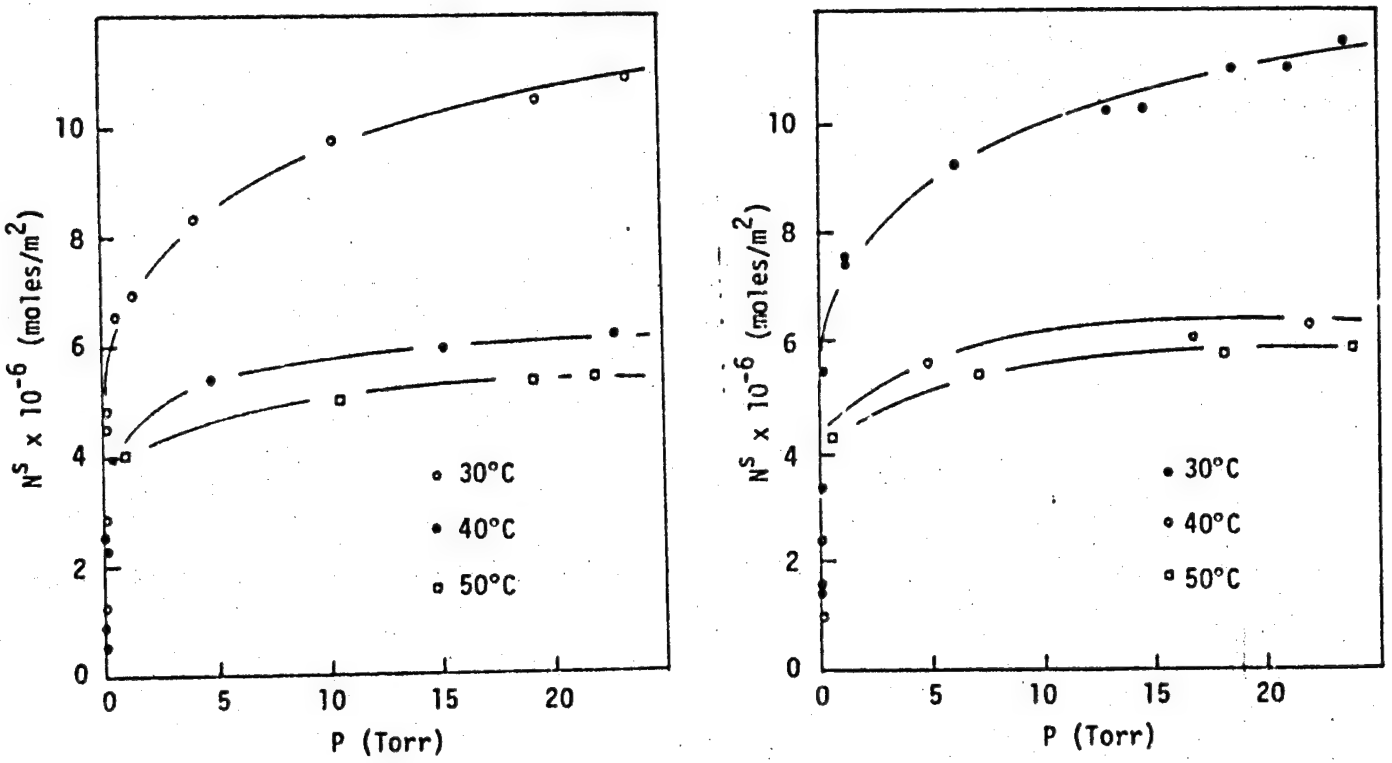

Figure 27. Temperature Dependence on Water Adsorption Isotherms of A2 (a) Outgassed at 200°C, (b) Outgassed at 400°C

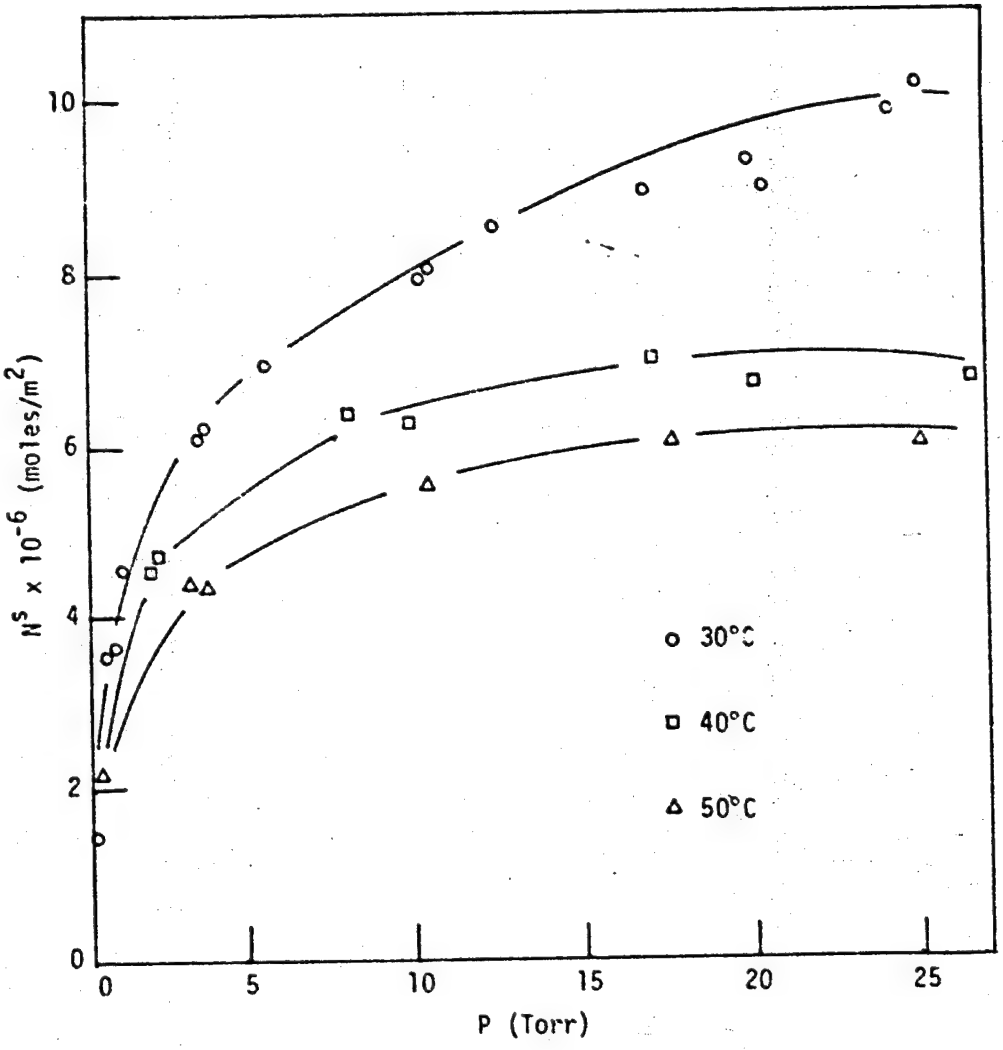

Figure 28. Temperature Dependence on Water Adsorption Isotherms of R1 Outgassed at 100°C

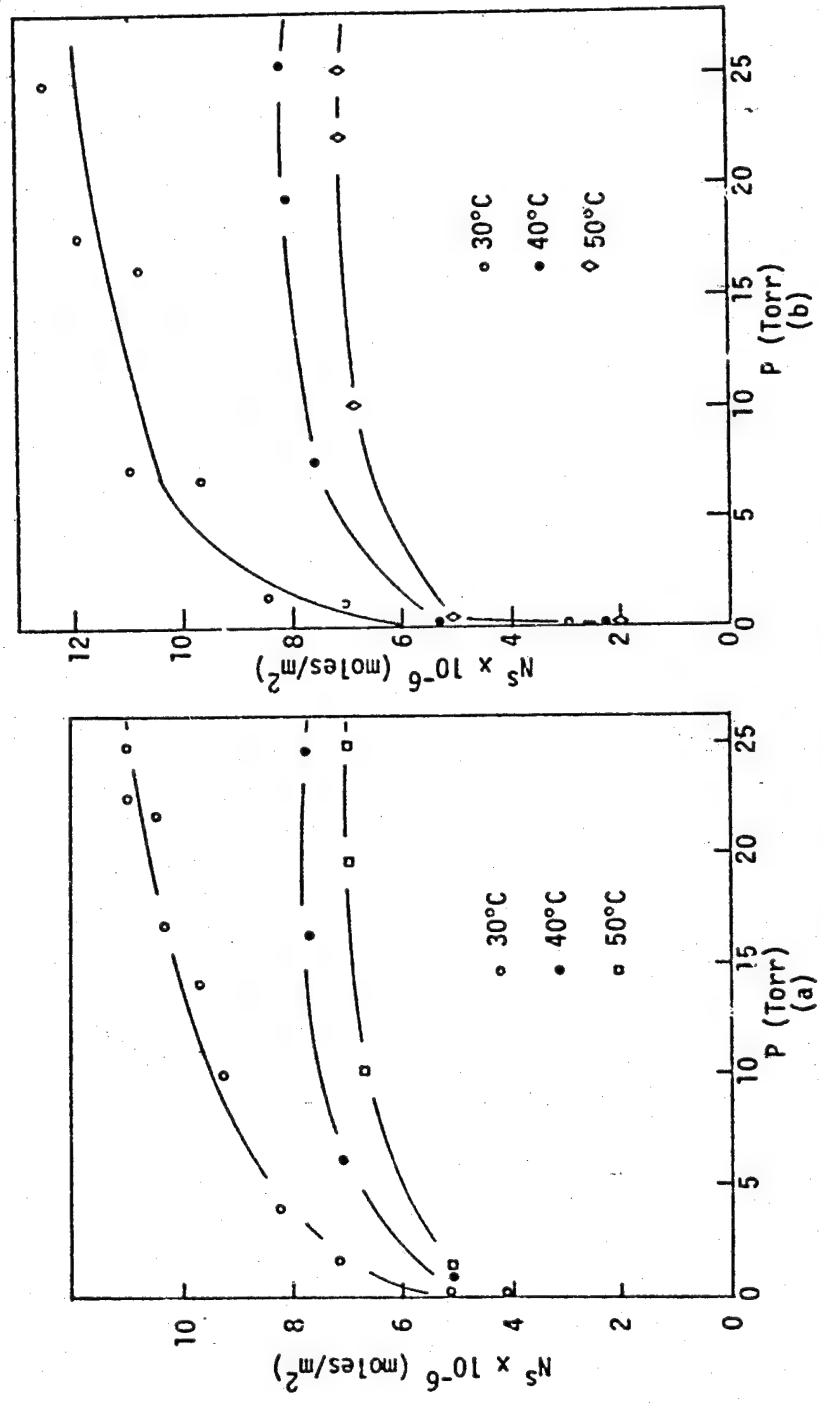

Figure 29. Temperature Dependence on Water Adsorption Isotherms of RI
(a) Outgassed at 200°C, (b) Outgassed at 400°C

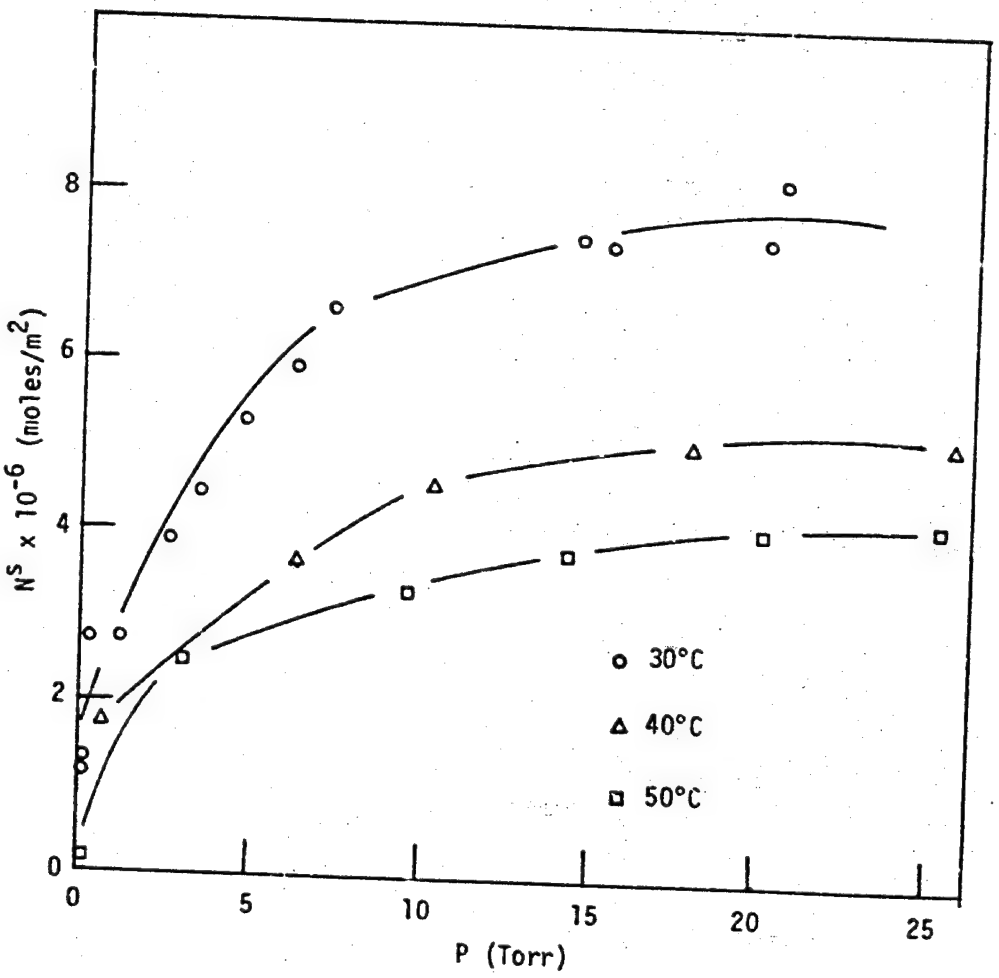

Figure 30. Temperature Dependence on Water Adsorption Isotherms of R3 Outgassed at 100°C

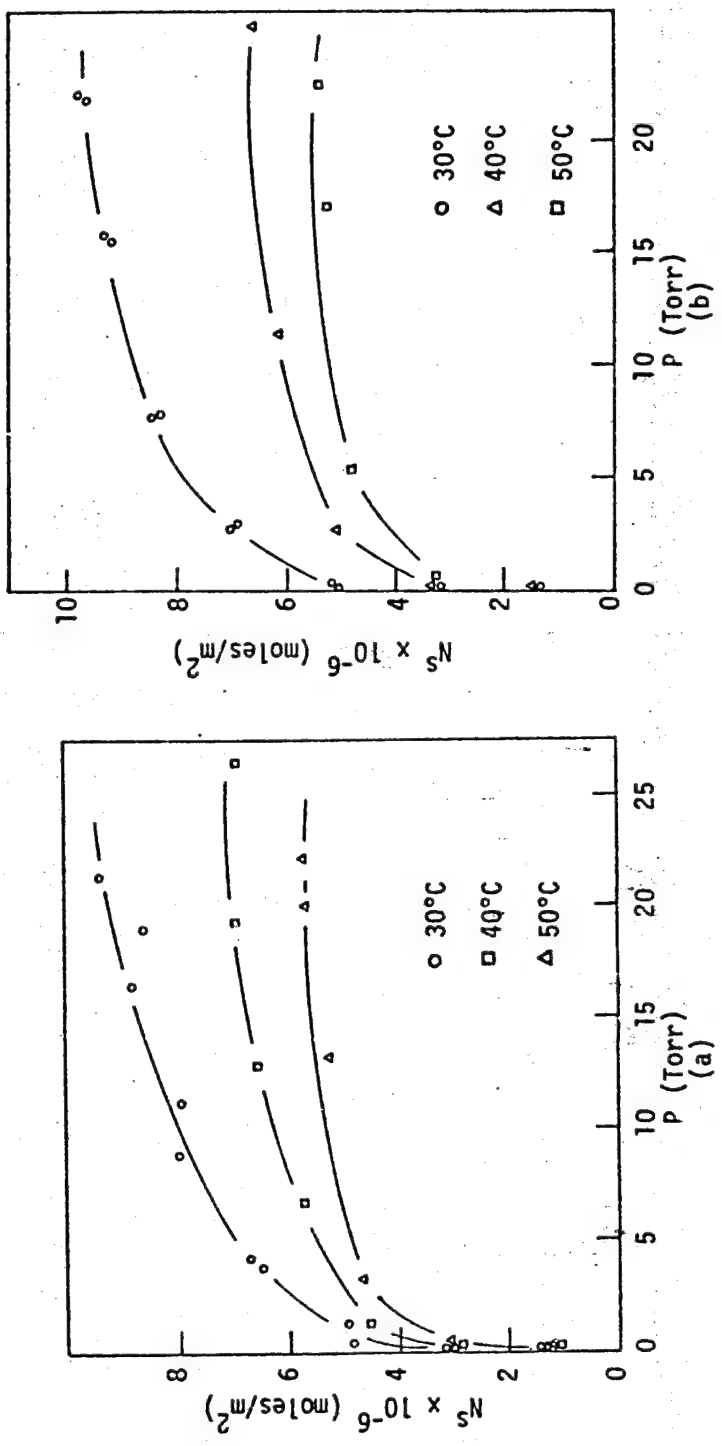

Figure 31. Temperature Dependence on Water Adsorption Isotherms of R3
(a) Outgassed at 200°C, (b) Outgassed at 300°C

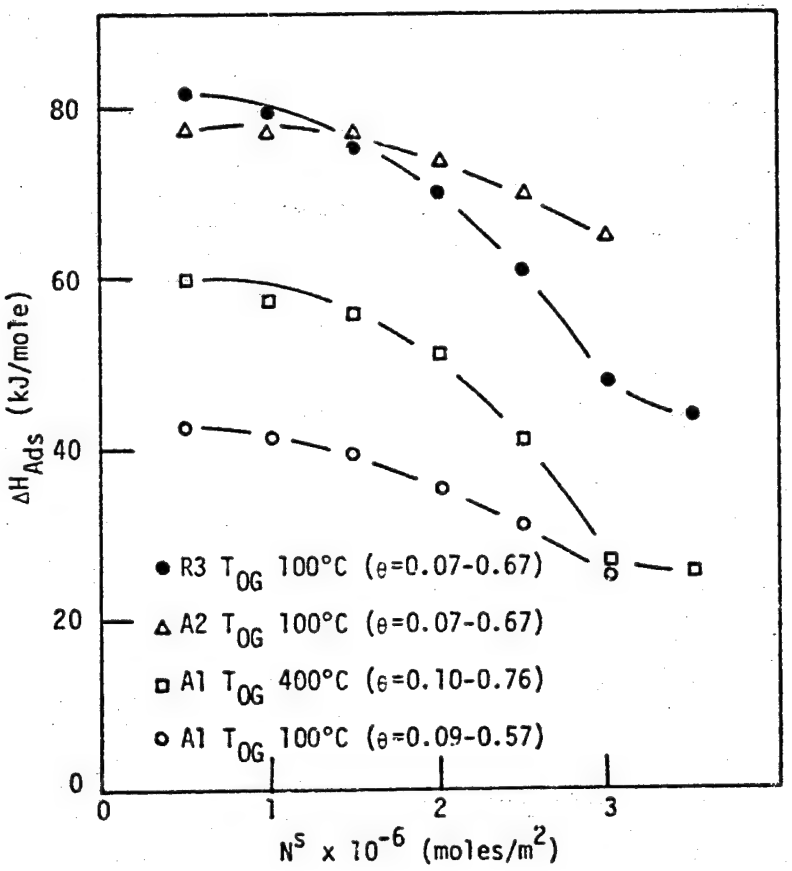

Figure 32. Isosteric Heats of Adsorption for Water on TiO_2 as a Function of Water Coverage

R3 and A2 powders outgassed at 100°C at a capacity of 50 x 10^{-8} moles/m^2. Jones and Hockey (28) estimated the heats of adsorption involved in the process of hydrogen bond formation between adsorbed water and surface hydroxyl groups to be 70-80 kJ $mole^{-1}$ based on the infrared data. This value is comparable with the isosteric heat values obtained for R3 and A2 powders outgassed at 100°C in the present study. Therefore, the major mechanism of rehydroxylation on R3 and A2 powders outgassed at 100°C is the formation of hydrogen bonds between water and hydroxyl groups.

Attempts were made to calculate the isosteric heats for R1, R3 and A2 at higher outgassing temperatures. Since the pressure values were very low for the isotherm at 30°C, a large scatter of the data points was observed. Due to these uncertainties in the low pressure values, the calculation of the isosteric heats of adsorption was not considered meaningful.

Since anatase gave low isosteric heats of adsorption, the behavior of its surface was further investigated by measuring heats of immersion as a function of surface coverage of water. The results are shown in Figure 33. There was a steady decrease in $\Delta_w H$ with increasing coverage, and it approached a value of 118 mJ/m^2 which is close to the surface enthalpy of liquid water, at a coverage (θ) of about 1.45. Thus, the adsorbed water on anatase is liquid-like on the surface. Using these data integral heats of adsorption were calculated and the values are listed in Table VI. A decrease in integral heats of adsorption with increasing coverage was observed.

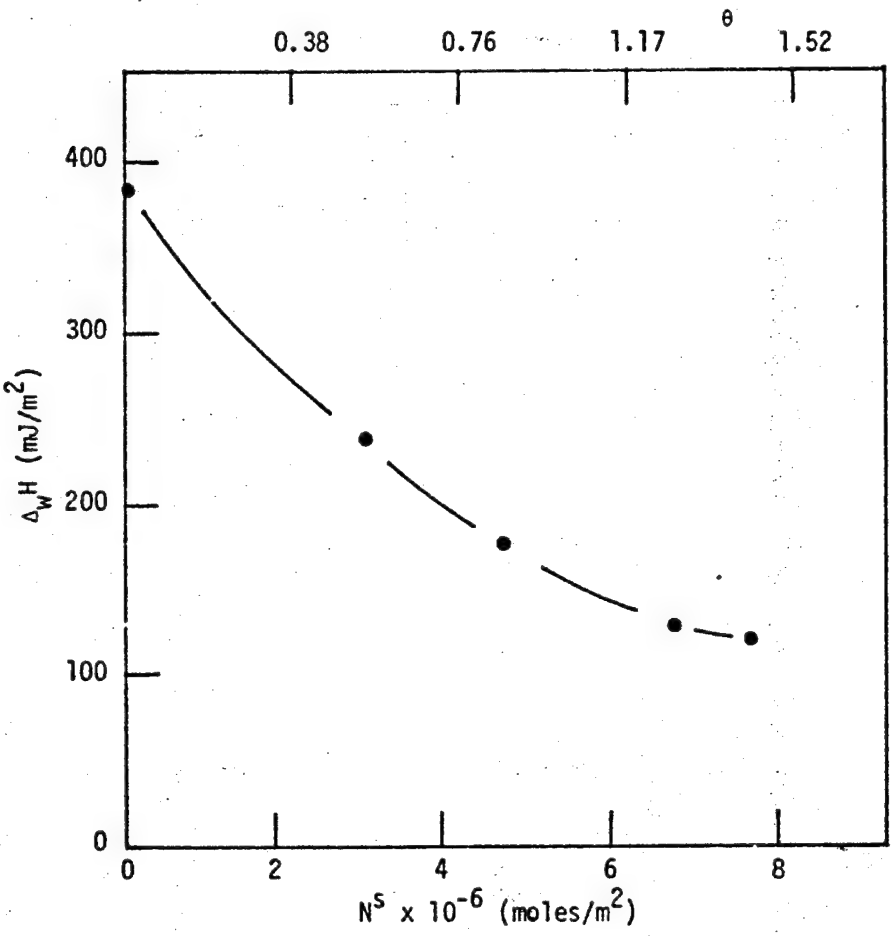

Figure 33. Heats of Immersion in Water of Al Outgassed at 100°C as a Function of Water Coverage

TABLE VI

INTEGRAL HEATS OF ADSORPTION OF Al OUTGASSED AT 100°C

Capacity (moles/m^2 x 10^{-8})	Integral heats of adsorption (kJ/mol)
280	92.7
455	86.8
650	81.1
740	77.4

C. INTERACTION WITH HCl

1. Heats of Immersion

Heats of immersion ($\Delta_w H$) of the five titania powders in 0.1N $HCl_{(aq)}$ and water at four outgassing temperatures are shown in Figure 34; the vertical lines indicate the increase in $\Delta_w H$ in $HCl_{(aq)}$ compared to that in water. All powders showed higher heats of immersion in $HCl_{(aq)}$ than in water. This shows that all the powders interact preferentially with $HCl_{(aq)}$. However, a very large increase in $\Delta_w H$ was observed for R1 and R2 powders. This heat was released over a 9 hour period. This high heat of immersion indicates that the reaction of $HCl_{(aq)}$ with R1 and R2 is very strong. Similar behavior has been observed by Bailey and Wightman (101) with pure alumina samples. However, the heats of immersion of titania in $HCl_{(aq)}$ have not been reported previously. In this study, the ESCA analysis indicated that an alumina coating was present on both R1 and R2 samples. Therefore, it is possible that there is partial dissolution of this alumina coating in $HCl_{(aq)}$. To further investigate the dissolution process, the HCl solutions after the immersion process were analyzed by atomic absorption spectroscopy. A large amount of aluminum was detected in the solution. ESCA analysis of the TiO_2 powder, after immersion in $HCl_{(aq)}$, showed a decrease in the Al/Ti atomic ratio but chlorine was not detected on the surface. All the above information provides evidence for the dissolution of alumina coating in HCl. The chemical reaction involved in dissolution can be expressed as

$$Al_2O_{3(s)} + 6\ HCl_{(aq)} \rightarrow 2\ Al^{+3}_{(aq)} + 6\ Cl^- + 3\ H_2O \qquad [20]$$

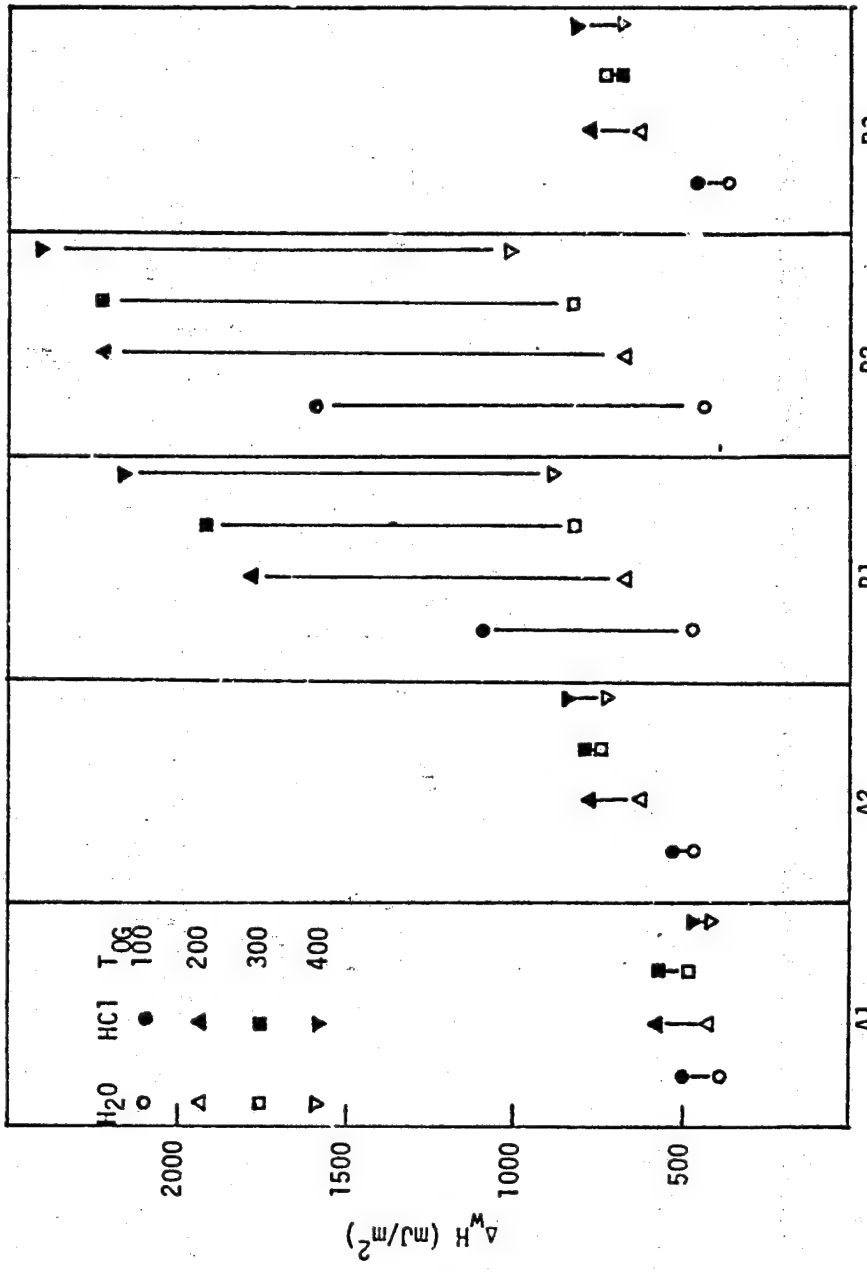

Figure 34. Heats of Immersion of TiO_2 in 0.1N $HCl_{(aq)}$ and Water

2. Adsorption and Readsorption Isotherms

Adsorption of HCl at different outgassing temperatures for A1 is shown in Figure 35. There is a small increase in adsorption with increasing outgassing temperature. This may be due to the progressive removal of adsorbed water molecules with increased outgassing temperature from reaction sites, facilitating the reaction with HCl. Reversibility of the adsorption process was determined by the readsorption isotherms. The readsorption isotherm for A1 sample after re-outgassing at 100°C is shown in Figure 36. The readsorption isotherm was significantly lower than the original adsorption isotherm. Thus, HCl molecules were strongly adsorbed on the titania surface and could not be completely removed by evacuation at 100°C. The readsorption isotherm after reoutgassing the same sample at 400°C was also lower than the original adsorption isotherm. This indicates that the strongly bound HCl on the A1 sample outgassed at 100°C could not be fully removed even by reoutgassing at 400°C. Adsorption and readsorption isotherms for A1 outgassed at 200°C and 400°C are shown in Figures 37 and 38. In both cases, the adsorption and readsorption isotherms were different and gave further evidence for the partial irreversible adsorption of HCl which cannot be removed by outgassing at 400°C.

The HCl adsorption isotherms for A2 is shown in Figure 39. A stronger dependence of adsorption capacity compared to A1 on outgassing temperature was observed. Since A2 had more adsorbed water and hydroxyl groups than A1 this behavior was consistent. The sites which are covered initially with water became more accessible for HCl adsorption once the water molecules are removed at higher outgassing temperatures. The

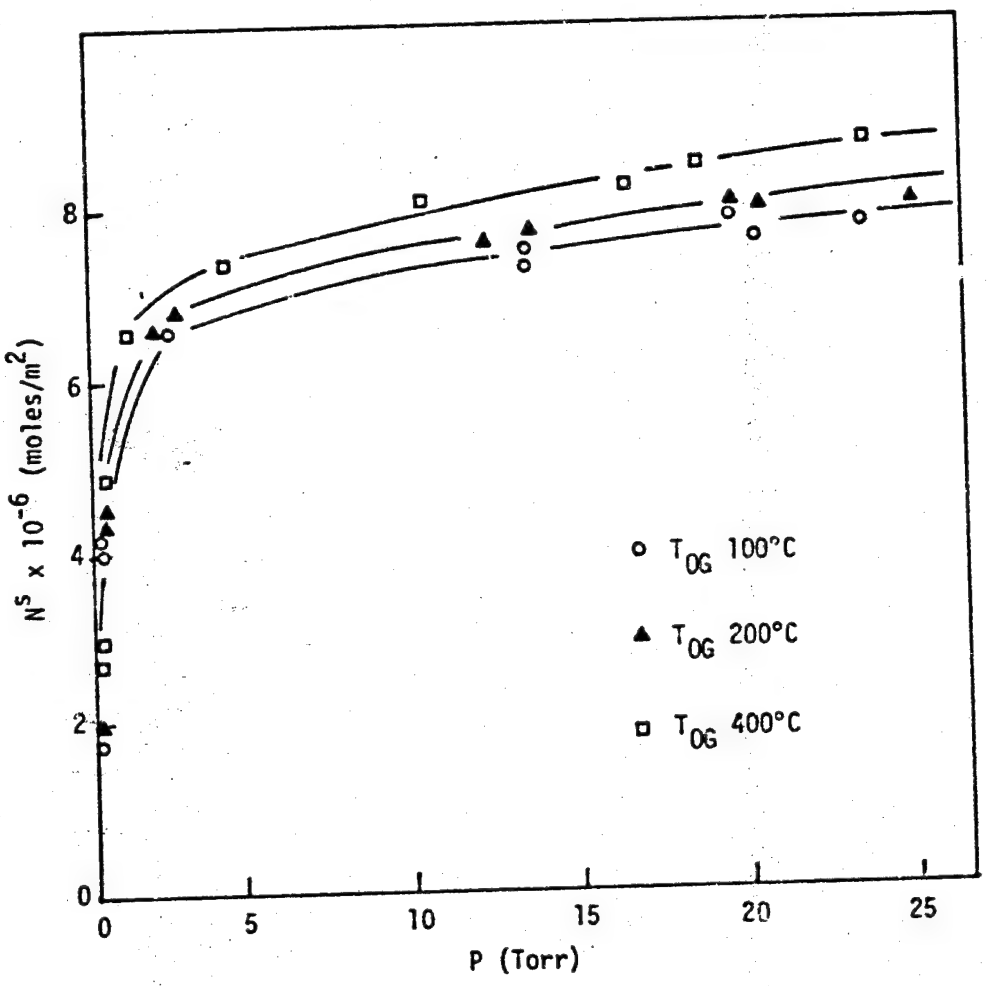

Figure 35. Adsorption Isotherms of Hydrogen Chloride on Al at 30°C

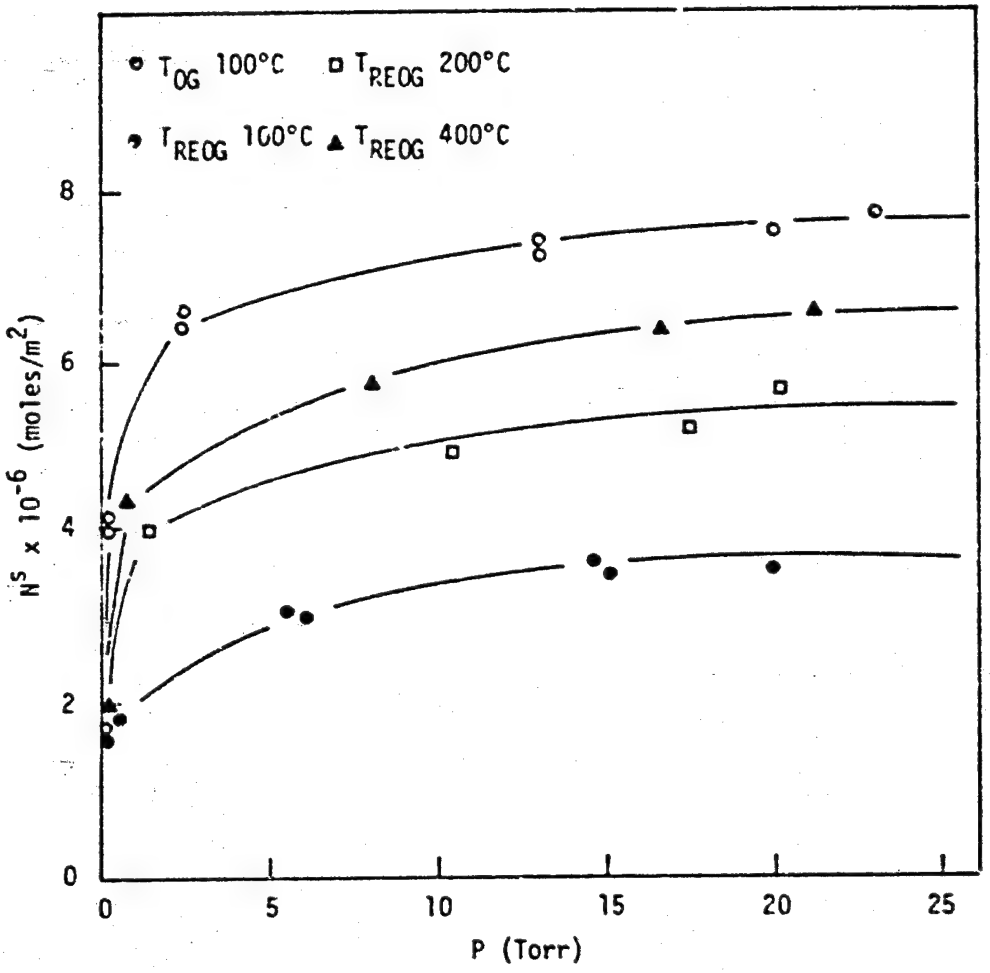

Figure 36. Adsorption and Readsorption Isotherms at 30°C of Hydrogen Chloride on Al Outgassed at 100°C

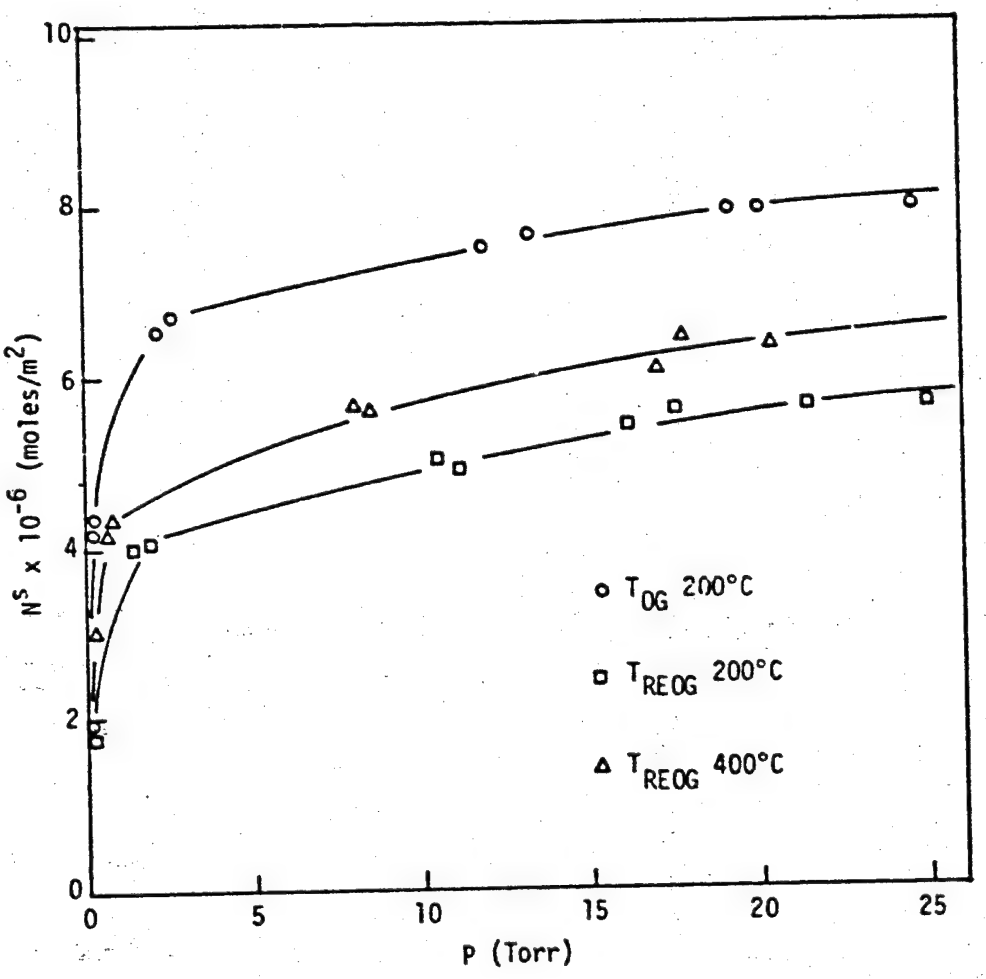

Figure 37. Adsorption and Readsorption Isotherms at 30°C of Hydrogen Chloride on Al Outgassed at 200°C

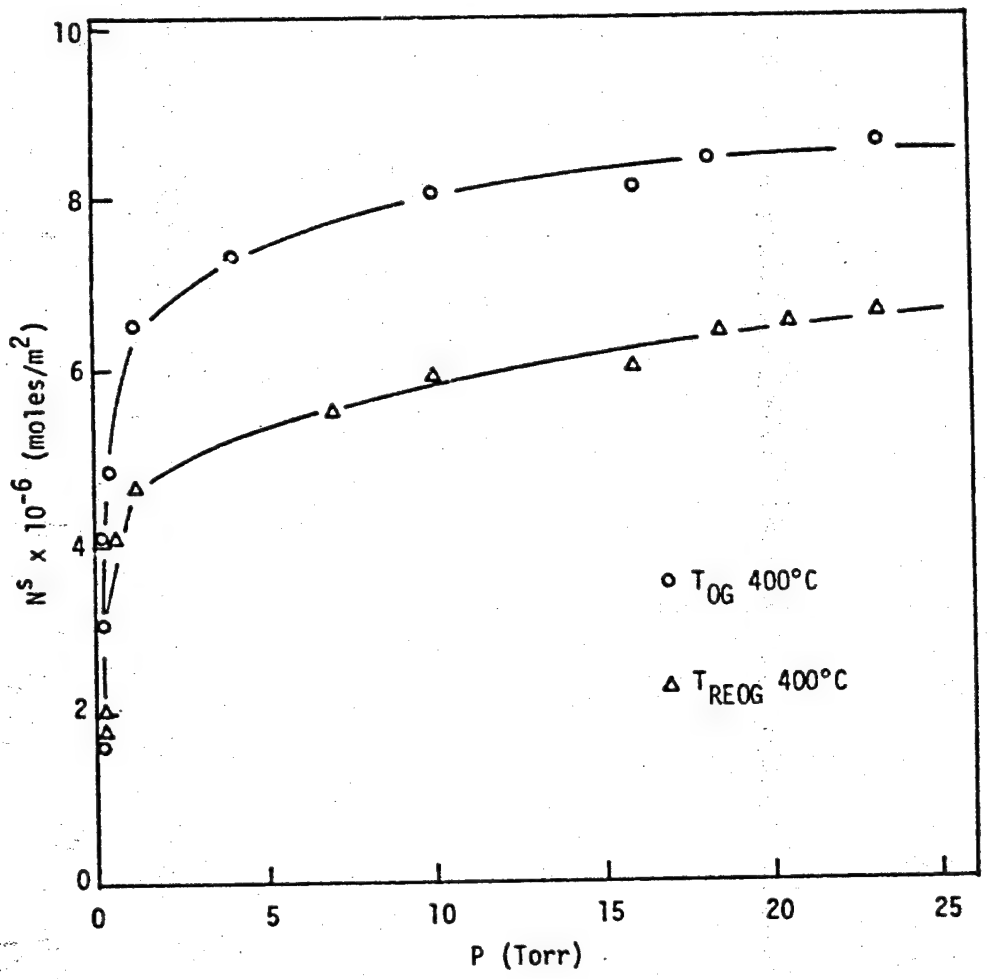

Figure 38. Adsorption and Readsorption Isotherms at 30°C of Hydrogen Chloride on Al Outgassed at 400°C

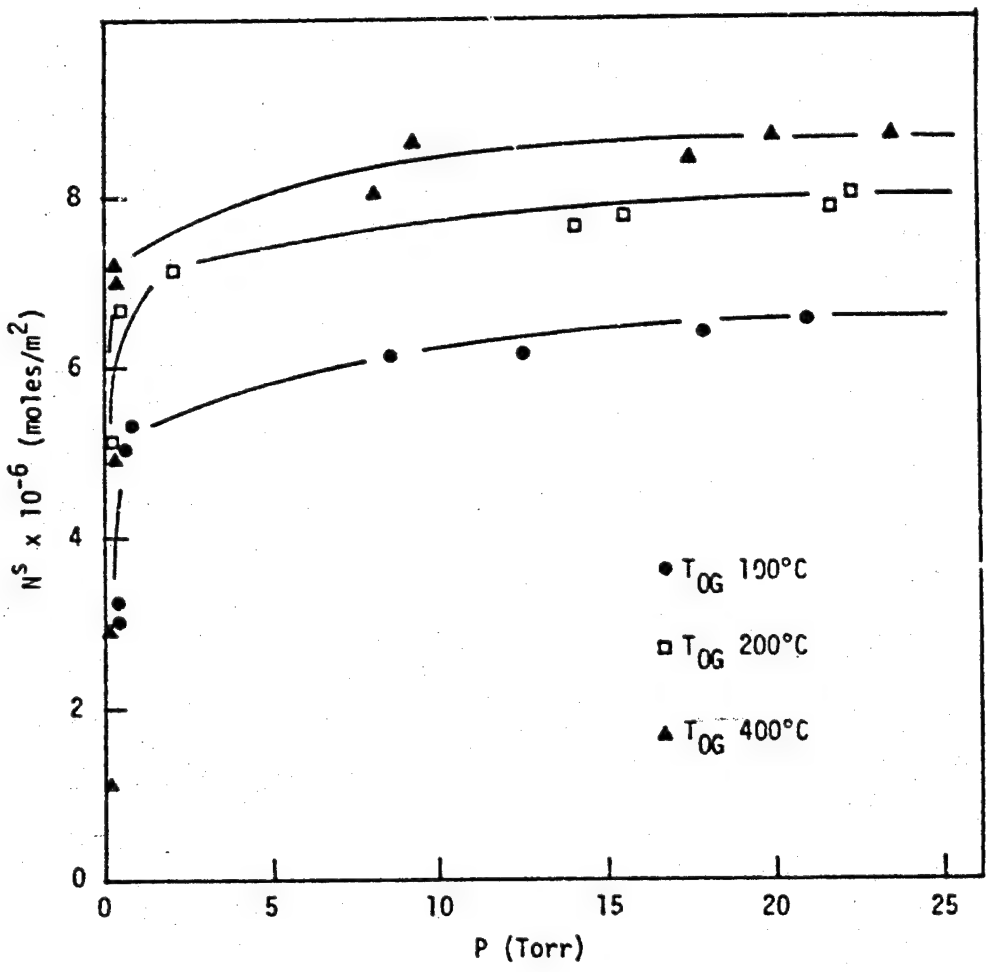

Figure 39. Adsorption Isotherms of Hydrogen Chloride on A2 at 30°C

adsorption and readsorption isotherms for A2 samples outgassed at 100°, 200° and 400°C are shown in Figures 40, 41 and 42, respectively. For all outgassing temperatures, the readsorption isotherms were lower than the original adsorption isotherms. Thus, A2 sample also adsorbed HCl strongly and the adsorbed HCl could not be removed completely by reoutgassing at 400°C.

The HCl adsorption isotherms for R3 showed a very strong dependence on outgassing temperature as shown in Figure 43. In contrast to the water adsorption isotherms, the HCl adsorption capacity did not decrease after outgassing at 400°C. The adsorption and readsorption isotherms for R3 powder outgassed at 100°, 200° and 400°C as shown in Figures 44, 45 and 46, respectively. For R3, at outgassing temperatures of 100° and 200°C, the readsorption isotherm was lower than the adsorption isotherm. However, after outgassing at 400°C the readsorption and adsorption isotherms were coincident. This indicates that HCl adsorbed on R3 sample can be removed completely by reoutgassing at 400°C. Thus, the adsorption of HCl on R3 was different from A1 and A2 sample powders. R3 was found to be acidic by the indicator method. Therefore, the reason for the lower adsorption capacity of acidic HCl onto R3 may be due to the acidic character of this surface. The adsorption of hydrogen chloride was measured after outgassing at 400°C and subsequent oxygen treatment. The adsorption isotherm after this oxygen treatment was slightly lower than the original isotherm obtained on R3 after outgassing at 400°C. The adsorption isotherm of hydrogen chloride measured after outgassing R3 at 200°C and subsequent oxygen treatment overlapped with the isotherm obtained on R3 outgassed at 200°C. The adsorption isotherms for alumina

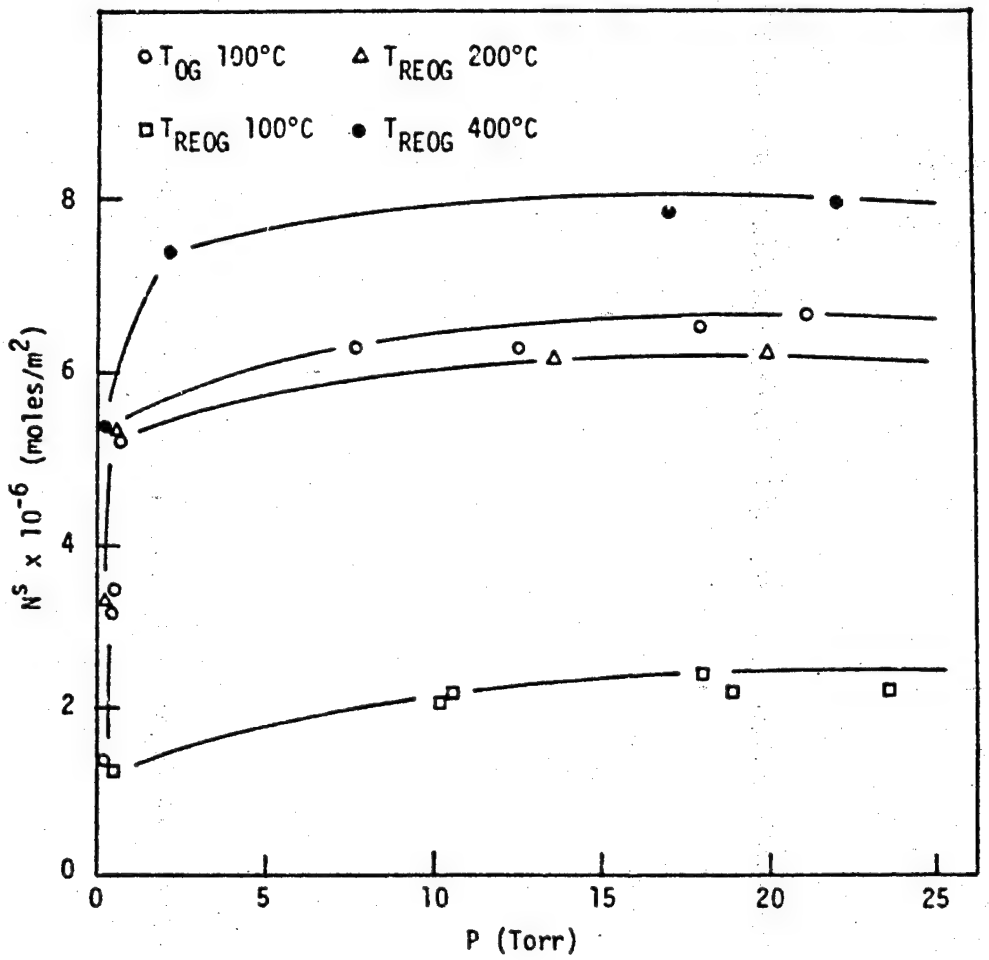

Figure 40. Adsorption and Readsorption Isotherms at 30°C of Hydrogen Chloride on A2 Outgassed at 100°C

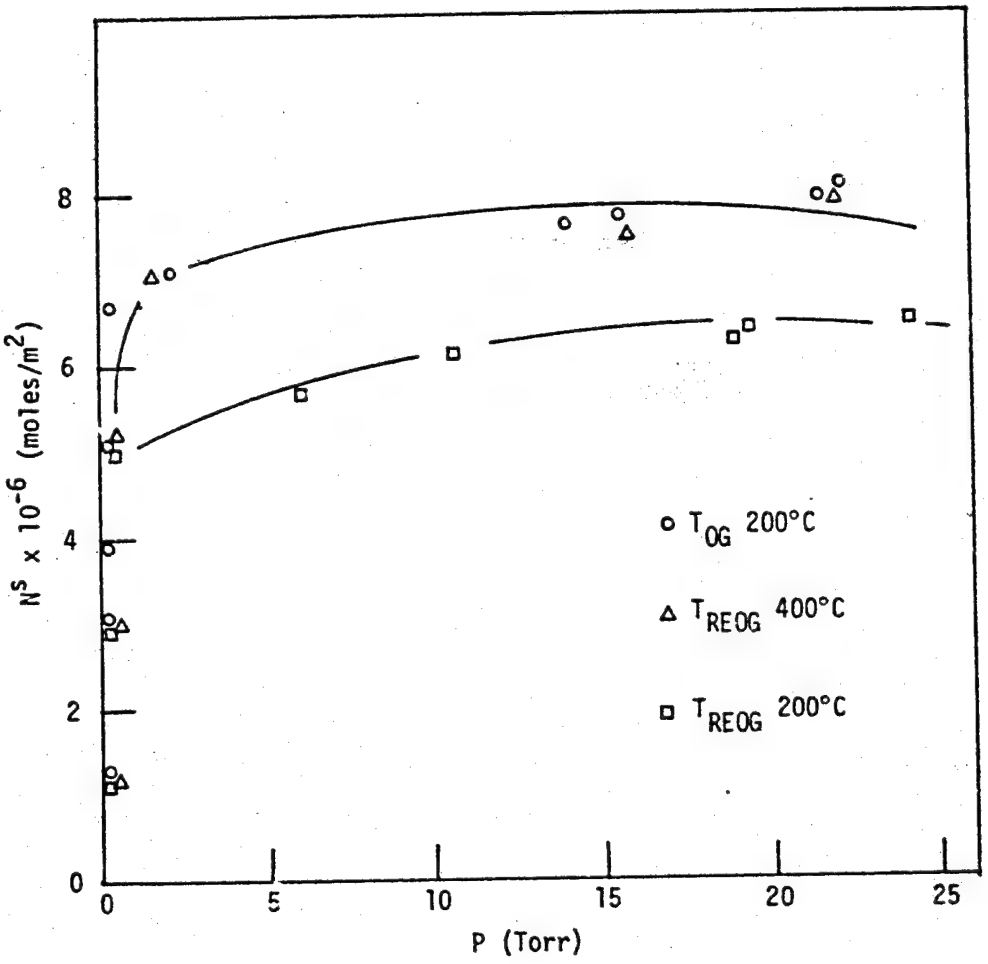

Figure 41. Adsorption and Readsorption Isotherms at 30°C of Hydrogen Chloride on A2 Outgassed at 200°C

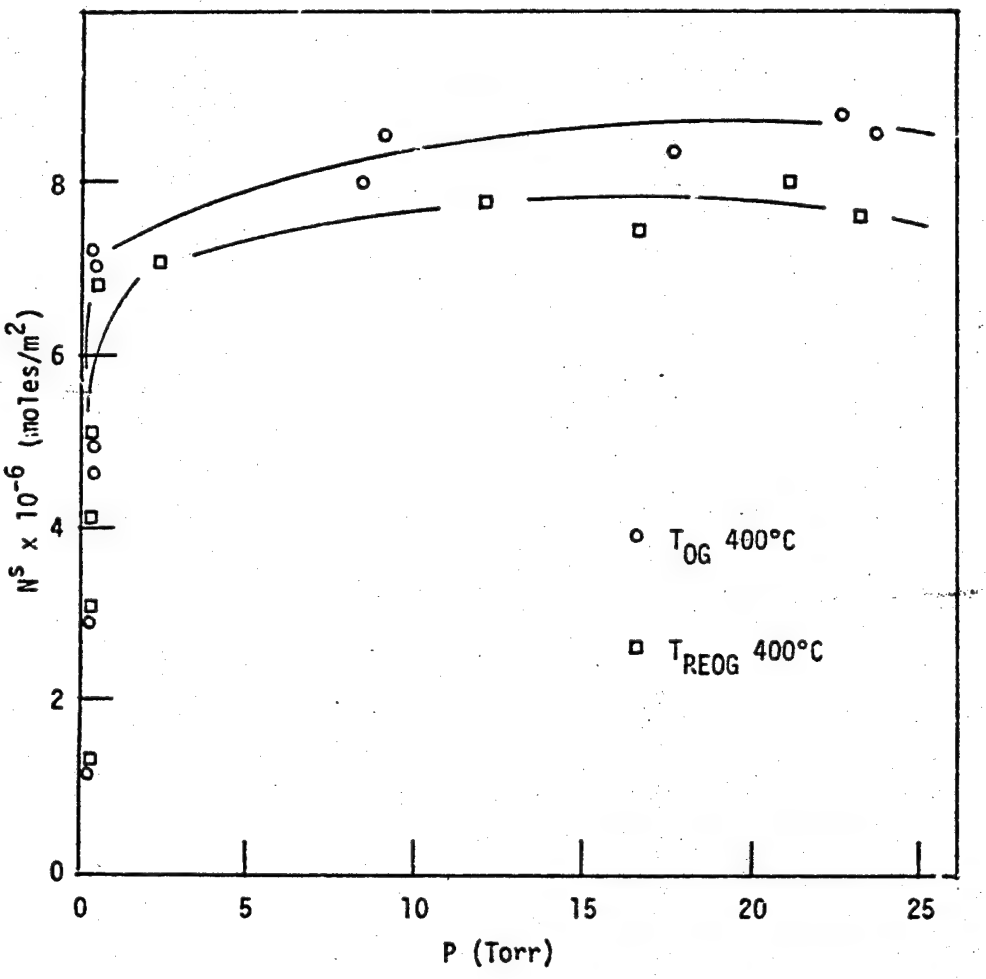

Figure 42. Adsorption and Readsorption Isotherms at 30°C of Hydrogen Chloride on A2 Outgassed at 400°C

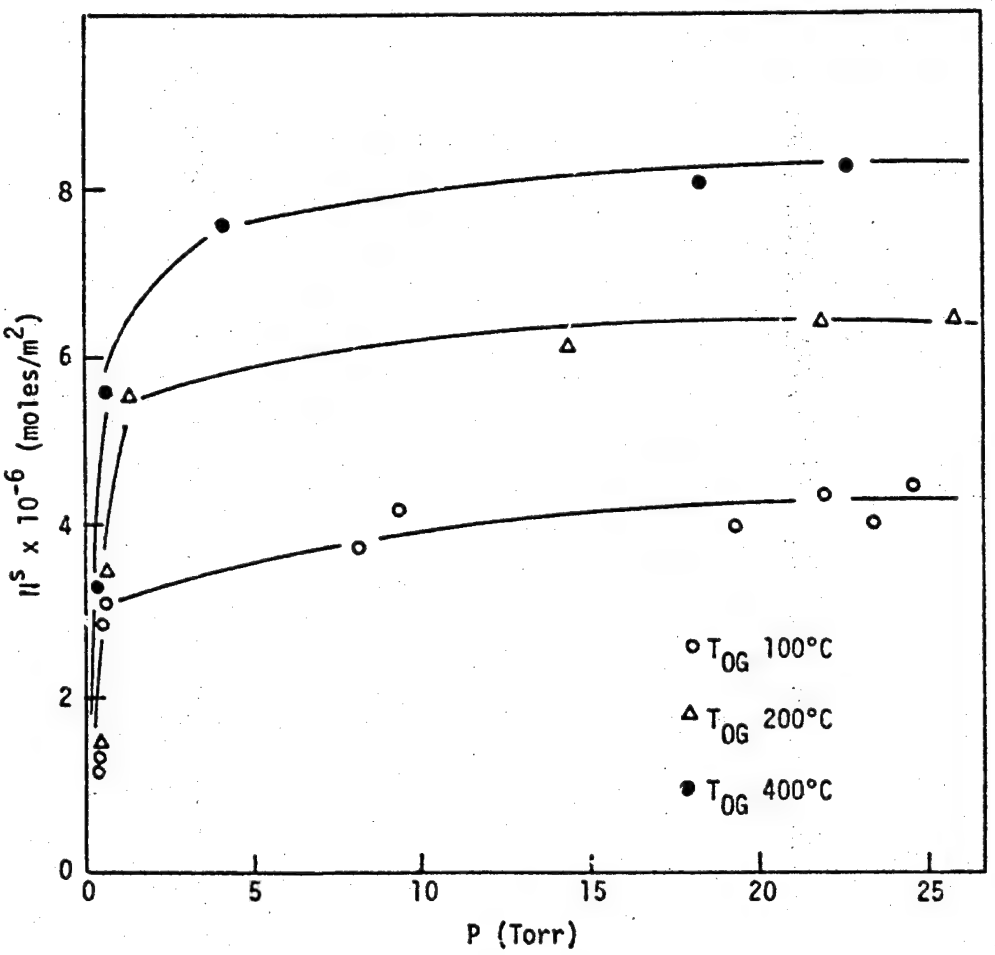

Figure 43. Adsorption Isotherms of Hydrogen Chloride on R3 at 30°C

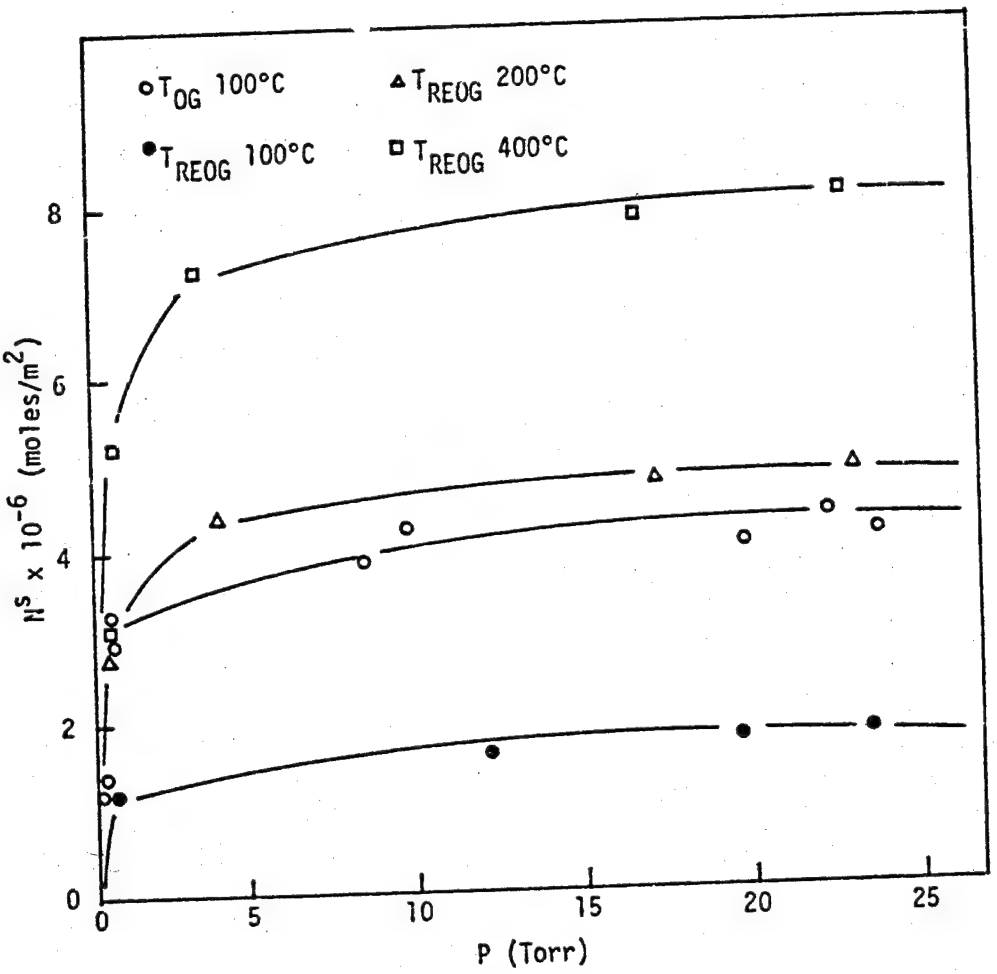

Figure 44. Adsorption and Readsorption Isotherms at 30°C of Hydrogen Chloride on R3 Outgassed at 100°C

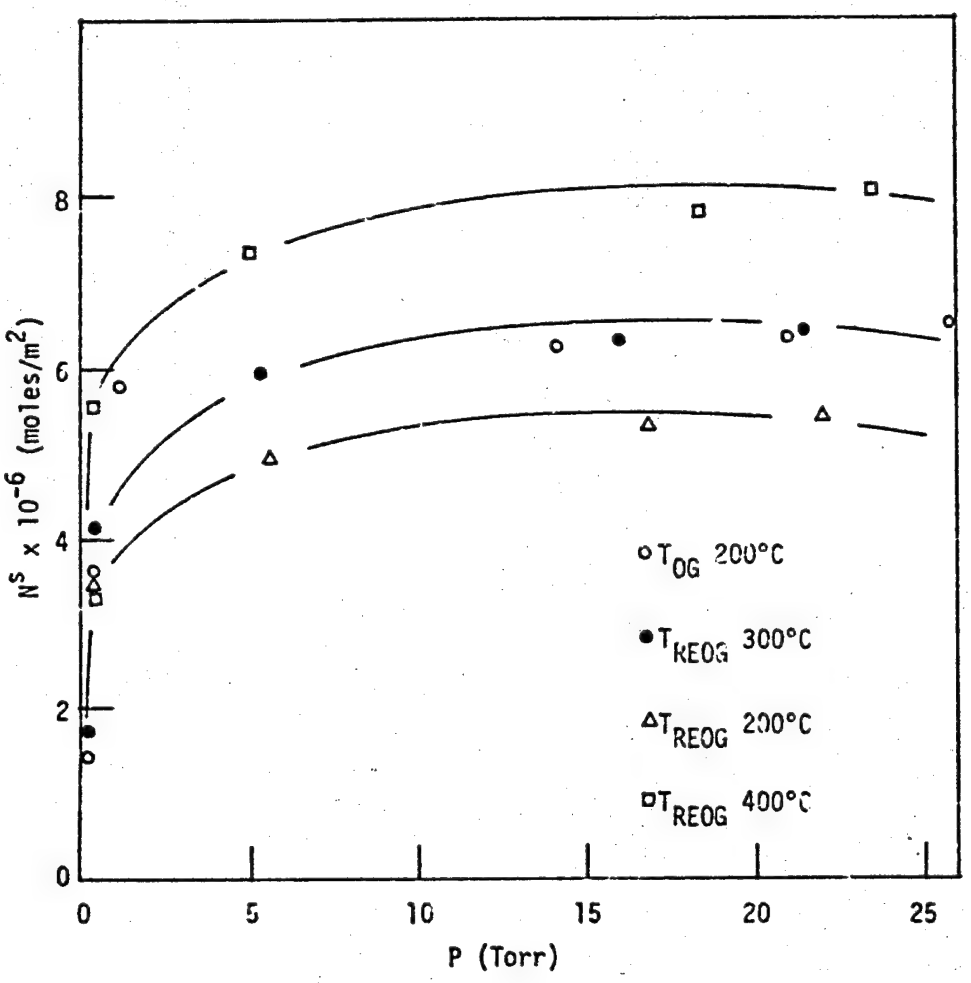

Figure 45. Adsorption and Readsorption Isotherms at 30°C of Hydrogen Chloride on R3 Outgassed at 200°C

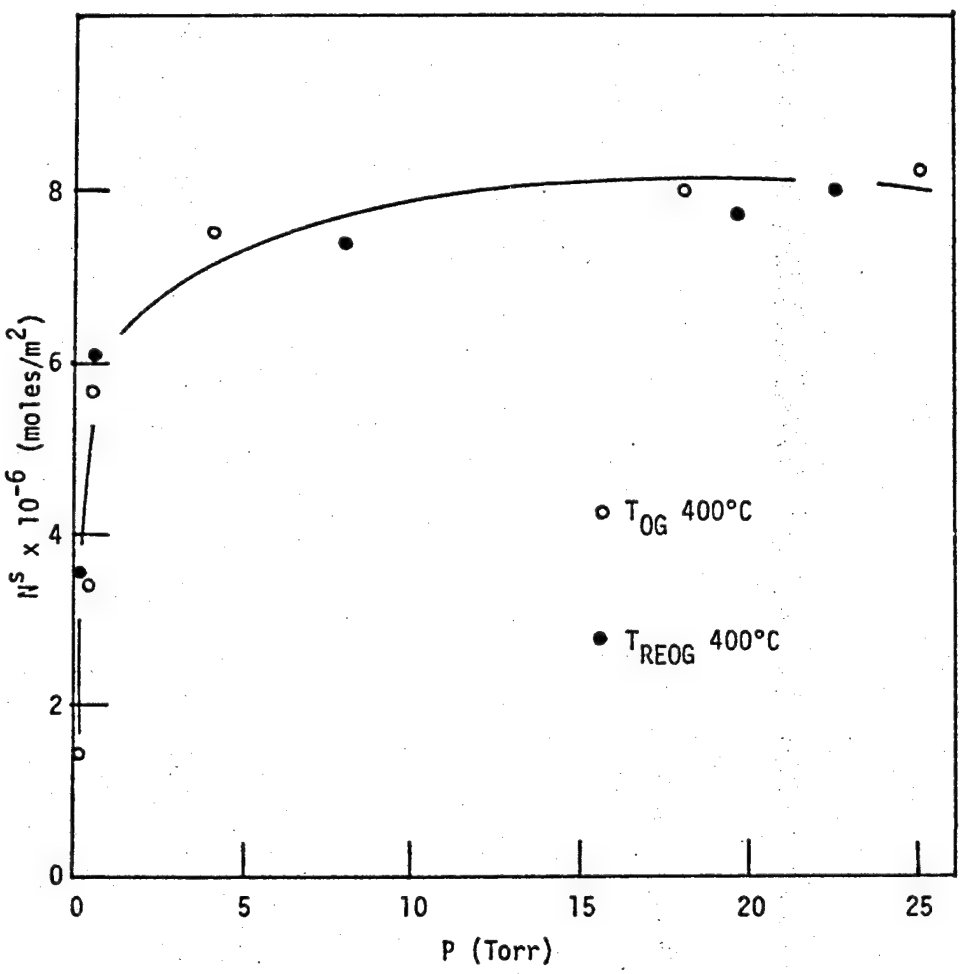

Figure 46. Adsorption and Readsorption Isotherms at 30°C of Hydrogen Chloride on R3 Outgassed at 400°C

coated samples R1 and R2 are shown in Figures 47 and 48, respectively. A dependence on outgassing temperature was observed in both cases. However this dependence was not as strong as was observed with water adsorption on the same samples. Thus, the water present on the surface did not strongly affect the adsorption of HCl on R1 and R2. The readsorption isotherms of HCl on R1 sample outgassed at 100°, 200° and 400°C are shown in Figures 49, 50 and 51, respectively. In all cases, the readsorption isotherms were lower than the original adsorption isotherms. Thus, HCl is strongly adsorbed onto R1 sample and could not be completely removed at 400°C. The readsorption isotherms for R2 outgassed at 100°, 200° and 400°C are shown in Figures 52, 53 and 54, respectively. Irreversible adsorption was also observed on R2 sample and adsorbed HCl again could not be removed at 400°C. The monolayer coverages (V_m) and cross sectional areas (σ) of HCl adsorbed on titania, calculated using the Langmuir equation [13], are shown in Table VII. The total monolayer coverages of adsorbed HCl on titania samples were calculated directly from the original adsorption isotherms and the amount of irreversibly adsorbed HCl was calculated from the readsorption isotherms. At an outgassing temperature of 100°C, A1 showed the highest total adsorption. Similar amounts were irreversibly adsorbed on A1 and A2 at this outgassing temperature. These two powders showed the highest amount of irreversible adsorption of HCl compared to other three samples outgassed at 100°C. After outgassing at 400°C, the total amount of HCl adsorption was similar on all pure titania powders. However, at this outgassing temperature, A1 had the largest amount of irreversibly adsorbed HCl and R3 had the least or comparatively no irreversible adsorption. Thus, A1 has the highest affinity for HCl

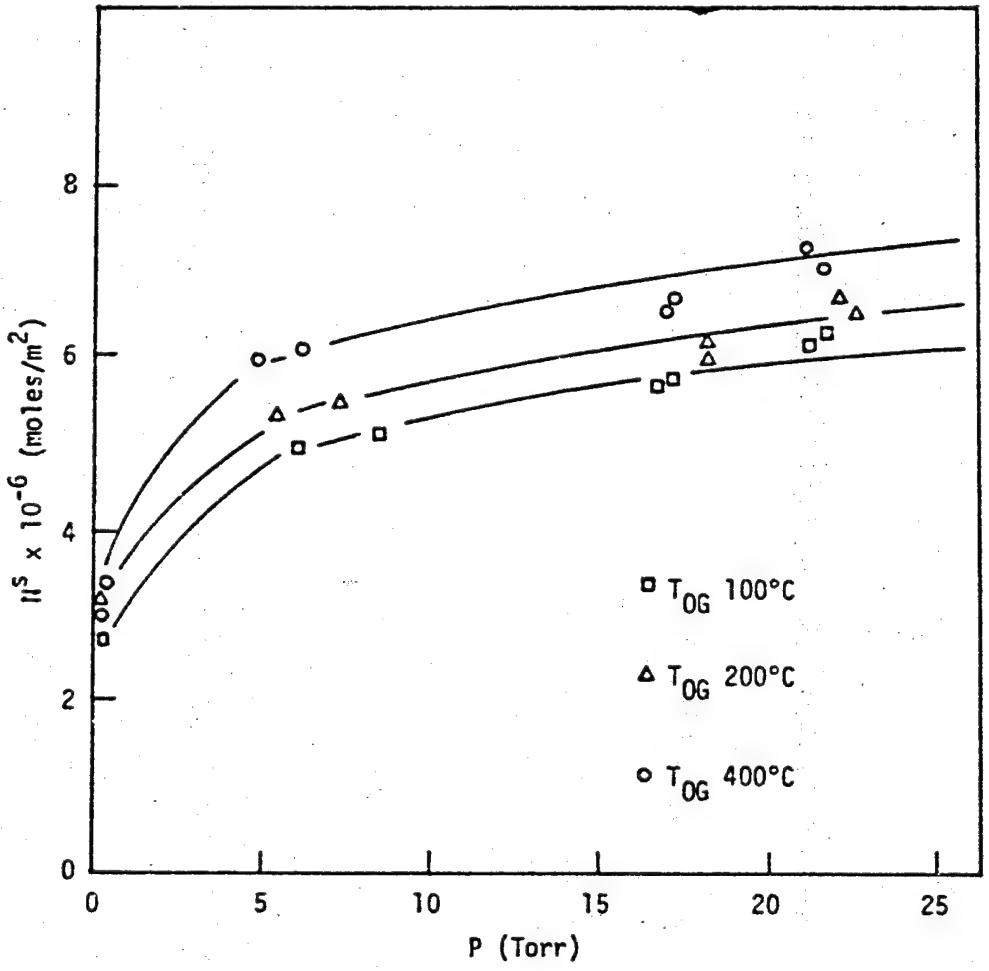

Figure 47. Adsorption Isotherms of Hydrogen Chloride on R1 at 30°C

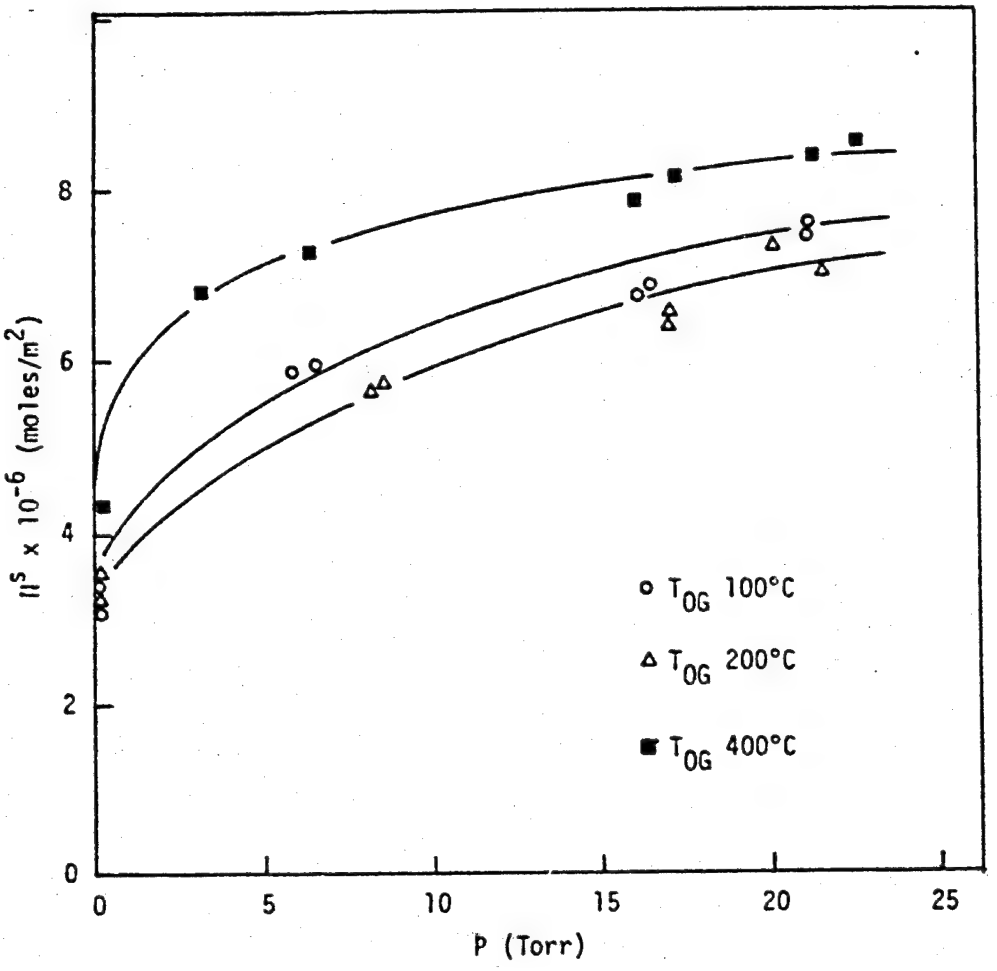

Figure 48. Adsorption Isotherms of Hydrogen Chloride on R2 at 30°C

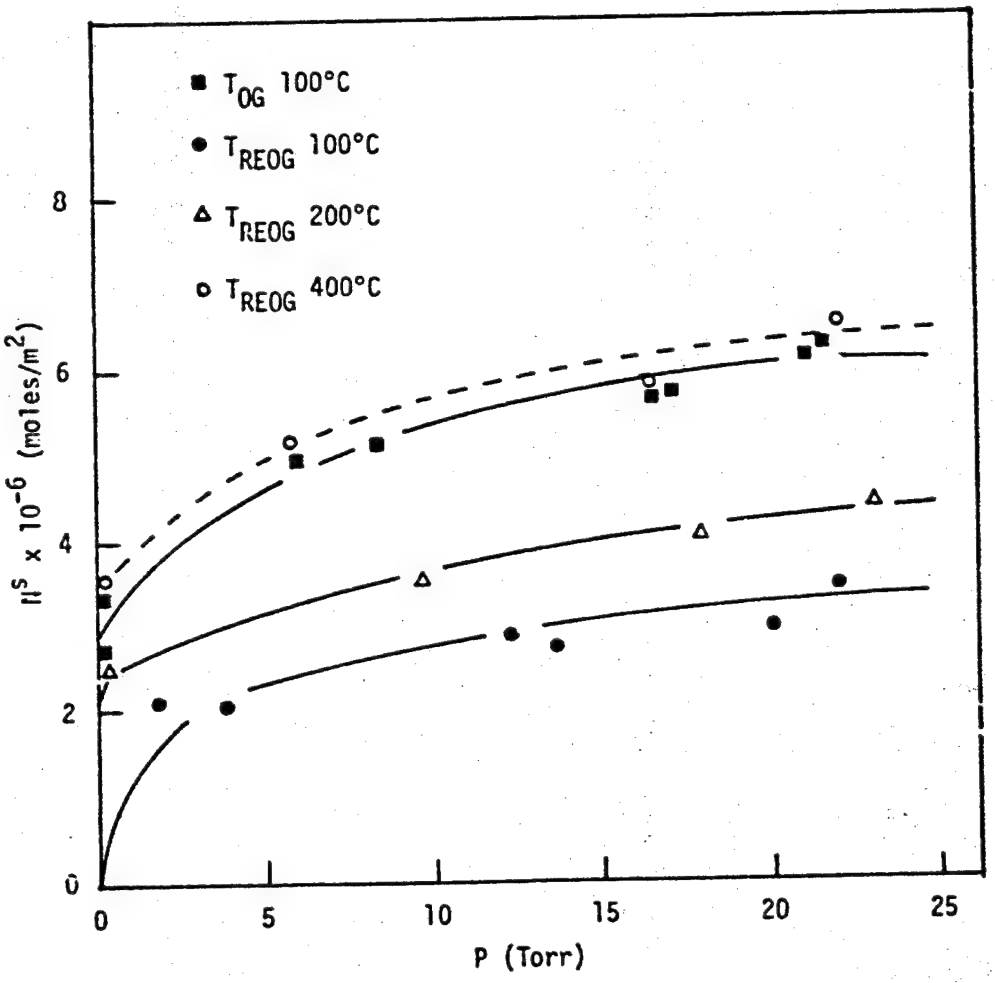

Figure 49. Adsorption and Readsorption Isotherms at 30°C of Hydrogen Chloride on R1 Outgassed at 100°C

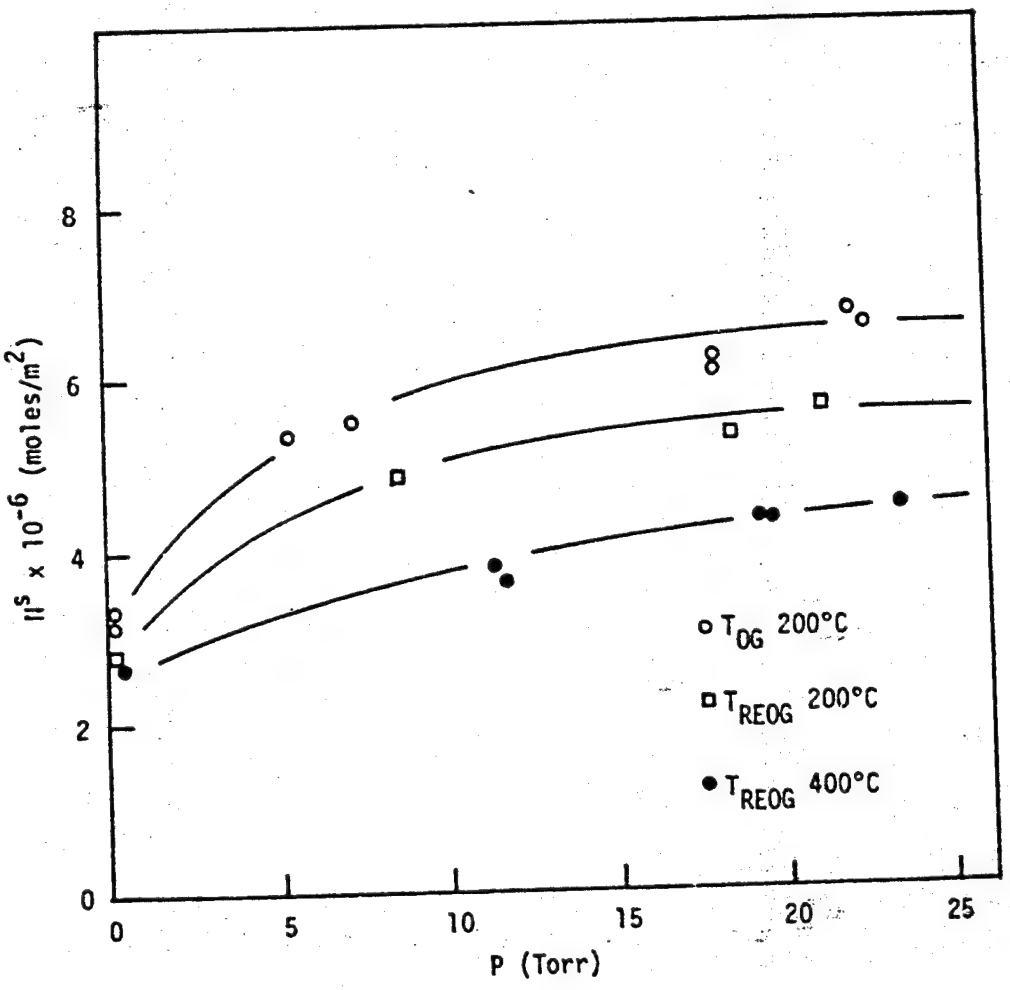

Figure 50. Adsorption and Readsorption Isotherms at 30°C of Hydrogen Chloride on R1 Outgassed at 200°C

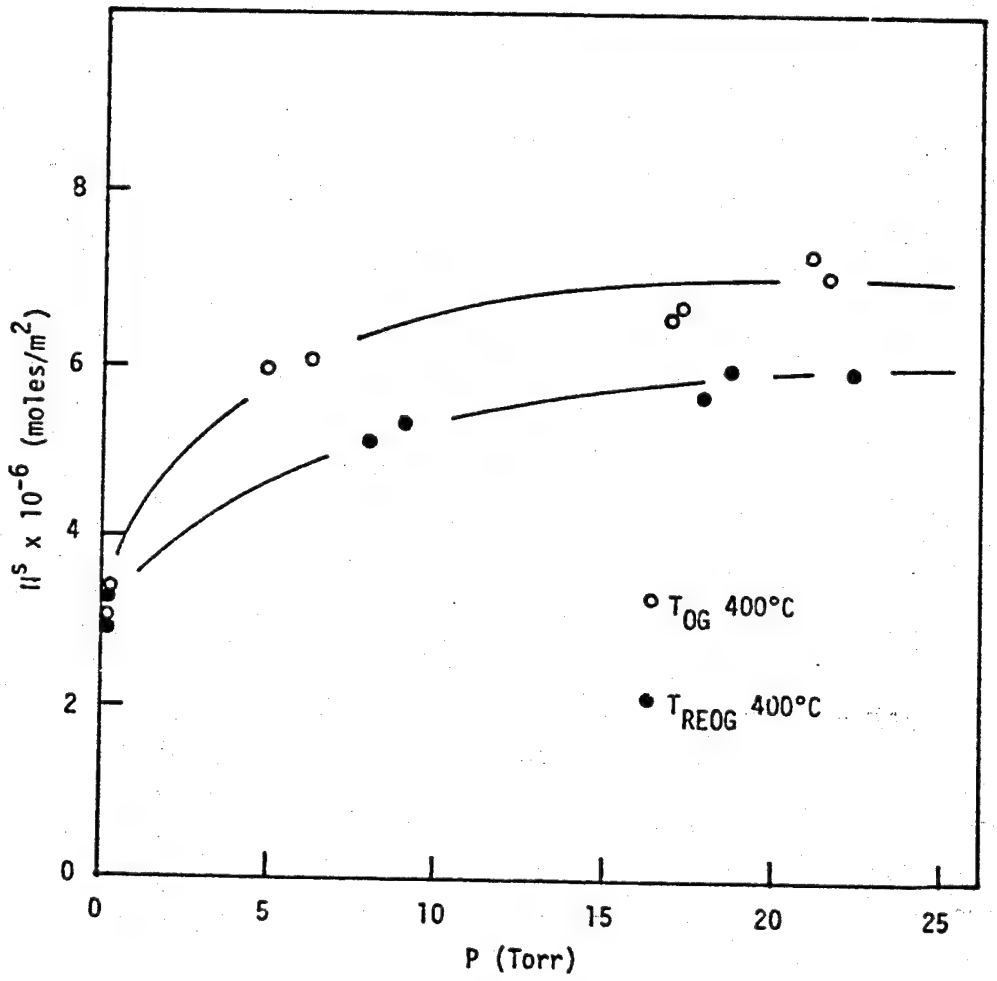

Figure 51. Adsorption and Readsorption Isotherms at 30°C of Hydrogen Chloride on R1 Outgassed at 400°C

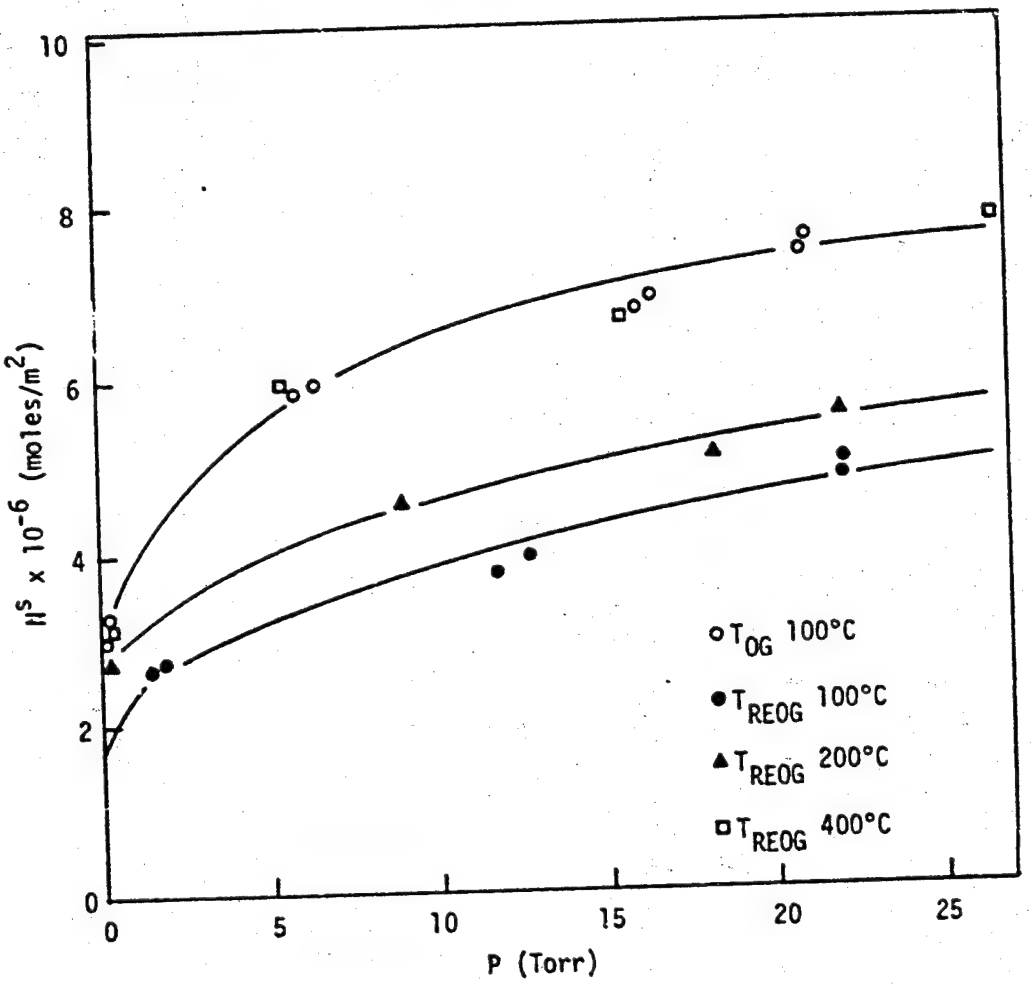

Figure 52. Adsorption and Readsorption Isotherms at 30°C of Hydrogen Chloride on R2 Outgassed at 100°C

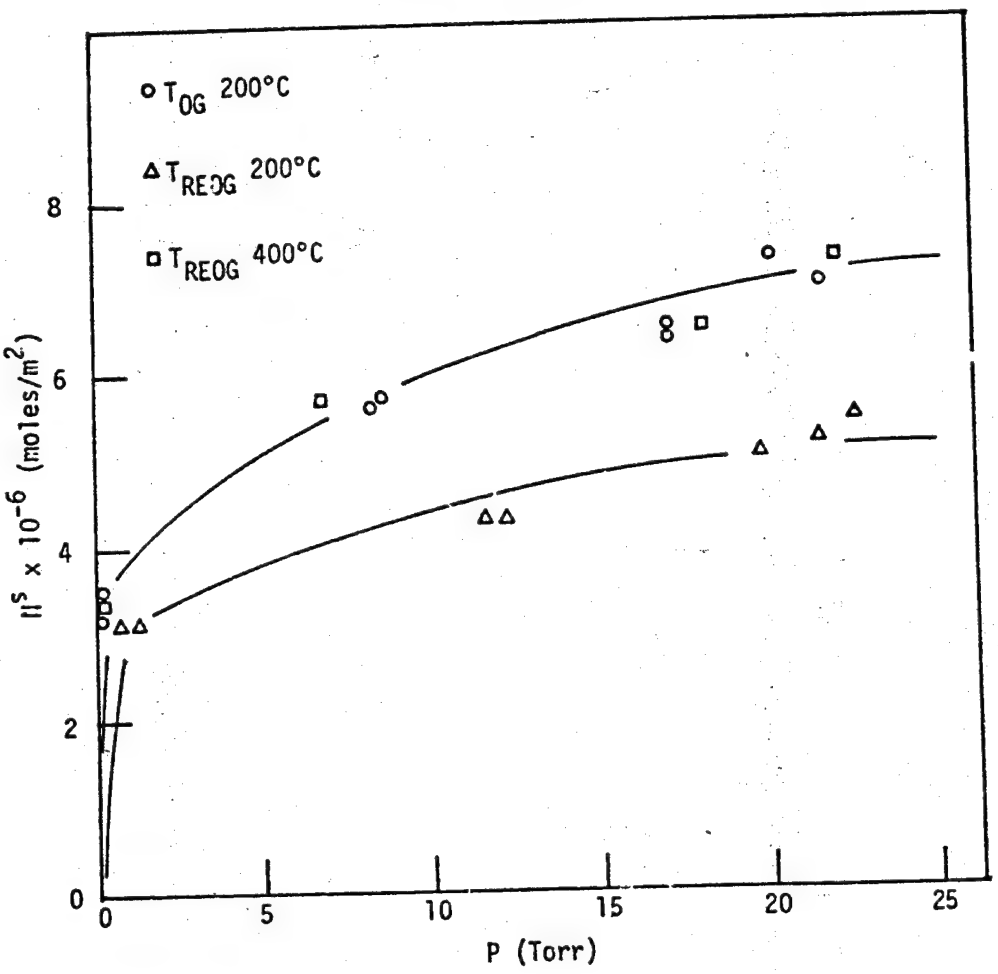

Figure 53. Adsorption and Readsorption Isotherms at 30°C of Hydrogen Chloride on R2 Outgassed at 200°C

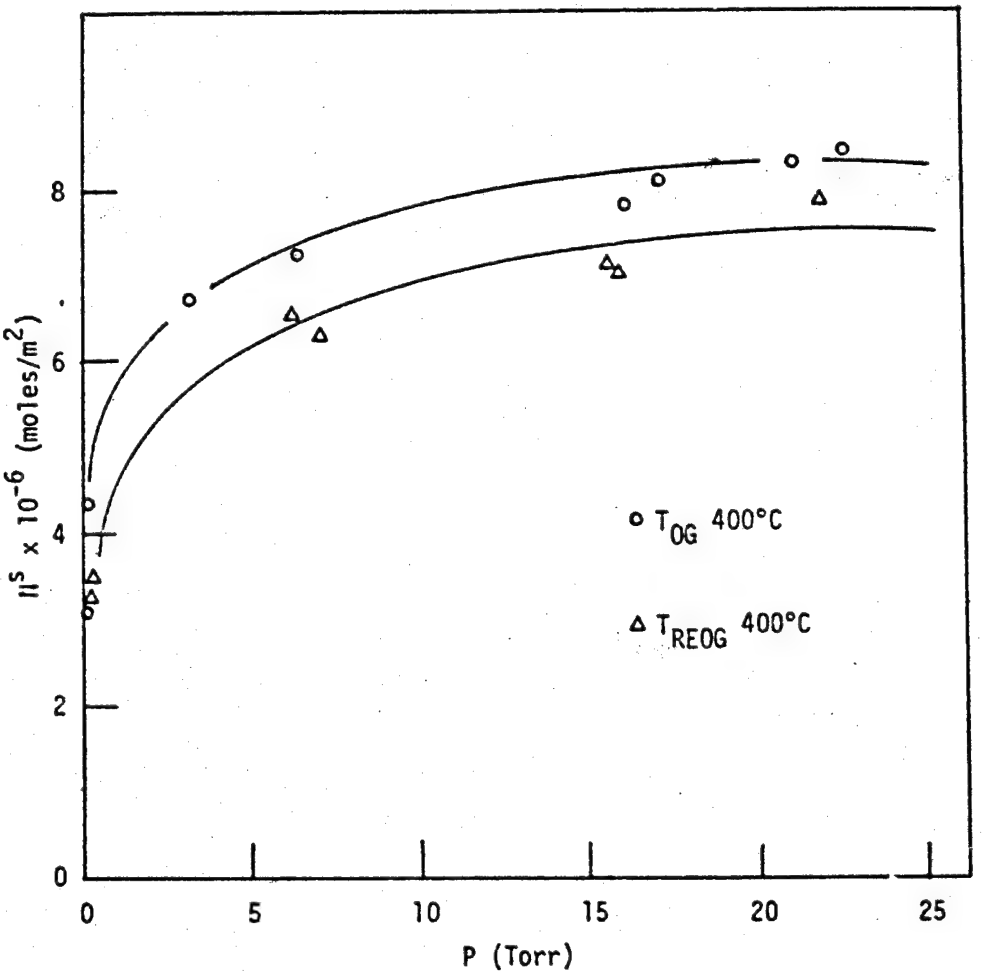

Figure 54. Adsorption and Readsorption Isotherms at 30°C of Hydrogen Chloride on R2 Outgassed at 400°C

TABLE VII

MONOLAYER COVERAGES AND CROSS SECTIONAL AREAS
FOR HCL ADSORPTION ON TiO_2

	A 1		A 2		R 3		R 1		R 2	
T_{OG} (°C)	$V_m \times 10^{-8}$ (mol/m^2)	σ (Å^2/mol)	$V_m \times 10^{-8}$ (mol/m^2)	σ (Å^2/mol)	$V_m \times 10^{-8}$ (mol/m^2)	σ (Å^2/mol)	$V_m \times 10^{-8}$ (mol/m^2)	σ (Å^2/mol)	$V_m \times 10^{-8}$ (mol/m^2)	σ (Å^2/mol)
Total Adsorption										
100	784	21	658	25	437	38	629	26	752	22
200	811	21	803	21	656	25	656	25	714	23
400	863	19	871	19	835	20	717	23	851	20
Irreversible Adsorption										
100	417	--	430	--	250	--	259	--	226	--
200	235	--	149	--	108	--	218	--	164	--
400	199	--	76	--	21	--	120	--	81	--
Reversible Adsorption										
100	367	--	228	--	184	--	370	--	526	--
200	576	--	654	--	548	--	438	--	714	--
400	664	--	795	--	814	--	597	--	770	--

adsorption. However, the lowest water adsorption capacity was found for Al from the water adsorption isotherms. Hence, there is no correlation between the number of hydroxyl groups present on the surface and the HCl adsorption capacity. Thus, hydroxyl groups are not the major species that would react with HCl. It is possible that the Ti$\diagup^{O}\diagdown$Ti groups are participating in the reaction. It is also interesting to note that the area occupied by one HCl molecule was similar in all pure TiO_2 powders after outgassing at 400°C as shown in Table VII.

For R3 powder, if the (110) plane is the predominantly exposed plane, it should possess 10.2 Ti ions per 100 $\mathring{A}^2$ (22). This would give an area of 19 $\mathring{A}^2$ for two Ti ions. This value is comparable with the area occupied by one molecule of HCl on R3 calculated using adsorption isotherms as shown in Table VII. Thus, one HCl molecule may be interacting with two Ti ions. The cross sectional areas of HCl adsorbed on γ-alumina (101) was 33 $\mathring{A}^2$/mol and on silica (102) was 47 $\mathring{A}^2$/molec. These values are significantly higher than that was observed on titania samples. However, the value obtained for α-alumina (101) of 18 $\mathring{A}^2$/mol was comparable with the value obtained for titania.

Using 16.6 $\mathring{A}^2$ as the area of the hydrogen chloride molecule obtained from liquid density calculations, the ratios of the surface area obtained from HCl adsorption (S_{HCl}) to the area obtained from nitrogen (S_{N_2}) were calculated and are shown in Table VIII. It is shown by the calculations that once the water molecules are removed by outgassing at 400°C, the majority of the surface 72-87% is occupied by HCl molecules. Thus, TiO_2 surface has a strong tendency for HCl adsorption.

TABLE VIII

S_{HCl}/S_{N_2} RATIOS

T_{OG}(°C)	A1	A2	R3	R1	R2
100	0.78	0.66	0.44	0.63	0.75
200	0.81	0.80	0.66	0.66	0.71
400	0.86	0.87	0.81	0.72	0.85

3. ESCA Analysis

ESCA Analysis was done to identify the elemental species present on the surface after HCl adsorption. A chlorine photopeak was observed on all the surfaces after adsorption of HCl. The binding energies of chlorine and Cl/Ti ratios are listed in Table IX. The values of the Cl/Ti ratio increased significantly after adsorption of HCl (line 3) compared to the fresh surface as shown in Table IX. The Cl/Ti ratio decreased by reoutgassing these samples at 100° and 400°C. Among the uncoated titania powders, A1 contained the largest Cl/Ti ratio after reoutgassing at 400°C while R3 did not contain any chlorine at this outgassing temperature. As described before, by HCl adsorption analysis it was found that A1 contained the largest amount of HCl after reoutgassing the exposed sample at 400°C while R3 contained the least. Therefore, the results from the ESCA analysis are in very good agreement with the analysis done with adsorption data. Furthermore, the Cl/Ti ratio for the TiO_2 surfaces after HCl reaction were significantly higher than the same ratio for alumina which was 0.022 (101) and silica which is 0.024 (102). The Cl/Al ratio on pure crystalline alumina is significantly lower than that was observed for alumina coated titania samples. The alumina coating may not be completely covering the titania surface. The alumina coating may not be crystaliine and, hence, it may be behaving different to the pure crystalline alumina powders.

In order to identify the nature of chlorine present after HCl adsorption, some chlorine-containing model compounds were investigated. The binding energies of the chlorine present in these model compounds are

TABLE IX

ESCA ANALYSIS OF TITANIA POWDERS AFTER REACTION WITH HCL

	T_{OG}(°C)	A 1		A 2		R 3		R 1	
		B.E.(eV)	Cl/Ti	B.E.(eV)	Cl/Ti	B.E.(eV)	Cl/Ti	B.E.(eV)	Cl/Ti
1	Fresh	197.6	0.048	---	---	---	---	197.4	0.038
2	400	197.7	0.020	---	---	---	---		
3	100+HCL	198.3	0.105	197.6	0.056	197.6	0.050	197.8	0.128
4	T_{REOG} 100	198.2	0.070	197.6	0.032	197.8	0.021	198.3	0.092
5	T_{REOG} 400	197.8	0.040	197.8	0.017	---	---	198.4	0.067

shown in Table X. The binding energy of chlorine present on the surface after adsorption of HCl is comparable with the chlorine present in NaCl, $CuCl_4$, $AlCl_3$ and $CrCl_3$. The chlorine in NaCl is ionic whereas chlorine in $CuCl_4$ is considered to be covalently bonded. Since the binding energies are relatively close for all cases it is difficult to distinguish between covalently bonded and ionic chlorine by ESCA analysis alone. Thus, chlorine present on the titania surface could have either ionic or covalent character.

4. Acidity Measurements

Results of the acidity measurements after adsorption of HCl on titania surfaces are given in Table XI. After the adsorption of HCl on the uncoated titanias (A1, A2 and R3) outgassed at 100°C, benzeneazodiphenylamine changed color from yellow to dark violet on the surface. Thus, each of these surfaces is highly acidic after HCl adsorption and the surface pK_a is <1.5. The alumina-coated R1 sample changed the color of methyl yellow from yellow to red but did not change the color of benzeneazodiphenyl amine. The R2 sample which is also alumina-coated changed the color of benzeneazodiphenyl amine from yellow to light violet. Thus, both alumina-coated samples were less acidic compared to the uncoated samples after HCl adsorption. Furthermore, the acidity of the uncoated samples was not affected by reoutgassing at 100°C, but both R1 and R2 showed a reduction of acidity at this outgassing temperature. After reoutgassing at 400°C, A1, R1 and R2 showed a large reduction in acidity (acidity >2.8) while A2 showed an acidity equal to 2.8. After reoutgassing at 400°C, R3 showed a color change with methyl yellow

TABLE X

BINDING ENERGIES OF Cl 2p PHOTOPEAK IN SOME MODEL COMPOUNDS

Sample	B.E. (eV)
Potassium perchlorate	206.5
Sodium chlorate	205.6
Sodium chloride	198.0
Copper chloride	196.6
Aluminum chloride	197.4
Chromium chloride	198.6

TABLE XI

ACIDITY MEASUREMENTS ON TiO_2 POWDERS AFTER HCL ADSORPTION

	Indicator	pK_a	T_{OG}	A 1	A 2	R 1	R 2	R 3
1	Benzeneazo--diphenylamine	1.5	100	Y → d.V.	Y → d.V.	Y → Y	Y → L.V.	Y → d.V.
			RE100	Y → V	Y → d.V.	Y → Y	Y → Y	Y → d.V.
			RE400	Y → Y	Y → Y	Y → Y	Y → Y	Y → Y
2	Methyl Yellow	2.8	100	Y → d.R.	Y → d.R.	Y → R	Y → R	Y → d.R.
			RE100	Y → R	Y → d.R.	Y → P	Y → P	Y → d.R.
			RE400	Y → Y	Y → P	Y → Y	Y → Y	Y → P
3	O-Nitro Phenol	7.0	100	Y → C	Y → C	Y → C	Y → Y	Y → C
			RE100	Y → C	Y → C	Y → C	Y → Y	Y → C
			RE400	Y → C	Y → C	Y → C	Y → Y	Y → C

Y = yellow, d.V. = dark violet, V = violet, C = colorless, R = red, d.R. = dark red, P = pink

($pK_a \leq 2.8$). However, a similar color change was observed when a fresh sample of R3 was outgassed at 400°C as shown in Table IV. Therefore, the acidity of exposed R3 after reoutgassing at 400°C was not due to the adsorbed HCl.

5. Infrared Analysis

To further investigate the interaction of HCl with TiO_2, the reaction was studied by infrared spectroscopy. The infrared spectra for A2 after outgassing at 200°C, after adsorption of HCl and after reoutgassing at 200°C are shown in Figure 55 and 56. It is clearly seen in Figure 55 that after reaction with HCl the two hydroxyl groups corresponding to 3650 cm^{-1} (hydrogen bonded) and 3710 cm^{-1} (isolated) were completely removed. Thus these two hydroxyl groups have reacted with HCl. In addition, a sharp peak at 3550 cm^{-1}, a broad band in the 3440-3000 cm^{-1} region and a band at 1600 cm^{-1} were formed. These values are consistent with the values obtained by Primet et al. (13). The two bands at 3440-3000 cm^{-1} and 1600 cm^{-1} gave evidence for the formation of molecular water during the reaction. The bending mode of water at 1600 cm^{-1} suggested that the water was monomeric. The sharpness of the band at 3550 cm^{-1} indicated the formation of additional hydroxyl groups in a well defined structure. After reoutgassing at 200°C it was not possible to reproduce the original spectrum. However, the band at 3420 cm^{-1} was reformed while the 3550 cm^{-1} band still remained. This is further confirming evidence for partial irreversibility of adsorption of HCl onto TiO_2.

6. Mechanism of the HCl Reaction With Titania Powders

Combining all the data obtained from adsorption isotherms, acidity

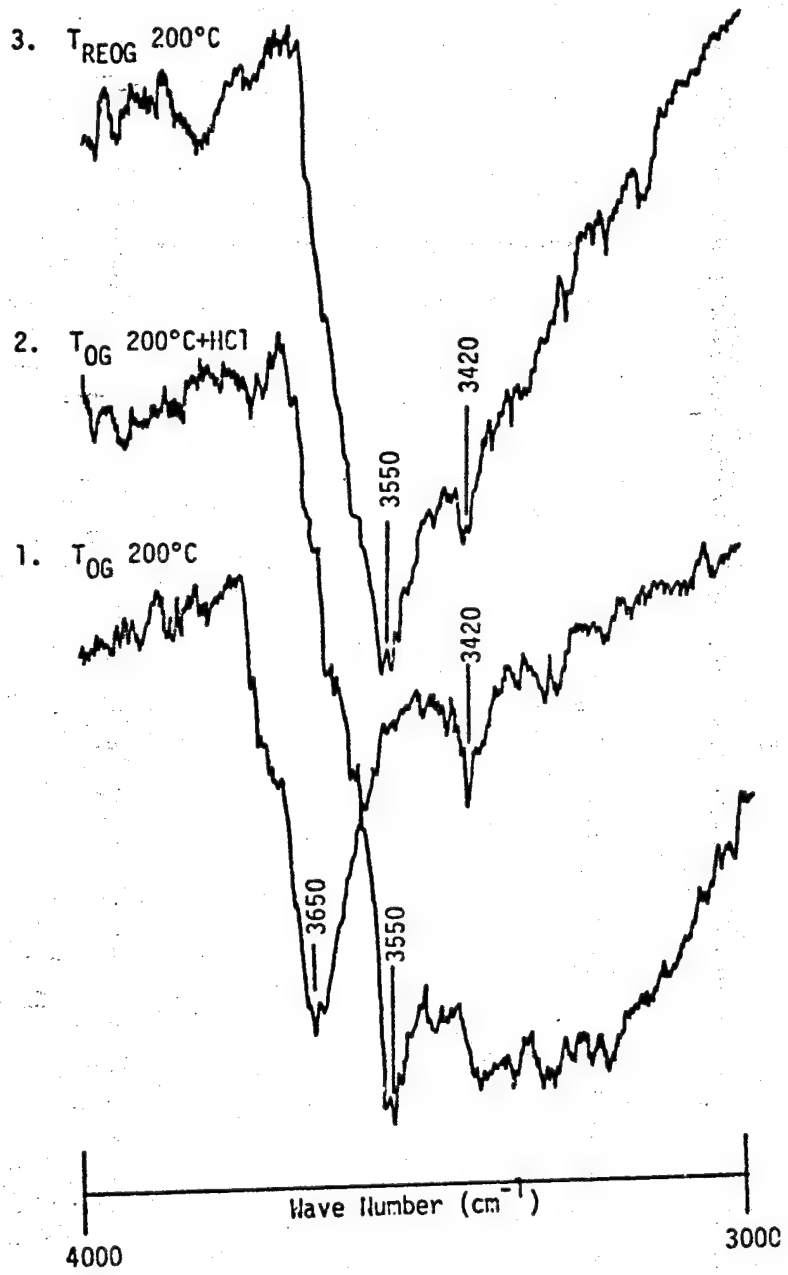

Figure 55. Infrared spectra (3000-4000 cm^{-1}) of A2 Outgassed at 200°C Before and After Hydrogen Chloride Adsorption

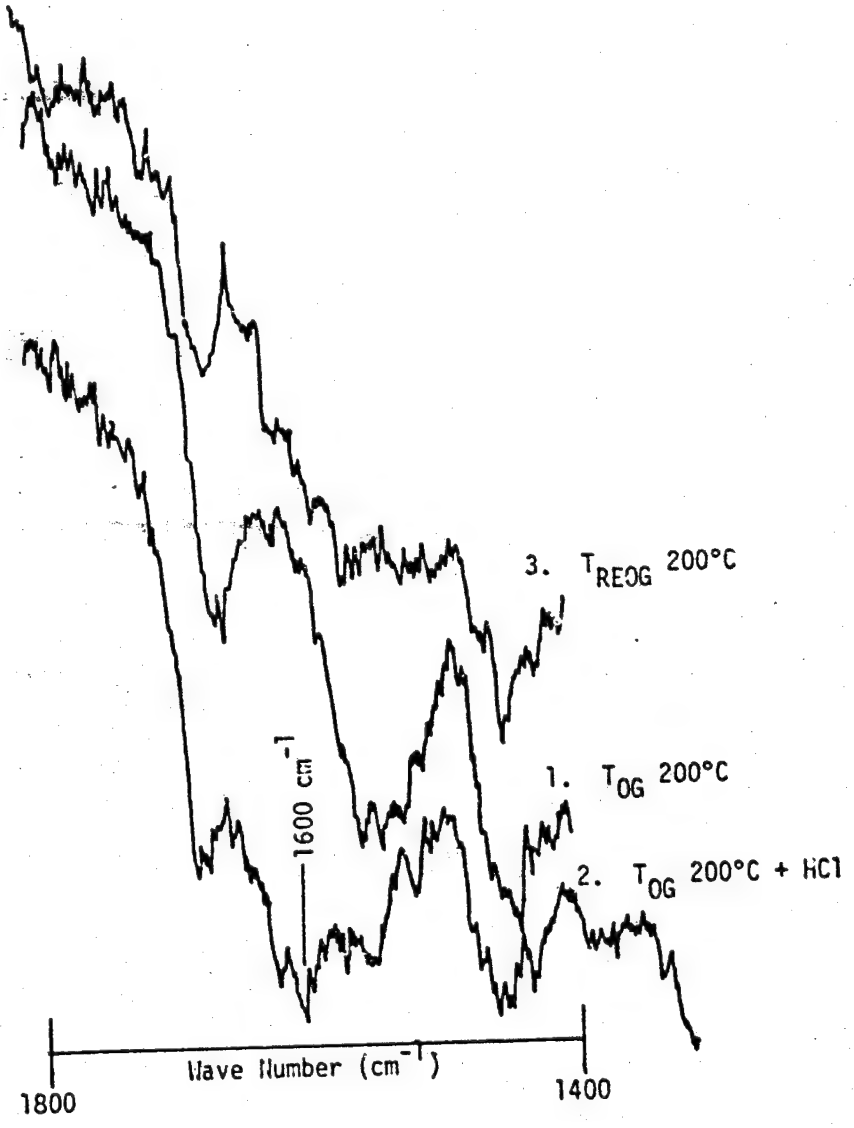

Figure 56. Infrared Spectra (1400-1800 cm^{-1}) of A2 Outgassed at 200°C Before and After Hydrogen Chloride Adsorption

measurements, ESCA analysis and infrared analysis, a mechanism for the reaction of titania surface with HCl is proposed. Both isolated and hydrogen bonded hydroxyl groups were reactive with hydrogen chloride as shown by infrared analysis. This could be summarized by the following reaction:

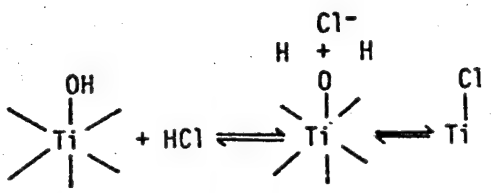

[21]

The final products were TiCl and H_2O. Since water was monomeric as observed from infrared analysis, it is possible that the species Ti H_2O^+ Cl^- is present on the surface, as shown by the intermediate state in reaction [21]. The formation of hydroxyl groups in a well defined structure as evidenced by sharp infrared band at 3550 cm^{-1}, could be explained by reaction [22].

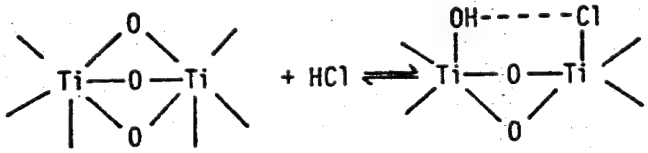

[22]

Since hydroxyl groups formed by this reaction were hydrogen bonded to chlorine atoms with a definite distance a sharp band was observed. This reaction also explains why the reaction of HCl with titania powders was independent of the number of hydroxyl groups on the surface as revealed by the adsorption data. From the calculation of the cross sectional area of HCl on the surface, it was found that two Ti ions were

involved with one HCl molecule. Therefore, this reaction involving Ti–O–Ti sites is also in agreement with the calculated cross sectional area of HCl. Hydroxyl groups that are formed by reaction [22] could not be removed by outgassing at 200°C but water could be removed at this outgassing temperature.

The surface species 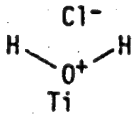 is responsible for the strong acidity observed on the surface after reaction with HCl and after reoutgassing at 100°C. Since these species were removed at an outgassing temperature of 400°C, strong acidity was not observed. The weak acid sites present on the surface may be due to the hydroxyl groups adjacent to chlorine atoms. Since chlorine is electronegative it could polarize the hydroxyl bond as shown in reaction [22] to give weakly acidic Bronsted sites.

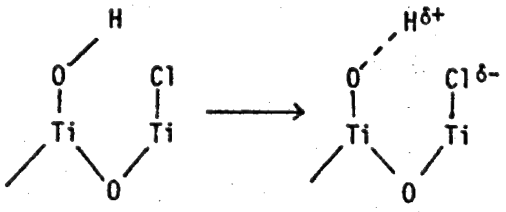

[23]

Part 2: Interaction of Polymer Adhesives with TiO_2, Ti and Ti-6-4 Powders

1. Interaction of Polymer Adhesives with Titania Powders

Heats of immersion of titania powders in polymer solutions were used to study the interaction with the polymer adhesives. The importance of proper wetting on adherend surfaces by adhesives has previously been recognized by various workers (89,90). Molecular forces of attraction cause the adhesive to wet and spread on the surface (90). Heats of immersion are a measure of the adhesion or interfacial forces between the liquid and the solid surface.

In this study, the heats of immersion of TiO_2 powders were measured in polymer solutions and in solvents. Any increase in the heat of immersion in the polymer solution compared to that in the solvent was used as a measure of the interaction between the polymer and the solid. This procedure has been used previously by Zettlemoyer et al. (103) to study the adsorption of surfactants from aqueous solutions onto Graphon. Heats of immersion of titania powders in LARC-13 solution, PPQ solution, DMF and xylene:m-cresol are shown in Table XII. It is clear that there is no significant difference between the heats of immersion of TiO_2 in DMF and in LARC-13 solution. This indicates that there is no preferential interaction of LARC-13 with any of the TiO_2 powders. Furthermore, similar heats of immersion values were obtained in xylene:m-cresol, and in PPQ solution for R3 powder. There was a small increase in the heats of immersion in PPQ compared to xylene:m-cresol for the R1 and A2 powders. However, for the A1 powder, there was a significant increase in the heat

TABLE XII

HEATS OF IMMERSION (mJ/m^2) AT 35°C OF
TITANIA POWDERS OUTGASSED AT ROOM TEMPERATURE

	A1	A2	R1	R3
DMF	287±10	353±20	308±11	297±26
LARC-13/DMF	314±27	384±35	323±37	328±10
Xylene:m-Cresol	261±17	269±10	230±3	228±40
PPQ/xylene:m-Cresol	445±17	315±24	289±6	256±5
Xylene	252	346	320	250
m-Cresol	339	269	434	212

of immersion ($\Delta_w H$) in PPQ solution compared to that in xylene:m-cresol. This increase in $\Delta_w H$ indicates that Al has a preferential interaction with PPQ. To further investigate this interaction, heats of immersion were measured as a function of concentration of PPQ in solution, and the results are shown in Figure 57. Nitrogen to titanium ratios obtained from ESCA analysis of the powders after immersion in the polymer solutions of different concentrations are also shown in Figure 57. It was clearly seen that both the N/Ti ratio and heats of immersion increase with increasing concentration of PPQ in solution. This further confirms the fact that Al has a preferential interaction with PPQ. It is important to identify the unique surface characteristics of Al which give rise to a preferential interaction with PPQ.

The lowest water adsorption capacity was found for the Al powder compared to other titania powders. This may be associated with the preferential interaction with organic polymer solution. The structures of the LARC-13 and PPQ are shown in Figure 58. It is also important to s understand the equilibrium between the PPQ and xylene:m-cresol as shown in Figure 59. Since m-cresol is an acidic solvent, the equilibrium favor production of H^+ ions. These H^+ ions can react with the lone pair of electrons on nitrogen to give positively charged PPQ. This positively charged PPQ should interact electrostatically with a negatively charged surface. From microelectrophoresis measurements (see Table III) it was found that Al had the highest negatively charged surface. Thus, the highest negatively charged Al surface interacts strongly with the positively charged PPQ.

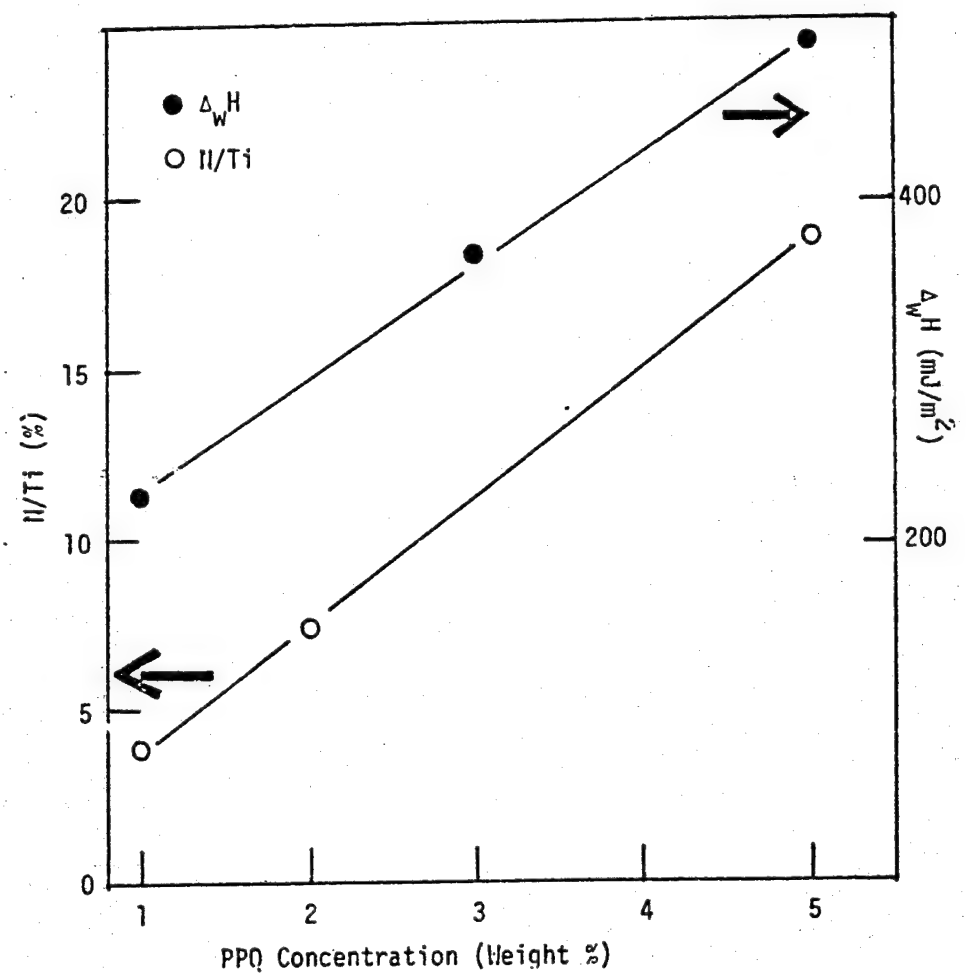

Figure 57. N/Ti Ratios and Heats of Immersion of Al as a Function of PPQ Concentration

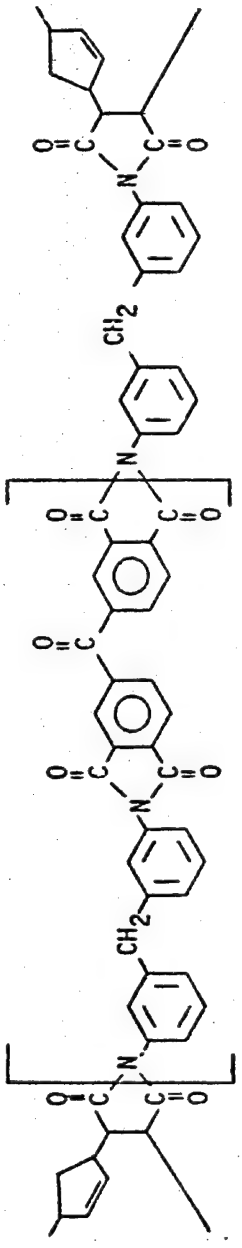

LARC-13 POLYIMIDE

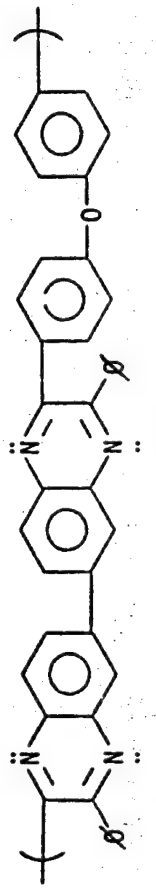

PPQ

Figure 58. Structures of LARC-13 Polyimide and Polyphenylquinoxaline

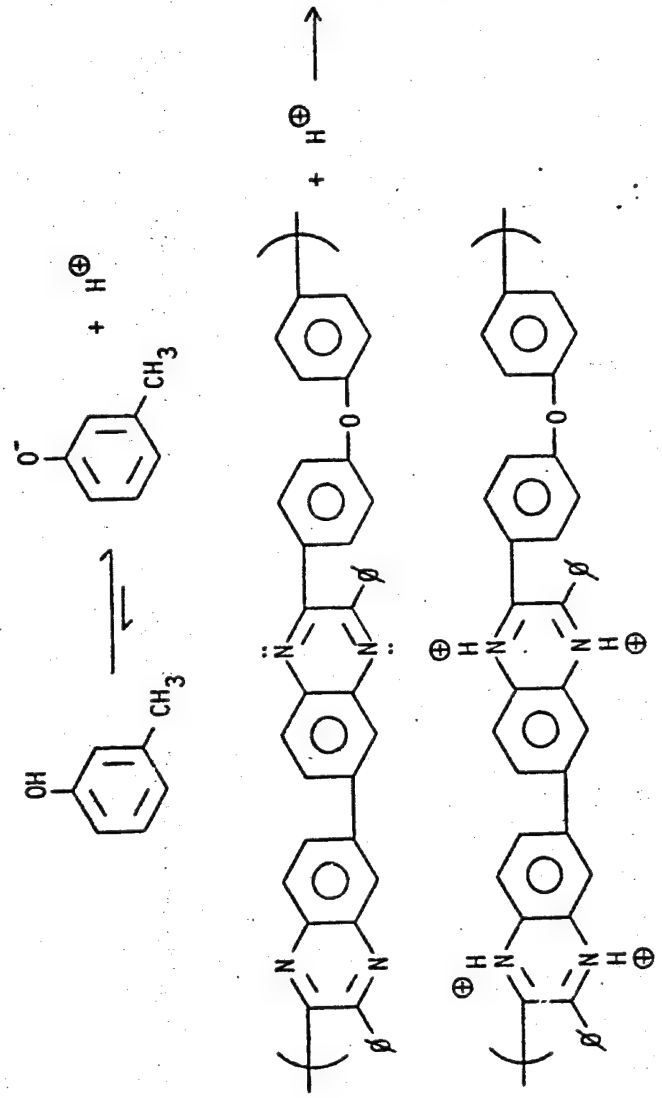

Figure 59. Equilibrium Between Polyphenylquinoxaline and Xylene:m-Cresol

2. Characterization of Ti and Ti 6-4 Metal Surfaces

The surface areas of Ti and Ti 6-4 metal powders as a function of outgassing temperature are shown in Figure 60. The surface areas of both powders were low, with Ti 6-4 having the lower surface area. A small increase in surface area was found for outgassing temperatures between 300° and 400°C for both powders.

Heats of immersion of the metal powders in water as a function of outgassing temperatures are shown in Figure 61. The heats of immersion values are higher than what was observed with titania powders at all outgassing temperatures as shown in Table XIII. The heats of immersion increase with increasing outgassing temperature. This behavior was also observed with titania powders. However, it is interesting to note the dramatic increase in heats of immersion on outgassing between 300°C and 400°C for both metal powders. To further investigate this, the Ti 6-4 powder was outgassed for 20 and 50 hours at 200° and 300°C, and the heats of immersion were measured. As shown in Figure 62, there was no change in the heats of immersion with outgassing time at 200°C. However, there was an increase in $\Delta_w H$ with increasing outgassing time at 300°C over a 50 hour period. Thus, the increase in heats of immersion observed between 300° and 400°C is a time dependent process. The long equilibriation time and large value of heat of immersion at 400°C was indicative of a strong chemical reaction. This may be due to the exposure of elemental Ti(0) at 400°C and its subsequent reaction with water. Elemental Ti can be exposed in two different ways at a higher temperature as shown in Figure 63. Metal can migrate through the oxide layer by a cation diffusion mechanism. However, this cation diffusion on pure Ti metal has been

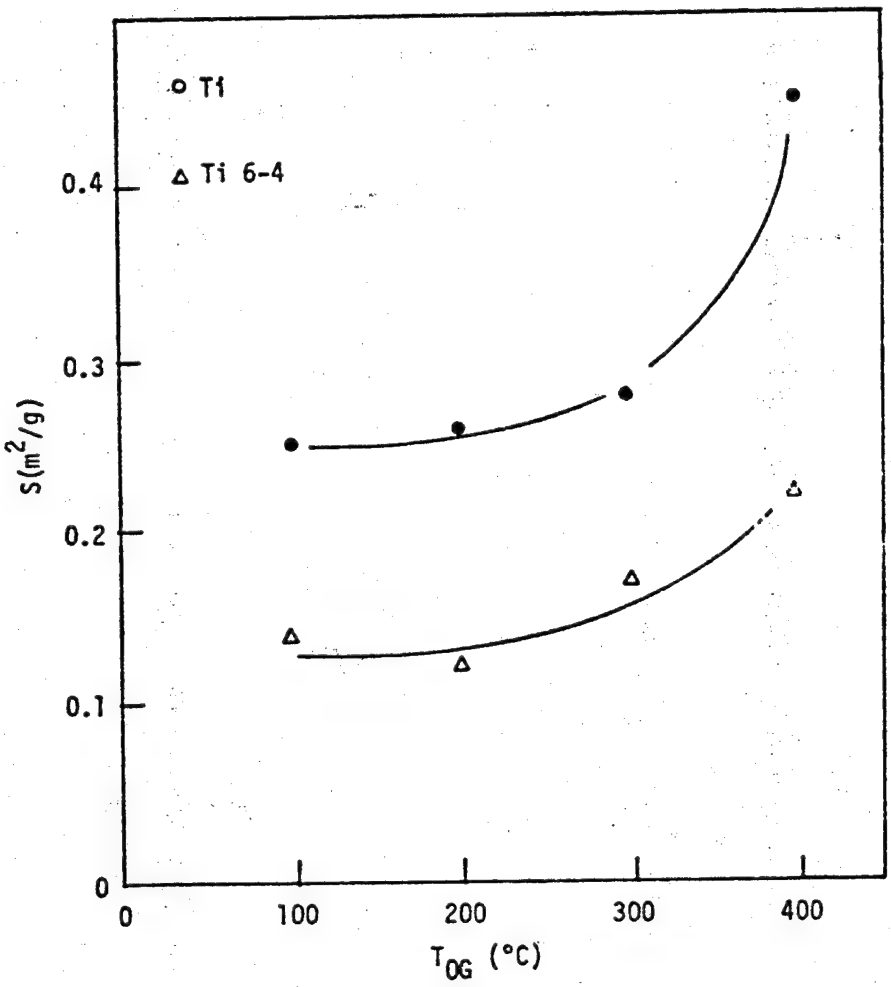

Figure 60. Surface Area of Ti and Ti 6-4 Powders as a Function of Outgassing Temperature

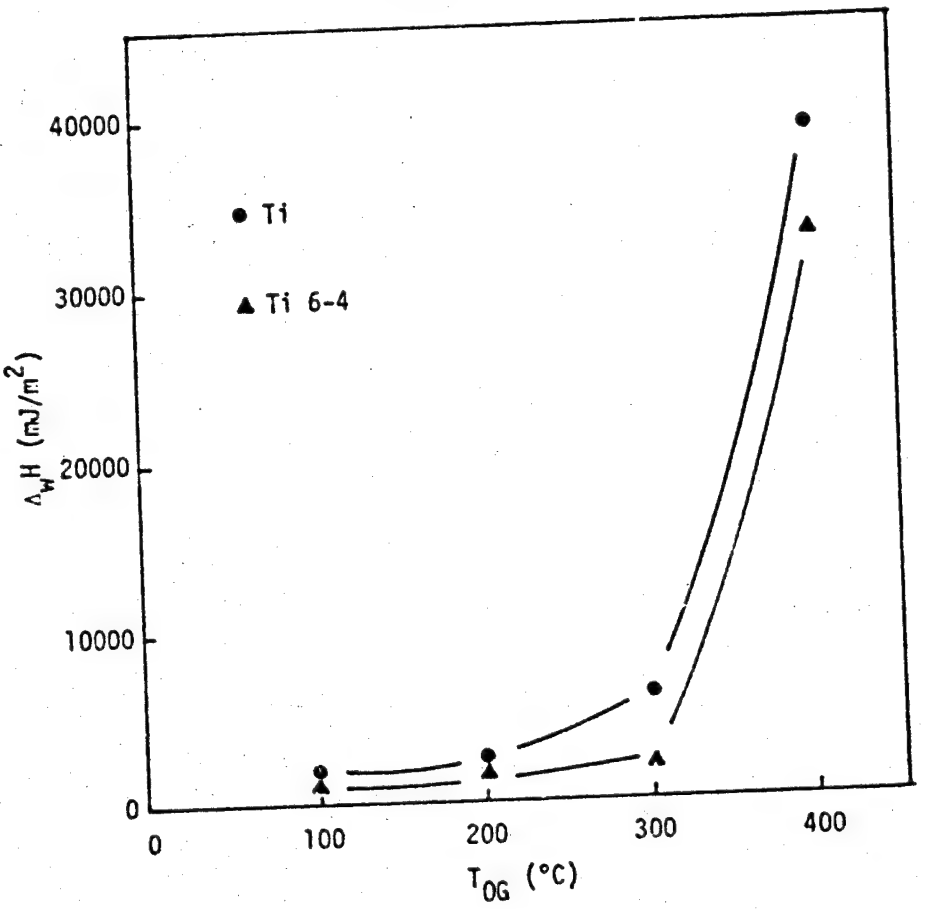

Figure 61. Heats of Immersion of Ti and Ti 6-4 Powders in Water as a Function of Outgassing Temperature

TABLE XIII

HEATS OF IMMERSION (mJ/m^2) OF TiO_2, Ti AND Ti 6-4 IN WATER

Sample	T_{OG} 100°C	T_{OG} 200°C	T_{OG} 300°C	T_{OG} 400°C
A1	382±15	423±19	474±3	425±28
A2	455±21	620±16	735±35	733±50
R1	466±18	669±26	818±37	886±40
R2	444±13	664±23	829±35	1006±12
R3	378±28	632	749	691
Ti	1424±129	2039±35	5929	38852±702
Ti 6-4	1071±36	1475±13	1829	32585

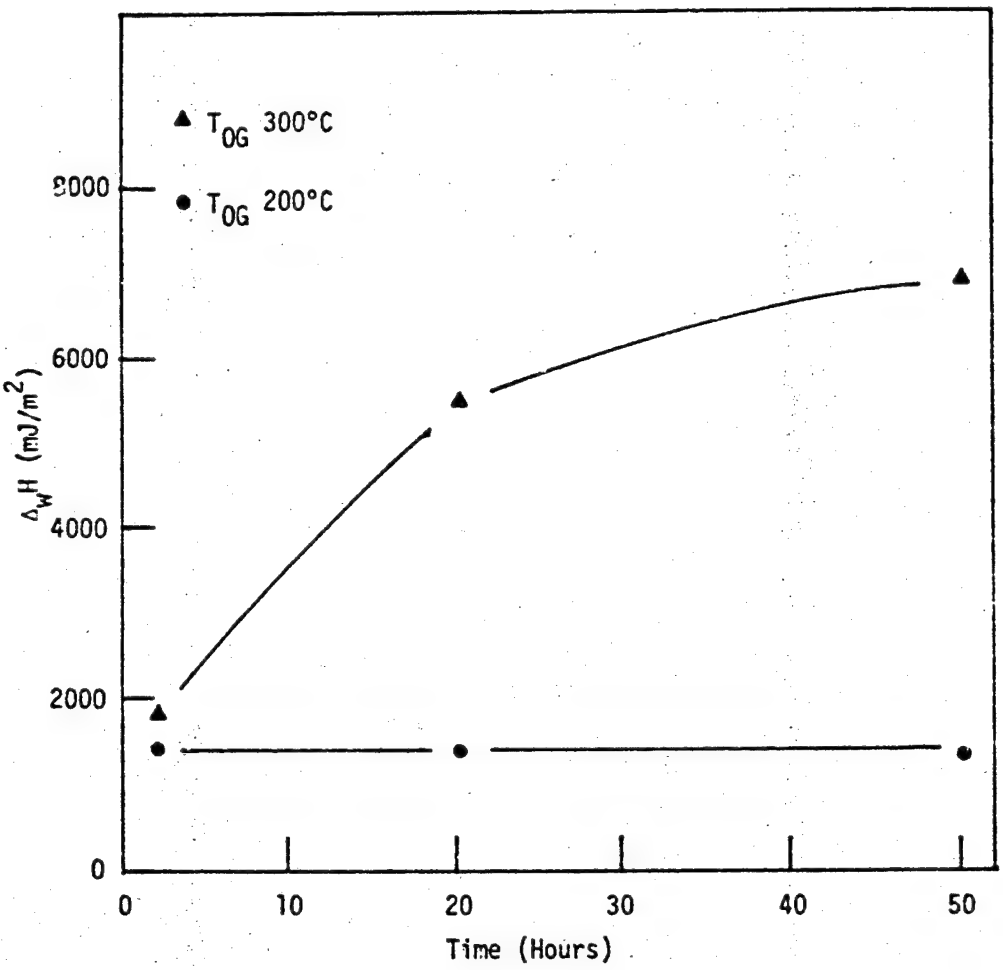

Figure 62. Heats of Immersion of Ti 6-4 as a Function of Outgassing Time

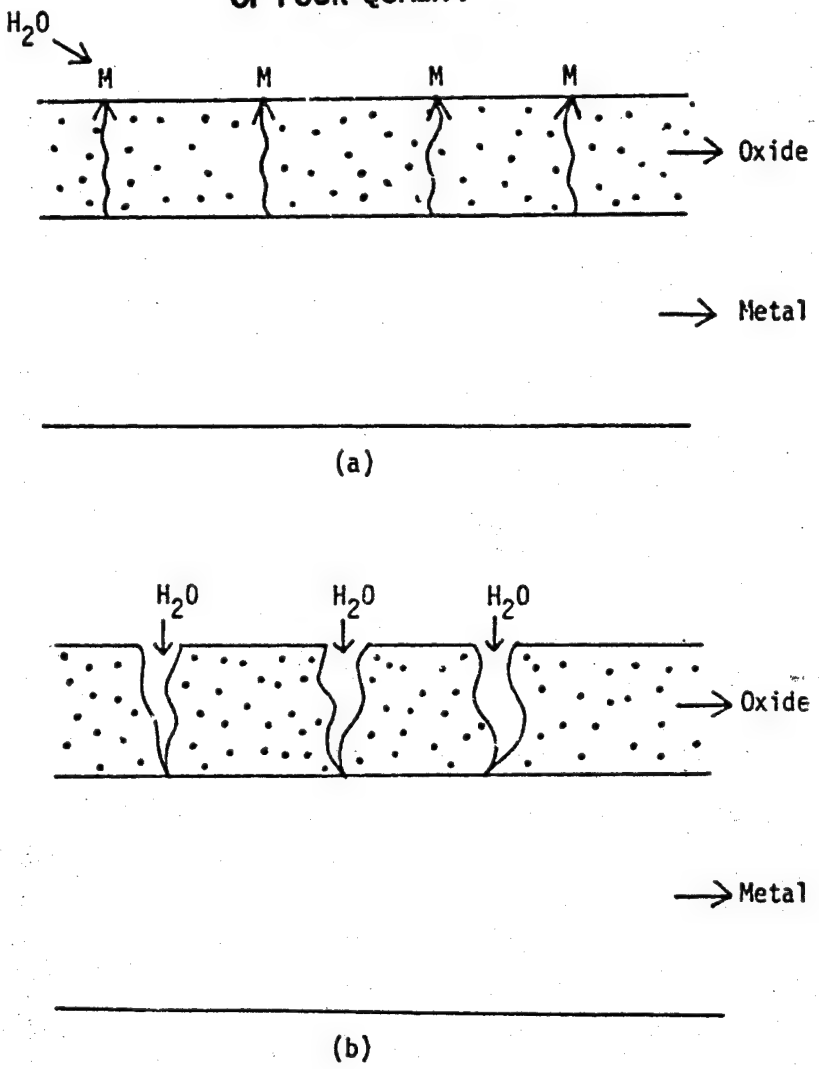

Figure 63. Mechanisms of Exposure of Elemental Metal at High Temperature: (a) Metal Migration (b) Cracking

observed previously only at 1000°C (9). The other mechanism is cracking of the oxide layer at temperatures >200°C. Here, water can penetrate through the cracks to react with the metal.

The SEM photomicrographs of untreated Ti and Ti 6-4 powders are shown in Figure 64. The surface of Ti is smooth compared to the surface of Ti 6-4. The Ti 6-4 consists of secondary particles. EDAX analysis showed only Ti on both samples. It is interesting to note that vanadium or aluminum were not detected on the Ti 6-4 sample. After outgassing at 400°C, apparent cracking of the Ti 6-4 surface was clearly observed at lower and higher magnifications as shown in Figures 65 and 66. However, similar crack features were not observed as distinctly on Ti surface after outgassing at 400°C as shown in Figure 67. Since there could be micro cracks which were not resolved at these magnifications, it is not possible to eliminate the possibility of cracking on the Ti surface. The EDAX analysis showed aluminum on Ti 6-4 after outgassing at 400°C. Therefore, aluminum has concentrated in the surface region after outgassing at 400°C.

To further investigate the possible mechanism of metal exposure, ESCA analysis was carried out on the metal powders at room temperature and after outgassing at 400°C in situ in the ESCA spectrometer. The results of this ESCA analysis are shown in Table XIV. Small amounts of elemental titanium was observed on both Ti and Ti 6-4 surfaces at room temperature. Trace amounts of Na and Al were observed on the Ti surface, while trace amounts of Al, V and N were observed on the Ti 6-4 surface. After outgassing at 400°C, there was no significant increase in the amount of elemental titanium on the Ti 6-4 surface. Thus, the

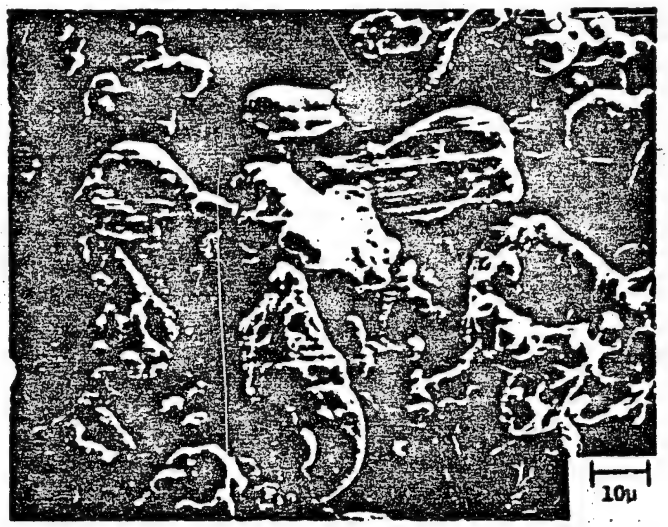

(a)

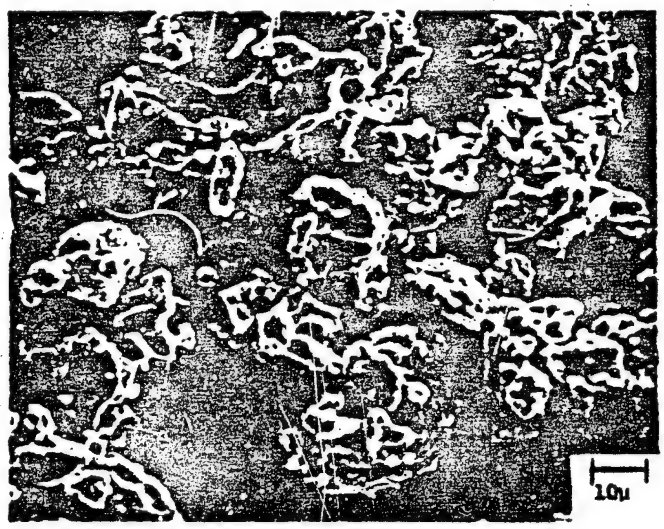

(b)

Figure 64. Scanning Electron Photomicrographs of (a) Ti and (b) Ti 6-4 at Room Temperature

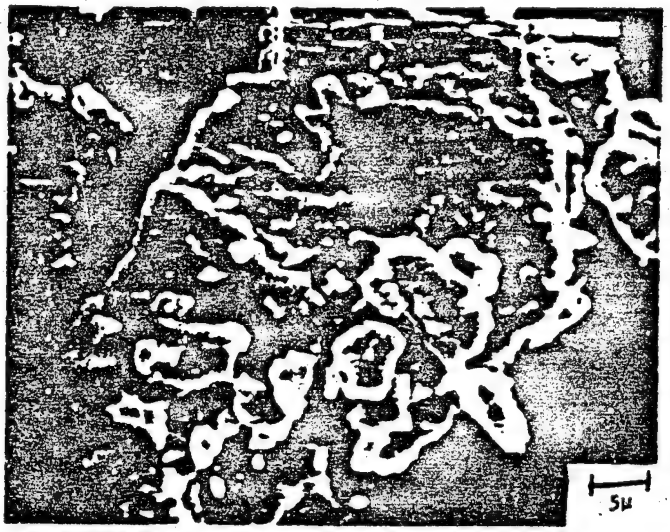

(a)

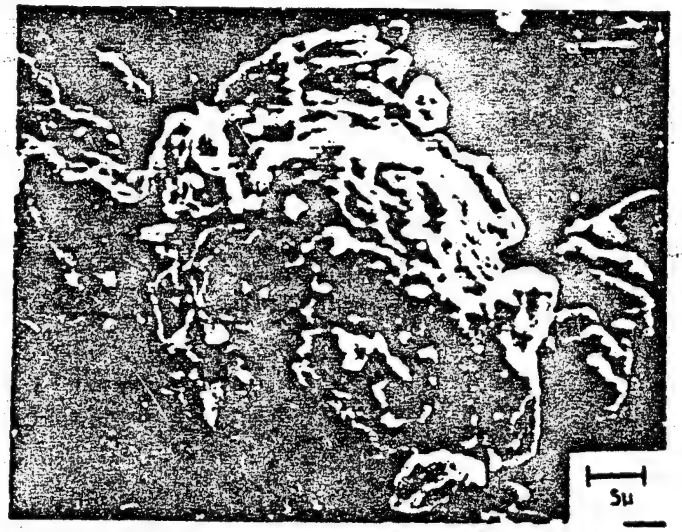

(b)

Figure 65. Scanning Electron Photomicrographs of Ti 6-4 (a) at Room Temperature (b) after Outgassing at 400°C

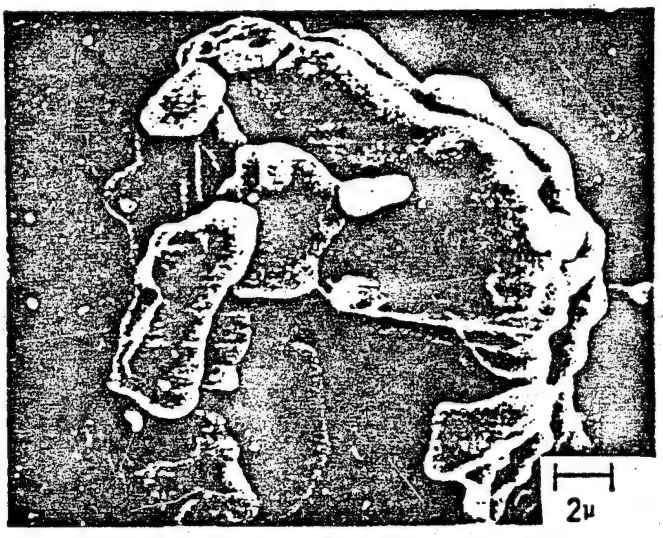

(a)

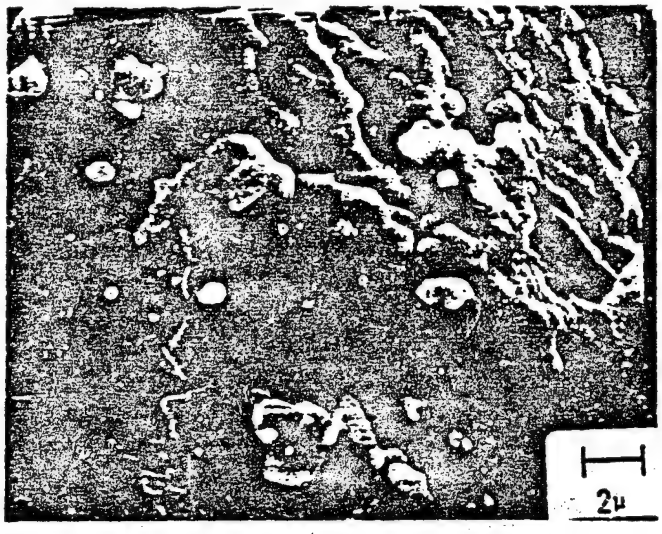

(b)

Figure 88. Scanning Electron Photomicrographs of Ti C-4 (a) at Room Temperature (b) after Outgassing at 400°C

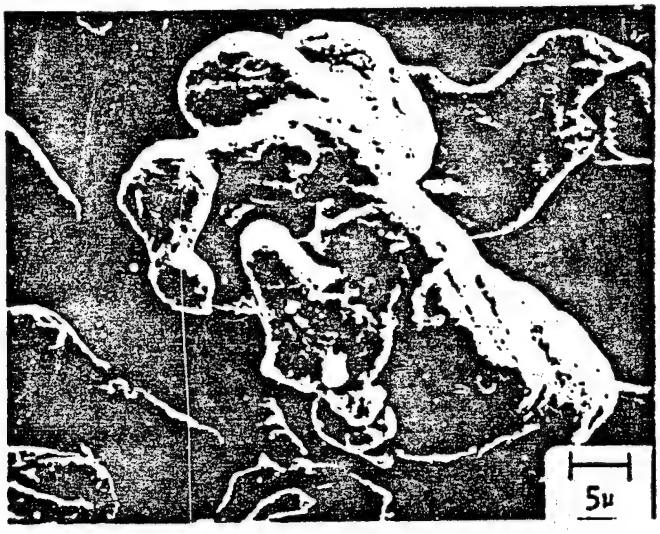

(a)

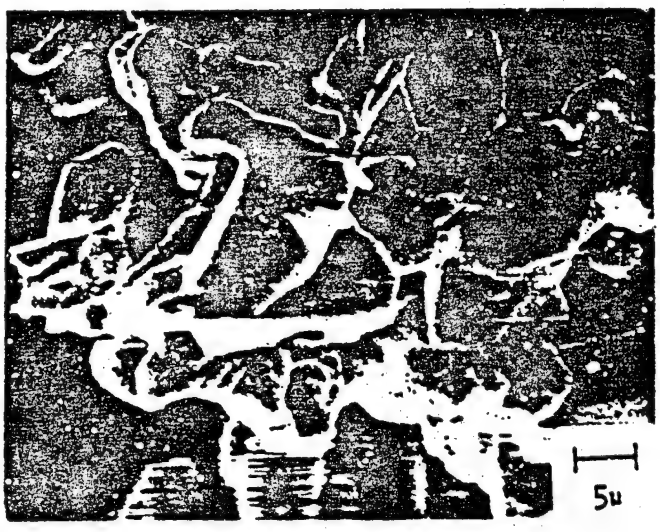

(b)

Figure G7. Scanning Electron Photomicrographs of Ti (a) at Room Temperature (b) after Outgassing at 400°C

TABLE XIV

ESCA ANALYSIS OF Ti AND Ti 6-4 POWDERS

Element	Ti		Ti OGT 400		Ti 6-4		Ti 6-4 OGT 400	
	B.E.(ev)	A.F.	B.E.(ev)	A.F.	B.E.(ev)	A.F.	B.E.(ev)	A.F.
C 1s	(284.6)	0.430	(284.6)	0.18	(284.6)	0.502	(284.6)	0.32
Al 2S	118.6	0.018	118.9	0.03	118.2	0.029	118.7	0.032
N 1s	---	---	---	---	399.2	0.010	398.7	0.02
Na 1s	1070.5	0.006	1071.7	0.02	---	---	---	---
O 1s	529.3	0.430	529.9	0.64	529.6	0.365	530.0	0.480
Ti(iv) $2p_3$	457.9	0.120	458.0	0.12	458.0	0.079	458.4	0.107
Ti(0) $2p_3$	453.6	0.001	453.6	0.004	453.4	0.001	454.1	0.003
V $2p_3$	---	---	---	---	516.0	0.005	521.2	0.03

mechanism for the exposure of elemental titanium at 400°C is probably not cation diffusion. Thus, heats of immersion is a new way to study the nature of the oxide layer on metal surfaces. It gives evidence for the possible mechanism of bond failure in thermally aged samples.

Heats of immersion of Ti and Ti 6-4 powders in water after heating at 400°C in air for two hours and subsequent outgassing at 100°C, 200°C, 300°C and 400°C are shown in Table XV. After heating at 400°C in air, heats of immersion at an outgassing temperature of 200°C were lower than that at an outgassing temperature of 100°C for both samples. The heats of immersion values in water after outgassing at 400°C were similar for the heated and fresh Ti samples. However, for Ti 6-4 after heating in air at 400°C, the heats of immersion in water were significantly lower than the fresh sample after outgassing at 400°C. The oxide layer on Ti 6-4 may have grown thicker after heating at 400°C in air. Therefore, the exposure of elemental Ti through this thick oxide layer was less and this gave rise to low heats of immersion in water. Scanning electron photomicrographs of Ti and Ti 6-4 after heating at 400°C in air are shown in Figure 68. The surfaces have not visibly changed as a result of heating. If cracking of the oxide layer occurred, very large fissures did not result. EDAX analysis showed the presence of aluminum on the Ti 6-4 surface after this heat treatment. Thus, similar to the observation made after heating in vacuum at 400°C, by heating the Ti 6-4 to 400°C in air, aluminum has concentrated in the surface region ($\sim$ 1μm).

Water vapor adsorption and readsorption isotherms at 30°C for Ti and Ti 6-4 after outgassing at 100°C are shown in Figure 69. The readsorption isotherm was significantly lower than the adsorption isotherm for

TABLE XV

HEATS OF IMMERSION (mJ/m^2) OF Ti AND Ti 6-4 HEATED IN AIR AT 400°C

T_{OG}(°C)	Ti Heated at 400°C	Ti 6-4 Heated at 400°C
100	6688	3878
200	2654	1216
300	2568	1445
400	37832	23020

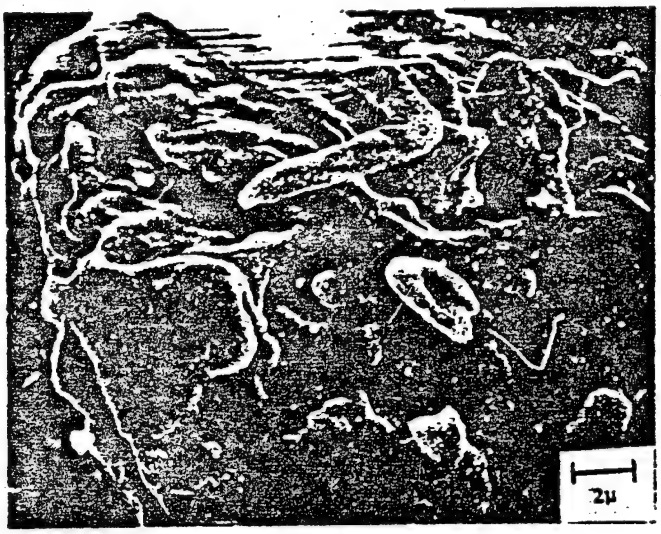

(a)

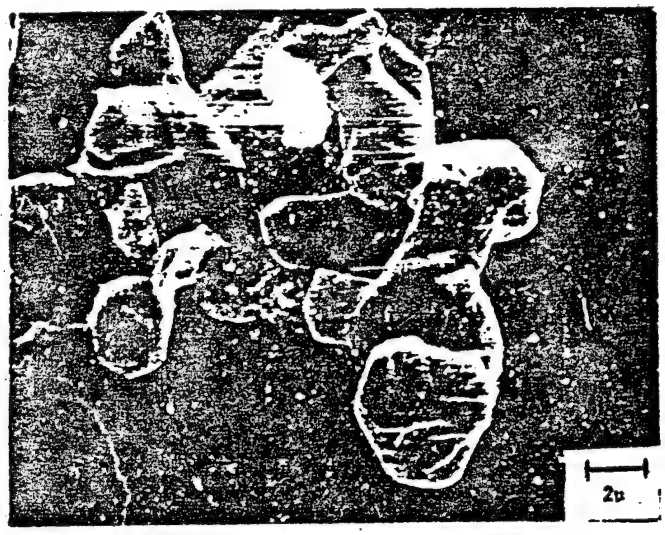

(b)

Figure 68. Scanning Electron Photomicrographs of (a) Ti 6-4 (b) Ti Heated in Air at 400°C

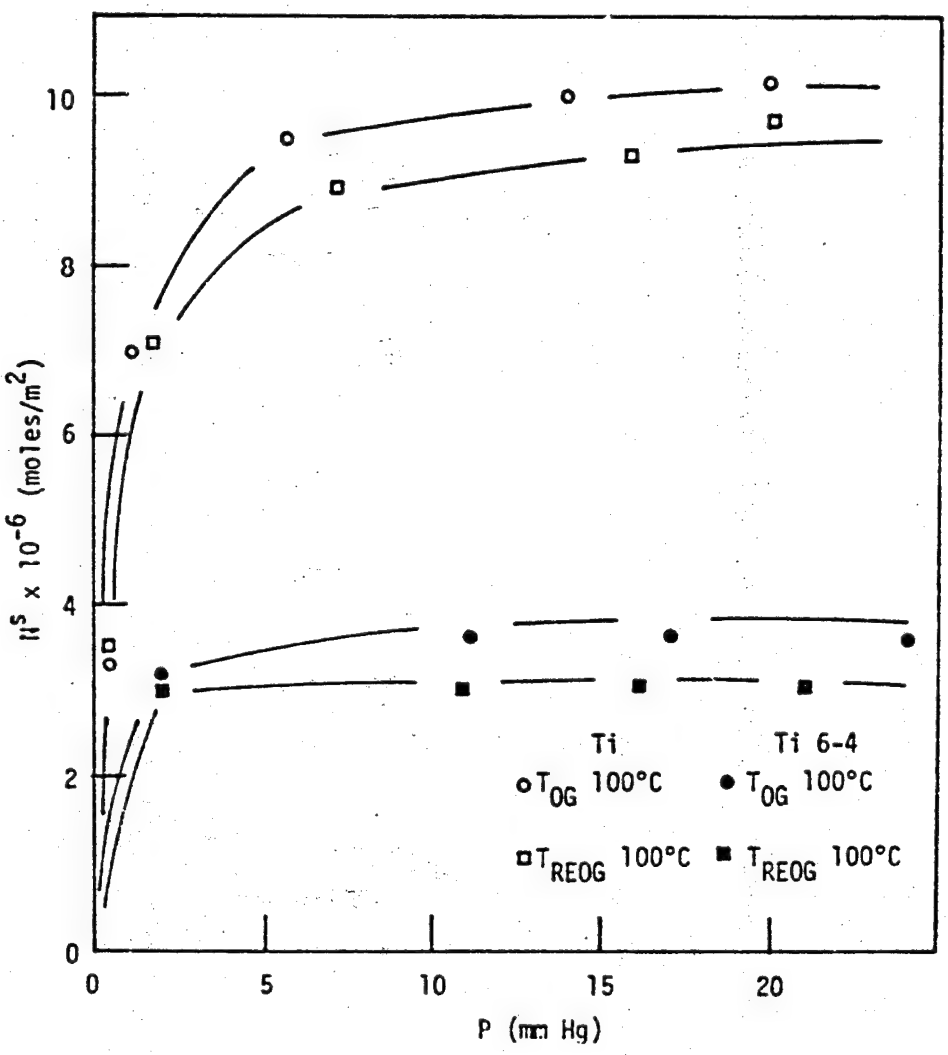

Figure 69. Adsorption and Readsorption Isotherms at 30°C for Water on Ti and Ti 6-4 Outgassed at 100°C

both Ti and Ti 6-4 powders. This indicated that there was irreversible adsorption of water vapor after outgassing at 100°C. Furthermore, a lower water adsorption capacity was observed for Ti 6-4 compared to Ti. The water vapor isotherms at 30°, 40° and 50°C for Ti outgassed at 100°C are shown in Figure 70. The adsorption was lower at 50°C compared to that at 30°C. However, the temperature dependence on isotherms was not very strong. This temperature dependence of water vapor adsorption was not seen for Ti 6-4 after outgassing at 100°C. This may be due to the irreversibility of the adsorption process.

3. Interaction of Polymer Adhesives PPQ and LARC-13 with Ti and Ti 6-4 Metal Powders

The heats of immersion of Ti, Ti 6-4 metal powders after outgassing at room temperature in solutions of PPQ, LARC-13, DMF and xylene:m-cresol are shown in Table XVI. The heats of immersion in LARC-13 solutions were significantly higher than those in DMF for both the Ti and Ti 6-4 powders. Thus, LARC-13 interacts preferentially with Ti and Ti 6-4 metal powders in contrast to the observations on crystalline titania powders. The difference in the heats of immersion between DMF and LARC-13 solutions were greater on Ti 6-4 than that on Ti powder. The heats of immersion for two metal powders in PPQ solutions were significantly higher than the heats of immersion in xylene:m-cresol. This indicates that PPQ also preferentially interacts with metal powders. The interaction was again more significant on Ti 6-4 compared to that on Ti surface. This may be attributed to the lower water adsorption capacity of Ti 6-4 compared to Ti. Both PPQ and LARC-13 are

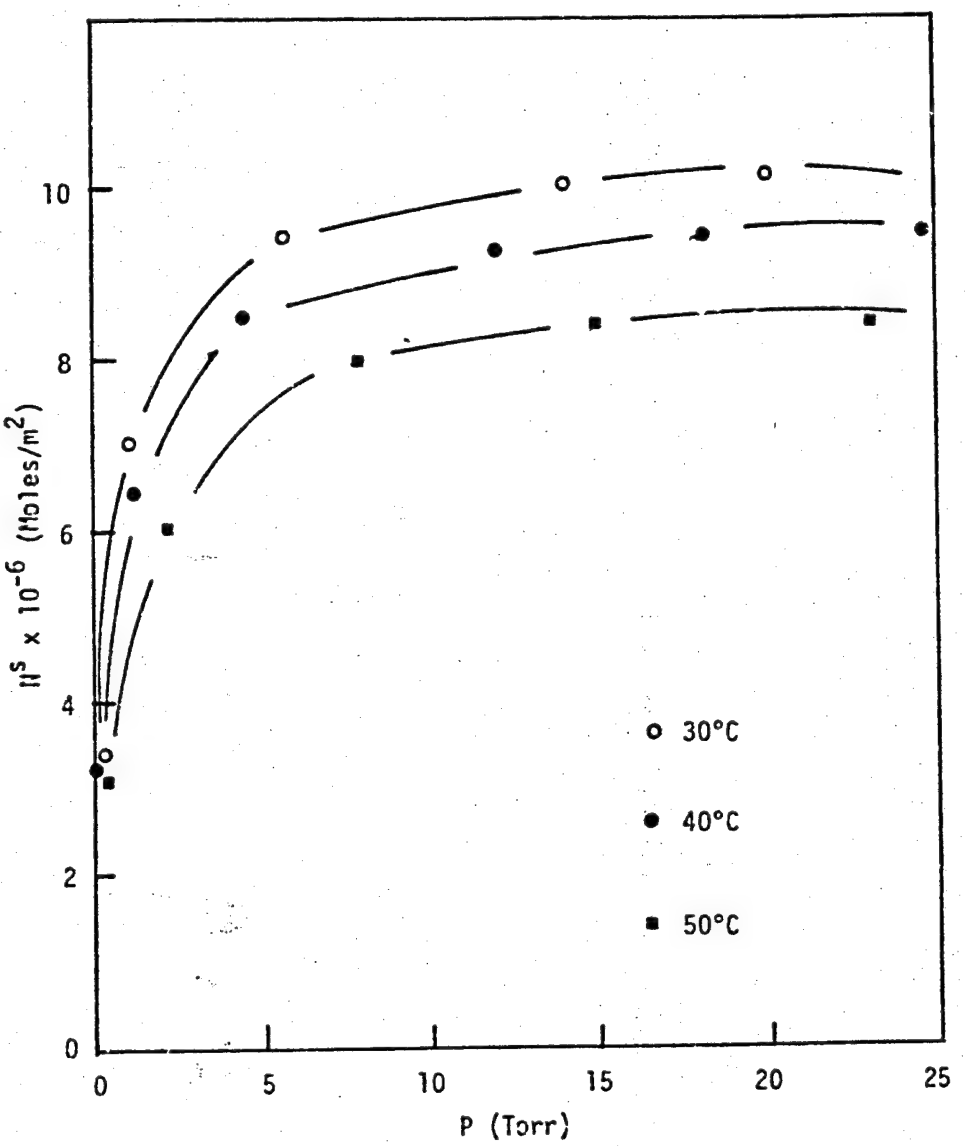

Figure 70. Temperature Dependence on Water Adsorption Isotherms of Ti Outgassed at 100°C

TABLE XVI

HEATS OF IMMERSION (mJ/m^2) OF Ti, Ti 6-4, AND Ti 6-4 AFTER PRETREATMENTS

SAMPLE	DMF	LARC-13/DMF	XYLENE:m-CRESOL	PPQ/XYLENE:m-CRESOL
Ti	1065±153	1492±60	891±54	1262±147
Ti 6-4	233±70	745±36	284±90	693±4
Ti 6-4 Turco	1077±100	2484±150	924±60	2319±200
Ti 6-4 Phosphate Fluoride	1445±150	3298±200	1276±150	2073±250

used to bond Ti 6-4 in metal structures. Since molecular attractive forces contribute to the heats of immersion, the above observations serve to re-emphasize that molecular forces play an important role in metal-polymer bonding.

It is also interesting to note the marked differences between the pure crystalline titania powders and the oxide surfaces present on the metal powders as shown in Table XVII. This indicates that crystalline titania powders are not a good choice to simulate the oxide surfaces on Ti or Ti 6-4 coupons.

Heats of immersion of Ti in LARC-13 solutions as a function of outgassing temperature are shown in Figure 71. The difference in heats of immersion between LARC-13 solution and DMF increased with increasing outgassing temperature up to 300°C. This is probably due to the removal of water molecules from adsorbing sites by high temperature outgassing, thus facilitating the reaction with LARC-13 polymer. However, at 400°C this difference was negligible, but the absolute values of heats of immersion were very high. This high value for the heat of immersion at 400°C is attributed to the reaction of elemental titanium metal with the solution. However, once the metal is exposed, the LARC-13 did not show any preferential interaction.

The heats of immersion of Ti 6-4 in LARC-13 solution, DMF, PPQ solution and m-cresol:xylene as a function of outgassing temperatures are shown in Figure 72. As observed with Ti in LARC-13 solution, the difference in the heats of immersion between the polymer solution and the solvent increased up to outgassing temperature of 300°C. The difference in the heats of immersion became negligible at 400°C. This again

TABLE XVII

COMPARISON OF THE PROPERTIES OF CRYSTALLINE TITANIA AND THE OXIDE LAYER PRESENT ON THE METAL POWDERS

Property	TiO_2	Ti and Ti 6-4
1. Heats of Immersion in water		High
(a) T_{OG} 100°C-300°C	400-800 mJ/m^2	1000-6000 mJ/m^2
(b) T_{OG} 400°C	400-1000 mJ/m^2	32000-39000 mJ/m^2
2. Water vapor Adsorption	Fully Reversible	Partially Reversible
3. Surface Area	10-50 m^2/g	0.1-0.2 m^2/g - low
4. Interaction with LARC-13 solution	No preferential Interaction	Preferential Interaction
5. Interaction with PPQ solution	Only Al shows preferential Interaction	Preferential Interaction

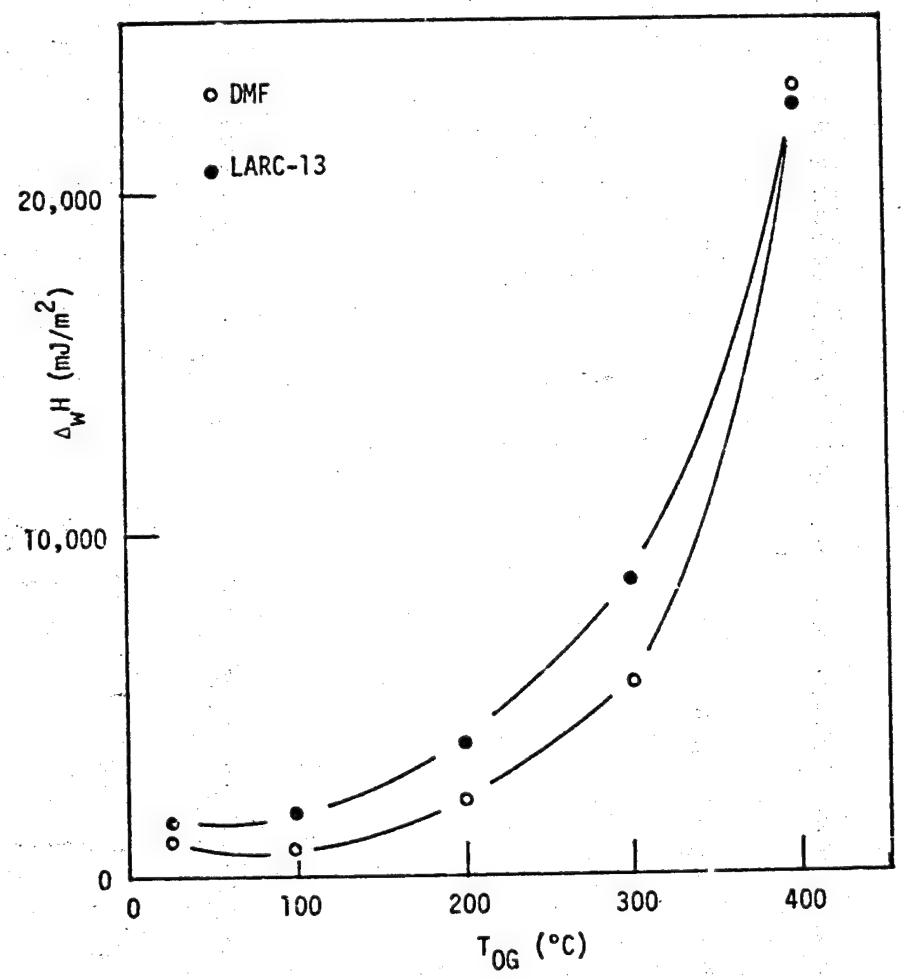

Figure 71. Heats of Immersion of Ti in LARC-13 and DMF as a Function of Outgassing Temperature

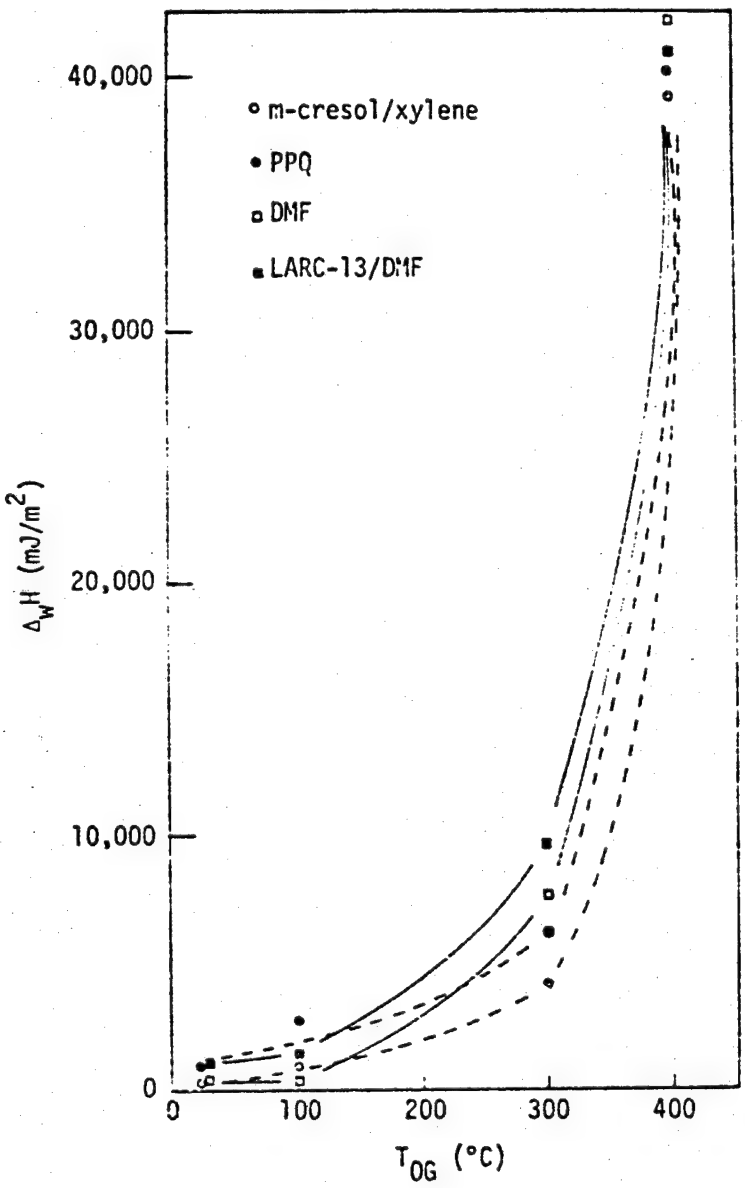

Figure 72. Heats of Immersion of Ti 6-4 in Polymer Solutions as a Function of Outgassing Temperature

indicates that once the elemental metal was exposed to the polymer solution, a levelling effect in which no preferential interaction with PPQ and LARC-13 on Ti 6-4 surface was observed.

The heats of immersion of Ti in PPQ solution and in xylene:m-cresol as a function of outgassing temperature are shown in Figure 73. The difference in heats of immersion between the polymer and the solvent increased with increasing outgassing temperature. However, at 400°C the heat of immersion in PPQ solution was significantly higher than that in the m-cresol:xylene. Therefore, once the elemental titanium was exposed at 400°C, PPQ interacted preferentially with the Ti surface. This behavior was not observed with Ti 6-4 and PPQ. EDAX analysis showed the presence of aluminum after outgassing the Ti 6-4 at 400°C. Thus, this difference in the interaction with PPQ at outgassing temperature could be due to the presence of aluminum on Ti 6-4 surface.

4. Pretreated Ti 6-4 Surfaces

The properties of Ti 6-4 powders after Turco and phosphate-fluoride pretreatments were investigated in this study since significant improvements in adhesive bonding have been observed following these pretreatments.

The surface areas of Ti 6-4 pretreated with Turco and phosphate-fluoride processes were 0.25 m^2/g and 0.24 m^2/g, respectively. There is an appreciable increase in surface area after both the pretreatments. The scanning electron photomicrographs of the Ti 6-4 powders after the two pretreatments are shown in Figure 74. There were no significant differences in powder morphology after either pretreatment. EDAX

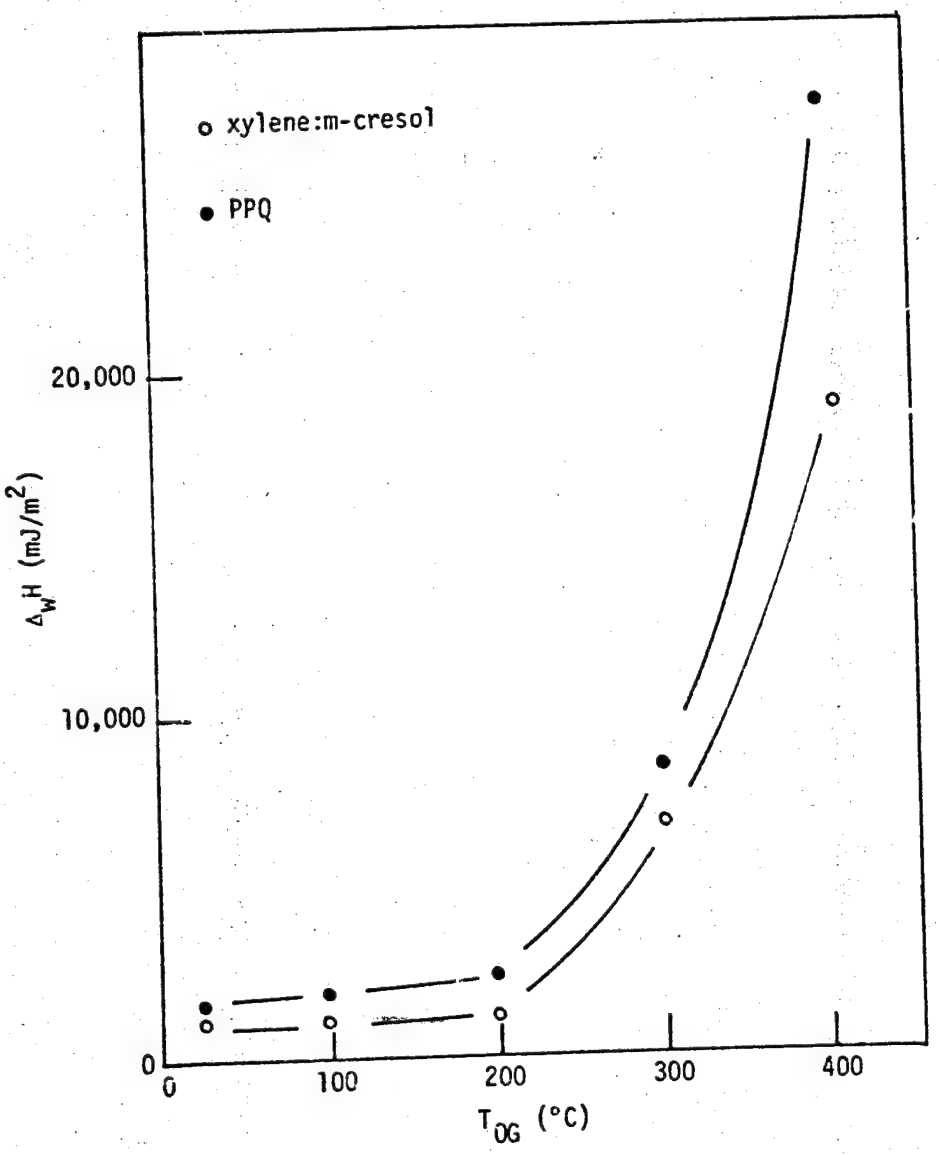

Figure 73. Heats of Immersion of Ti in PPQ Solution as a Function of Outgassing Temperature

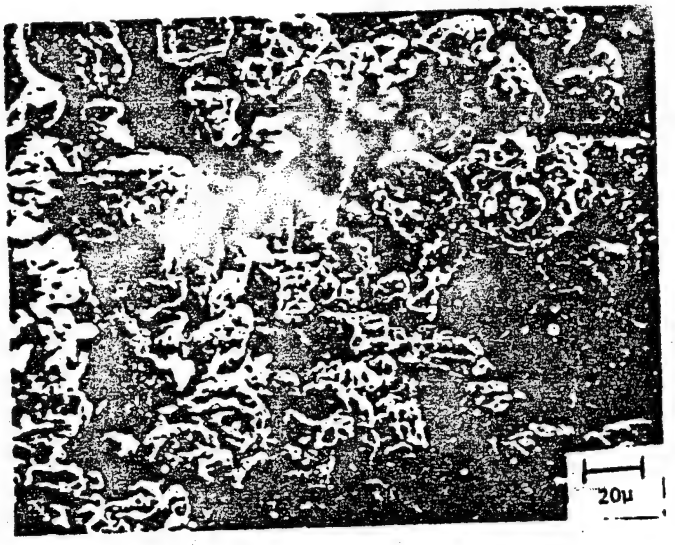

(a)

(b)

Figure 74. Scanning Electron Photomicrographs of Ti 6-4 after (a) Turco (b) Phosphate-fluoride Pretreatments

analysis showed the presence of aluminum on the phosphate-fluoride etched surface.

Heats of immersion of Ti 6-4 after the phosphate-fluoride and Turco pretreatments in water are shown in Figure 75. The heats of immersion were similar up to a 200°C outgassing temperature. However, at 300°C, heats of immersion values were slightly higher on the pretreated surfaces than on the untreated surface. At 400°C, the phosphate-fluoride etched surface showed a significantly higher heat of immersion value compared to both Turco etched and fresh Ti 6-4 surfaces. It has been shown by previous workers (85) that the Ti 6-4 surface pretreated with phosphate-fluoride process results in a thin oxide layer. Therefore, exposure of elemental titanium through this thin oxide layer would be easier. Hence, after phosphate-fluoride pretreatment, a higher value of heats of immersion in water was observed.

The heats of immersion of untreated and pretreated Ti 6-4 in polymer solutions and solvents are shown in Table XVI. It is clearly seen that the difference in heats of immersion between the polymer solution and solvents have increased considerably after pretreatment of the Ti 6-4. Thus, there is calorimetric evidence that pretreatment processes can enhance the bonding between the polymers and Ti 6-4 surface. The preferential interactions of LARC-13 and PPQ were similar on Ti 6-4 after the Turco pretreatment as noted by the difference in heats of immersion in the solvent and polymer solution. However, interaction between LARC-13 and phosphate-fluoride pretreated Ti 6-4 was significantly stronger than the interaction with PPQ. Thus, this heat of immersion study further

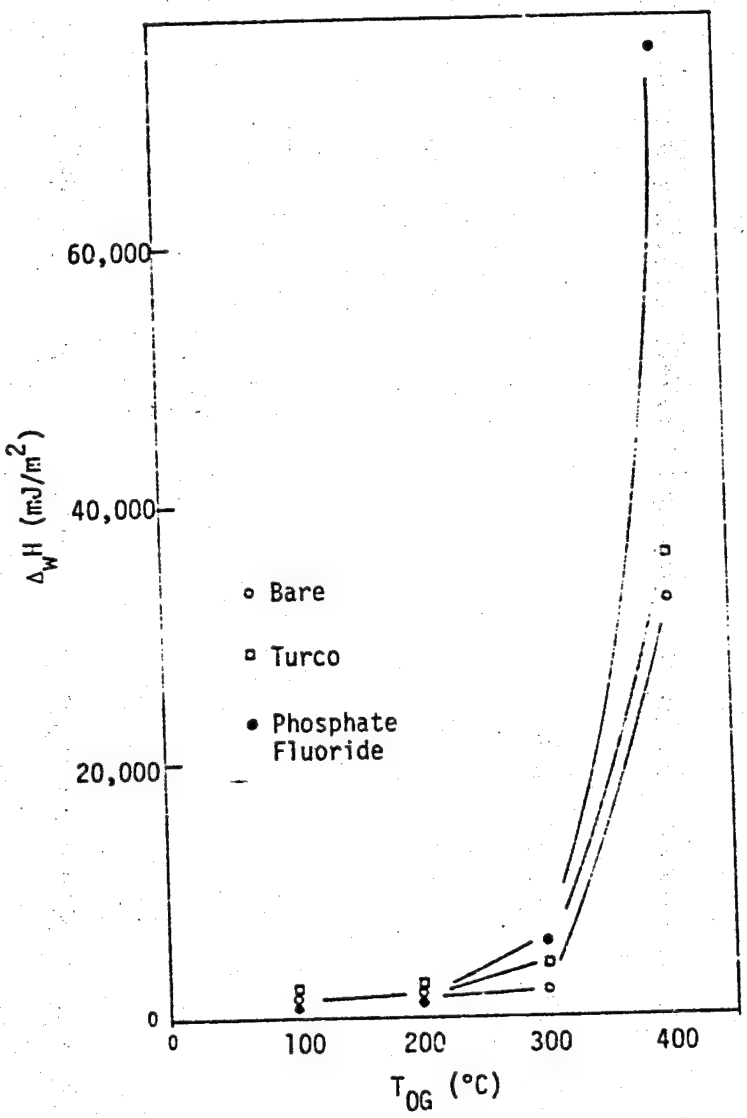

Figure 75. Heats of Immersion of Ti 6-4 after Turco and Phosphate-fluoride Pretreatments

establishes the importance of surface pretreatment in metal-polymer bonding. It gives further evidence for the bonding mechanism involving molecular forces of attraction in the adhesion process.

V. SUMMARY

A summary follows of the interaction between water and hydrogen chloride with both anatase and rutile TiO_2 powders.

X-ray diffraction analysis showed that powder A1 was 100% anatase, A2 was 87% anatase and 13% rutile, and R1, R2 and R3 were 100% rutile. SEM/EDAX analysis showed secondary particles giving only Ti signals. ESCA analysis showed that the two rutile powders R1 and R2 were alumina-coated. Chlorine, phosphorus and potassium were detected on A1 powder. The indicator method showed that R1, R2, A1 and A2 powders were basic ($pK_a > 7.6$). This basicity was unchanged by outgassing at 400°C. Powder R3 was found to be acidic ($pK_a \sim 1.5$) and a decrease in acidity ($pK_a \sim 2.8$) was found after outgassing at 400°C. A drastic reduction in acidity ($pK_a > 7.6$) was found after oxygen treatment on R3 outgassed at 400°C.

Microelectrophoresis analysis showed that A1 had the highest negatively charged surface, while R3 had the highest positively charged surface. Surface charge was not affected on A1, A2, R1 and R2 powders by outgassing at 400°C while a decrease in positive charge was observed on R3 powder. Infrared analysis of A2 showed the presence of three kinds of hydroxyl groups, namely isolated, hydrogen bonded and bridged hydroxyl groups. Powder A1 showed less dependence of the heat of immersion in water on outgassing temperature (100-400°C) than the other titania powders. A2, R1 and R2 showed an increase in heats of immersion with increasing outgassing temperature. R3 showed a maximum in the heat of immersion at 300°C.

Water adsorption capacity of A1 powder was not affected by increasing outgassing temperature from 100 to 400°C. This was attributed to the presence of phosphorus which can replace the hydroxyl groups on the A1 surface. A2, R1 and R2 showed an increase in water adsorption capacity with increasing outgassing temperature similar to the heat of immersion data. This is due to the successive removal of hydroxyl groups with different energies at higher outgassing temperatures. R3 showed an increase in heats of immersion with increasing outgassing temperature and a decrease at 400°C. This decrease in adsorption capacity, heats of immersion, surface acidity and surface charge at 400°C was attributed to the irreversible condensation of hydroxyl groups. Isosteric heats of adsorption of water on R3 and A2 outgassed at 100°C were comparable to the heats of adsorption involved in the formation of hydrogen bonds between adsorbed water molecules and surface hydroxyl groups. Powder A1 after outgassing at 100° and 400°C showed low isosteric heats of adsorption.

Adsorption of HCl at 30°C on all titania powders outgassed at 100°, 200° and 400°C showed a dependence on the outgassing temperature. This dependence was highest for R3 powder while it was lowest for A1 powder. Part of the HCl was irreversibly adsorbed at 30°C on all titania powders and could not be completely removed by reoutgassing at 100°C. For A1, A2, R1 and R2 powders this irreversibly adsorbed HCl could not be even removed by reoutgassing at 400°C. However, adsorbed HCl on R3 powder was completely removed by reoutgassing at 400°C. A1 showed the highest HCl adsorption while R3 showed the lowest. Thus, HCl adsorption was found to be independent of the number of hydroxyl groups present on the surface.

Titania surfaces were found to be strongly acidic ($pK_a < 1.5$) after HCl adsorption. ESCA analysis showed the presence of Cl on all titania samples after HCl adsorption. It was not possible to distinguish whether the chlorine was ionic or covalently bonded. Infrared analysis of A2 after HCl adsorption showed the formation of new type of hydroxyl groups and water. Based on the experimental data a mechanism for the HCl reaction was proposed involving both $Ti\overset{O}{\diagdown\diagup}Ti$ sites and Ti-OH sites. Heats of immersion of titania in aqueous HCl was higher than in water. Further, the heat of immersion was very high in HCl for R1 and R2 powders due to dissolution of the alumina coating.

A summary follows of the heats of immersion of TiO_2, Ti and Ti 6-4 powders in water, polymer primer solution and solvents. Heats of immersion of Ti and Ti 6-4 metal powders in water were significantly higher than for the titania powders. The heats of immersion increased with increasing outgassing temperature and an anomalous increase was observed between 300° and 400°C. Further, the heat of immersion was independent of outgassing time at 200°C but increased for longer outgassing times at 300°C. These results were attributed to exposure of water to elemental titanium as a result of cracking of the thin oxide surface layer at 400°C. SEM photomicrographs of Ti showed evidence of cracking at 400°C. ESCA analysis did not support the possibility of metal migration through the oxide layer.

LARC-13 polyimide did not interact preferentially with any of the titania powders. However, polyphenylquinoxaline (PPQ) interacted preferentially with Al powder. Both polymers LARC-13 and PPQ interacted preferentially with Ti and Ti 6-4 powders as gauged by the larger heats

of immersion of the powders in the polymer solutions compared to the solvents.

A very high heat of immersion in water was observed after outgassing phosphate-fluoride etched Ti 6-4 sample at 400°C compared to the Turco etched sample. This could be due to the presence of a thinner oxide layer for the phosphate-fluoride etched powder. Both pretreated Ti 6-4 samples showed enhanced interaction with both LARC-13 and PPQ.

REFERENCES

1. Hendricks, C. L.; "Evaluation of High Temperature Structural Adhesives for Extended Service", NASA Contract NAS1-15605 Semi Annual Report, Boeing Aerospace Co., June 1979.
2. Baun, W. L.; "Surface Characterization of Titanium and Titanium Alloys". Part I: Effect on Titanium -6Al-4V Alloy of Commercial Treatments", Technical Report AFML-TR-76-29, Part 1, 1976.
3. Hamilton, W. C.; Lyerly, G. A.; Appl. Polym. Symp., 1972, 19, 105-124.
4. Dwight, D. W.; Counts, M. E.; Wightman, J. P.; Colloid and Interface Science, Vol. III, Ed. Kerker, M.; 143-156, Academic Press, New York, 1976.
5. Beck, B.; Siriwardane, R.; Wightman, J. P.; "A Fundamental Approach to Adhesion, Synthesis, Surface Analysis, Thermodynamics and Mechanics", NASA Report, NSG-1124, 1981.
6. Mason, J. G.; Siriwardane, R. V.; Wightman, J. P.; J. Adhes., 1981, 11, 315.
7. Benninghoven, A.; Bispinck, H.; Ganschow, O.; Wiedmann, L.; Appl. Phys. Lett., 1977, 31, 1.
8. Motte, F.; Coddet, C.; Sarrazin, P.; Azzopardi, M.; Beson, J.; Oxid. Met., 1976, 10, 113.
9. Wiseman, T. J.; "Inorganic White Pigments", Ed. Parfitt, G. D.; Sing, K.S.W.; Characterization of Powder Surfaces, Academic Press, 1976.

10. Chemical Engineering News, April 27, 1981.

11. Munuera, G.; Stone, F. S.; Trans. Faraday Soc., 1971, 67, 205-238.

12. Boutin, H.; Prask, H.; Iyengar, R. D.; J. Catal., 1967, 9, 309-12.

13. Primet, M.; Basset, J.; Mathieu, M. V.; Prettre, M.; J. Phys. Chem., 1970, 74, 15.

14. Day, R. E.; Prog. Org. Coatings, 1973/4, 2, 269.

15. Garey, C. L.; Ed. "Physical Chemistry of Pigments in Paper Coating", Tappi Press, 1977.

16. Cotton, F. A.; Wilkinson, G.; "Advanced Inorganic Chemistry", Interscience Publishers, 1966.

17. Yates, D.J.C.; J. Phys. Chem., 1961, 65, 746.

18. Dawson, P. T.; J. Phys. Chem., 1967, 71, 4.

19. Day, R. E.; Parfitt, G. D.; Trans. Faraday Soc., 1967, 63, 708.

20. Herrington, K. D.; Lui, Y. K.; J. Colloid Interface Sci., 1970, 34, 3.

21. Primet, M.; Pichat, P.; Mathieu, M. V.; J. Phys. Chem., 1971, 76, 9.

22. Jones, P.; Hockey, J. A.; Trans. Faraday Soc., 1971, 67, 679.

23. Jones, P.; Hockey, J. A.; Trans. Faraday Soc., 1971, 67, 2669.

24. Munuera, G.; Moreno, F.; Gonzalez, F.; "Reactivity of Solids", Ed. Anderson, J. S., 681, Chapman and Hall, 1972.

25. Munuera, G.; Stone, F. S.; Trans. Faraday Soc., 1971, 67, 205.

26. Munuera, G.; Z. Phys. Chem. Neue Folge, 1972, 78, 113.

27. Jackson, P.; Parfitt, G. D.; Trans. Faraday Soc. I, 1972, 68, 896.

28. Jones, P. D.; Hockey, J. A.; Trans. Faraday Soc. I, 1972, 68, 907.

29. Iwaki, T.; Komura, M.; Miura, M.; Bull. Chem. Soc. Jap., 1972, 45, 2343.

30. Day, R. E.; Parfitt, G. D.; Peacock, J.; J. Colloid Interface Sci., 1974, 46, 17.

31. Yates, D. E.; James, R. O.; Healy, T. W.; Trans. Faraday Soc. I, 1980, 76, 1.

32. Dawber, G.; Guest, L. B.; Thermochimica Acta., 1973, 6, 411.

33. Nagao, M.; Yunoki, K.; Muraishi, H.; Morimoto, T.; J. Phys. Chem., 1978, 82, 9.

34. Parfitt, G. D.; Ramsbotham, J. R.; Rochester, C. H.; Trans. Faraday Soc., 1971, 67, 3100.

35. Parfitt, G. D.; Ramsbotham, J.; Rochester, C. H.; J. Colloid Interface Sci., 1972, 11.

36. Tschapek, M.; Wasowski, C.; Torres Sanchez, R. M.; J. Electroanal. Chem., 1976, 74, 167.

37. Parks, G. A.; Chem. Rev., 1965, 65, 177.

38. Healy, T. W.; Fuerstenau, D. W.; Colloid Sci., 1965, 20, 376.

39. Berube, Y. G.; DeBruyn, P. L.; J. Colloid Interface Sci., 1968, 27, 2.

40. Berube, Y. G.; DeBruyn, P. L.; J. Colloid Interface Sci., 1968, 28, 1.

41. Levine, S.; Smith, A. L.; Discuss. Faraday Soc., 1971, 52, 290.

42. Kumagi, S.; Fukushima, S.; J. Colloid Interface Sci., 1972, 56. 227.

43. Parfitt, G. D.; Ramsbotham, J.; Rochester, C. H.; Trans. Faraday Soc., 1971, 67, 579.

44. Primet, M.; Pichat, P.; Mathieu, M. V.; J. Phys. Chem., 1971, 75, 9.

45. Parfitt, G. D.; Ramsbotham, J.; Rochester, C. H.; Trans. Faraday Soc., 1971, 67, 1500.

46. Boehm, H. P.; Discuss. Faraday Soc., 1971, 52, 264.

47. Boehm, H. P.; Advan. Catal., 1971, 22, 347.

48. Parfitt, G. D.; Ramsbotham, J.; Rochester, C. H.; Powder Technol., 1973, 7, 9.

49. Day, R. E.; Parfitt, G. D.; Peacock, J.; Discuss. Faraday Soc., 1971, 54, 356.

50. Furlong, D. N.; Rouquerol, F.; Rouquerol, J.; J. Colloid Interface Sci., 1980, 75, 1.

51. Eltekov, Y. A.; Khopina, N. V.; Kiselev, A. V.; Kovaleva, N. N.; J. Colloid Interface Sci., 1974, 47, 3.

52. Dollimore, D.; Pearce, J.; J. Colloid Interface Sci., 1974, 40, 2.

53. Day, R. E.; Eltekov, Y. A.; Parfitt, G. D.; Thompson, P. C.; Trans. Faraday Soc., 1969, 65, 266.

54. Pope, M. I.; Sulton, D. J.; Powder Technol., 1974, 10, 251.

55. James, R. O.; Stiglich, P. J.; Healy, T. W.; Trans. Faraday Soc., 1975, 71, 142.

56. Basilova, H.; Collect. Czech. Chem. Commun., 1975, 40,-3100.

57. Boonstra, A. H.; Mutsaers, C.A.H.; J. Phys. Chem., 1975, 79, 16.

58. Leal, O.; Andrew, P.; Z. Phys. Chem., 1974, 88, 215.

59. Iyengar, R. D.; Codell, M.; Gisser, H.; Weisberg, J.; Z. Phys. Chem., Neue Foldge, 1974, 89, 5325.

60. Iyengar, R. D.; Kellerman, R.; J. Colloid Interface Sci., 1971, 5.

61. Bickley, R. I.; Stone, F. S.; J. Catal., 1973, 31, 389.

62. Munuera, G.; Rives-Arnau, V.; Sauceda, A.; Trans. Faraday Soc., 1979, 75, 736.

63. Gravelle, P. C.; Juillet, F.; Meriaudeau, P.; Teichner, S. J.; Trans. Faraday Soc., 1971, 67, 140.

64. Fukuzawa, S.; Sanuer, K. M.; Kwan, T.; J. Catal., 1968, 11, 364.

65. Che, M.; Naccache; C.; Imelik, B.; J. Catal., 1972, 24, 328.

66. Anderson, S.L.T.; Trans. Faraday Soc. I, 1979, 76, 1356.

67. Chung, Y. W.; Lo, W. J.; Somorjai, G. A.; Surface Sci., 1977, 64, 588.

68. Morimoto, T.; Kittaka, S.; J. Colloid Interface Sci., 1980, 78, 2.

69. Pope, M. I.; Sutton, S. I.; Powder Technol., 1974, 9, 273.

70. Iwaki, T.; Bull. Chem. Soc. Jap., 1973, 46, 1631.

71. Taylor, L., Ed.; "Metals Handbook, Atlas of Microstructure of Industrial Alloys", 7, 321, Am. Soc. Metals, Metals Park, 1972.

72. Shih, H. D.; Jona, F.; Appl. Phys., 1977, 12, 311.

73. Senzaki, K.; Kuriyama, K.; Kawaski, K.; Surface Sci., 1976, 55, 697.

74. Dumas, P.; John, C. S.; Oxid. Met., 1976, 10.

75. Quarto, F. D.; Doblhofer, K.; Gerisher, H.; Electrochim. Acta., 1978, 23, 195.

76. St. Clair, A. K.; St. Clair, T. L.; Polym. Eng. Sci., 1976, 16, 314.

77. St. Clair, T. L.; Progar, D. J.; Proc. 24th, 1979 Natl. SAMPE Symp., 24, 1081.

78. Stegar, V. Y.; 12th National Sampe Conference, Oct. 7, 1980.

79. Hergenrother, P. M.; Macromolecules, 1974, 7, 575.

80. Hergenrother, P. M.; Polym. Eng. Sci., 1976, 16.

81. Allen, K. W.; Alsalim, H. S.; J. Adhes., 1974, 6, 229.

82. Wegman, R. F.; Appl. Polym. Symp., 1972, 19, 385.

83. Liverly, G. W.; "Improved Surface Treatments of Titanium Alloys for Adhesive Bonding", Technical Report, AFML-TR-73-270, 1974.

84. Hergenrother, P. M.; Progar, D. J.; Submitted to Adhesive Age.

85. Chen, W.; Dwight, D. W.; Wightman, J. P.; "A Fundamental Approach to Adhesion", NASA Report, 1978.

86. Chen, W.; Dwight, D. W.; Kiang, W. R.; Wightman, J. P.; "Reduction of Contamination on Titanium Surface Studied by ESCA", Surface Contamination, Genisis, Detection and Control, Mittal, K. L., Ed., 2, 665, Plenum Press, New York, 1979.

87. Ditchek, B. M.; Breen, K. R.; Venables, J. D.; "Bondability of Ti Adherends", Naval Air Systems Command Final Report AIR-52032-B, 1980.

88. Ditcheck, B. M.; Breen, K. R.; Sun, T. S.; Venables, J. D.; Brown, S. R.; 12th National SAMPE Technical Conference, Oct. 7, 1980.

89. Huntsberger, J. R.; J. of Paint Technology, 1967, 39, 199.

90. DeLollis, N. J.; "Adhesion Theory Review and Critique", AEC Research Development Report, TID-4500, 1970.

91. Mittal, K.; J. Vac. Sci. Technol., 1976, 13.

92. Kinloch, A. J.; J. Adhes., 1979, 10, 193.

93. Gregg, S. S.; Sing, K.S.W.; "Adsorption Surface Area and Porosity", Academic Press, New York, 1967.

94. Skiles, J. A.; M.S. Thesis, Virginia Polytechnic Institute and State University, Blacksburg, Virginia, 1978.

95. Wagner, C. D.; "Handbook of X-ray Photoelectron Spectroscopy", 1st ed.: Perkin Elmer, Eden Prairie, Minn., 1979.

96. Scofield, J. H.; J. Electron Spectrosc. Relat. Phenom.", 1976, 8, 129.

97. Harkins, W. D.; The Physical Chemistry of Surface Films, Reinhold Publishing Corp., New York, 1957.

98. Finklea, H.; Private Communication.

99. Siriwardane, H. J.; Private Communication.

100. "Selected Powder Diffraction Data for Minerals", Joint Comm. on Powder Diffraction Standards, 1974, 2, 49.

101. Bailey, R. R.; Wightman, J. P.; J. Colloid Interface Sci., 1979, 70, 112.

102. Kang, Y.; Skiles, J.; Wightman, J. P.; J. Phys. Chem., 1980, 84, 1448.

103. Zettlemoyer, A. C.; Schneider, C. H.; Skewis, J. D.; "Second International Congress of Surface Activity", Vol. III, 472, Academic Press, New York, 1957.

APPENDIX I

COMPUTER PROGRAM FOR THE CALCULATION OF ISOSTERIC HEAT

ORIGINAL PAGE IS
OF POOR QUALITY

```
      DIMENSION TITLE(18),GHED(6)
      DIMENSION A(25,5),Q(25),W(25,25),AT(5,25),AW(5,25)
     1 ,AWA(5,5),C(5)
    5 READ(5,100)NPROB,(TITLE(I),I=1,18)
  100 FORMAT(I5,18A4)
      IF(NPROB.LE.0)GO TO 99
      WRITE(6,200)(TITLE(I),I=1,18)
  200 FORMAT(1H1,18A4)
      READ(5,101)(GHED(I),I=1,6)
  101 FORMAT(18A4)
      WRITE(6,201)(GHED(I),I=1,6)
  201 FORMAT(//,'GRAPH HEADING:',18A4)
      READ(5,105)MAXDIM,MAXVAR,MEQ,MVAR
  105 FORMAT(4I5)
      WRITE(6,206)MAXDIM,MAXVAR,MEQ,MVAR
  206 FORMAT(//5X,' MAXIMUM NUMBER OF EQUATIONS', I5//
     1 5X,'MAXIMUM NUMBER OF VARIABLES',I5//
     2 5X,'PRESENT NUMBER OF EQUATIONS',I5//
     3 5X,'PRESENT NUMBER OF VARIABLES',I5//)
      CALL CMDATA(A,C,MEQ,MVAR)
      WRITE(6,204)
      DO 20 I=1,MEQ
   20 WRITE(6,205)(A(I,J),J=1,MVAR),W(I)
  205 FORMAT(1X,6(E12.5,2X)/)
  204 FORMAT(1H1,10X,'INPUT DATA  A-MATRIX AND RHS VECTOR'//)
      DO 30 I=1,MAXDIM
      DO 25 J=1,MAXDIM
   25 W(I,J)=0.0
   30 W(I,I)=1.0
      W(1,1)=1.00
      W(2,2)=  1.0
      CALL TRAPOS(A,AT,MAXDIM,MAXVAR,MEQ,MVAR)
      CALL MATMLT(AT,W,AW,MAXVAR,MAXDIM,MAXDIM,MVAR,MEQ,MEQ)
      CALL MATMLT(AW,A,AWA,MAXVAR,MAXDIM,MAXVAR,MVAR,MEQ,MVAR)
      DO 45 I=1,MVAR
      SUM=0.0
      DO 40 J=1,MEQ
   40 SUM=SUM + AT(I,J)*Q(J)
   45 C(I)=SUM
      CALL GAUSS(AWA,C,MAXVAR,MVAR)
      DO 50 I=1,MVAR
   50 WRITE(6,210)I,C(I)
  210 FORMAT(//5X,'VARIABLE NO.',I5,2X,'VALUE=',E12.5)
      CALL CMPLOT(A,J,C,MEQ,MVAR,GHED)
      GO TO 5
   99 STOP
      END


      SUBROUTINE TRAPOS(A,AT,MAXDIM,MAXVAR,MEQ,MVAR)
      DIMENSION A(MAXDIM,MAXVAR),AT(MAXVAR,MAXDIM)
      DO 10 I=1,MEQ
      DO 10 J=1,MVAR
   10 AT(J,I)=A(I,J)
      RETURN
      END
```

```
      SUBROUTINE MATMLT(A,B,C,M1,M2,M3,N1,N2,N3)
      DIMENSION A(M1,M2),B(M2,M3),C(M1,M3)
      DO 10 I=1,N1
      DO 10 J=1,N3
      SUM=0.0
      DO 20 K=1,N2
   20 SUM=SUM + A(I,K)*B(K,J)
   10 C(I,J)=SUM
      RETURN
      END

      SUBROUTINE GAUSS(A,B,NN,N)
      DIMENSION A(NN,NN),B(1)
      NM1=N-1
      IF(NM1.NE.0)GO TO 11
      B(1)=B(1)/A(1,1)
      RETURN
   11 CONTINUE
C     CHANGE ROWS AND DO FORWARD ELIMINATION
      DO 30 I=1,NM1
      XLARGE=1.E-15
      JCOUNT=0
      DO 15 J=I,N
      IF(ABS(A(J,I)) .GT. XLARGE) GO TO 10
      GO TO 15
   10 XLARGE=ABS(A(J,I))
      JCOUNT=J
   15 CONTINUE
      IF(JCOUNT.EQ.0)GO TO 60
      DO 20 K=1,N
      TEMP=A(I,K)
      A(I,K)=A(JCOUNT,K)
      A(JCOUNT,K)=TEMP
   20 CONTINUE
      TEMP=B(I)
      B(I)=B(JCOUNT)
      B(JCOUNT)=TEMP
      IP1=I+1
      DO 30 K=IP1,N
      Q=-A(K,I)/A(I,I)
      B(K)=Q*B(I) + B(K)
      DO 30 J=IP1,N
      A(K,J)=Q*A(I,J) + A(K,J)
   30 CONTINUE
      IF(A(N,N).EQ.0.0)GO TO 60
C     BACK SUBSTITUTION
      B(N)=B(N)/A(N,N)
      NP1=N+1
      DO 50 K=1,NM1
      Q=0.0
      NMK=N-K
      DO 40 J=1,K
      Q=Q + A(NMK,(NP1-J))*B(NP1-J)
   40 CONTINUE
      B(NMK)=(B(NMK)-Q)/A(NMK,NMK)
   50 CONTINUE
      IERROR=1
      RETURN
   60 IERROR=2
      WRITE(6,300)
  300 FORMAT(////'******** MATRIX IS SINGULAR ********'/)
      RETURN
      END
```

C-3

```
      SUBROUTINE CMDATA(A,C,MEQ,MVAR)
      COMMON/ONE/PM,VM
      DIMENSION X(20),Y(20),A(25,8),Q(25)
      READ(5,100)PM,VM
  100 FORMAT(2F10.2)
      WRITE(6,101)PM,VM
  101 FORMAT(2X,'PM=',F10.2,3X,'VM=',F10.2)
      DO 10 I=1,MEQ
   10 READ(5,110)X(I),Y(I)
  110 FORMAT(2F10.3)
      DO 15 I=1,MEQ
      A(I,1)=(PM/VM)/X(I) - 2.0/VM + (1.0/(PM*VM))*X(I)
      A(I,2)=1.0/X(I)
      A(I,3)=X(I)
      A(I,4)=X(I)**4
      A(I,5)=X(I)**5
      A(I,6)=Y(I)
   15 C(I)=1.0/Y(I)- (1.0/VM -X(I)/(VM*PM))
      RETURN
      END
```

```
FUNCTION VAL(XX,C,MVAR)
COMMON/ONE/PM,VM
DIMENSION C(6)
CON=(1.0-2*C(1))/VM+ C(1)*(PM/VM)/XX +(C(1)-1.0)*XX/(PM*VM)
VAL=1.0/CON
RETURN
END
```

ORIGINAL PAGE IS
OF POOR QUALITY

```
      SUBROUTINE CMPLOT(A,G,C,MEQ,MVAR,GHED)
      DIMENSION X(27),Y(27),A(25,6),G(25),C(6),GHED(6)
      DATA LMASK1/-30584/,LMASK2/-21846/
      AMAX=4.000
      ALAX=6.0
      CALL PLOTS(0,0,50)
      DO 10 I=1,MEQ
      X(I)=A(I,5)
      Y(I)=A(I,6)
      WRITE(6,1005)X(I),Y(I)
 1005 FORMAT(2X,'X',F10.5,2X,'Y',F10.5)
   10 CONTINUE
      CALL SCALE(X,ALAX,MEQ,1)
      CALL SCALE(Y,ALAX,MEQ,1)
      X(MEQ+1)=0.0
      Y(MEQ+1)=0.0
      Y(MEQ+2)=10.
      SCLX=X(MEQ+2)
      SCLY=Y(MEQ+2)
      CALL PLOT(1.0,1.0,-3)
      NLAX=ALAX
      MLAX=5*NLAX
      CALL GRID(0.0,0.0,MLAX,0.2,MLAX,0.2,LMASK1)
      CALL GRID(0.0,0.0,NLAX,1.0,NLAX,1.0,LMASK2)
      SCL1=X(MEQ+1)
      SCL2=X(MEQ+2)
      CALL AXIS(0.0,0.0,6HX AXIS,-6,ALAX,0.0,SCL1,SCL2)
      SCL1=Y(MEQ+1)
      SCL2=Y(MEQ+2)
      CALL AXIS(0.0,0.0,6HY AXIS,6,ALAX,90.0,SCL1,SCL2)
      CALL PLOT(0.0,0.0,3)
      DO 20 I=1,MEQ
      XP=X(I)/SCLX
      WRITE(6,1000)I
 1000 FORMAT(2X,'POINT',I5)
      YP=Y(I)/SCLY
      CALL PLOT(XP,YP,3)
      CALL SYMBOL(XP,YP,0.1,11,0.0,-1)
   20 CONTINUE
      CALL PLOT(0.0,0.0,3)
      CALL NEWPEN(2)
      DO 30 I=1,100
      XX=XMAX*FLOAT(I)/100.0
      YY=VAL(XX,C,MVAR)
      XX=XX/SCLX
      YY=YY/SCLY
      CALL PLOT(XX,YY,2)
   30 CONTINUE
      YLOC=ALAX-0.5
      CALL SYMBOL(0.5,YLOC,0.2,GHED,0.0,24)
      CALL PLOT(0.0,0.0,999)
      RETURN
      END
```

APPENDIX II

ADSORPTION ISOTHERMS CURVE FITTED USING COMPUTER PROGRAM